An *in vitro* model of murine middle ear epithelium

Apoorva Mulay[a], Khondoker Akram[a], Debbie Williams[b], Hannah Armes[a,c], Catherine Russell[a], Derek Hood[b] Stuart Armstrong[d], James P Stewart[d], Steve DM Brown[b], Lynne Bingle[c], Colin D Bingle [a].

[a]Academic Unit of Respiratory Medicine, Department of Infection, Immunity and Cardiovascular Disease, University of Sheffield, Sheffield, UK.

[b]MRC Mammalian Genetics Unit, Harwell, UK

[c]Oral and Maxillofacial Pathology, Department of Clinical Dentistry, University of Sheffield, Sheffield, UK

[d]Institute of Infection and Global Health, University of Liverpool, Liverpool, UK.

Running title: An *in vitro* model of murine middle ear epithelium

Corresponding author: Colin Bingle PhD, Academic Unit of Respiratory Medicine, Department of Infection, Immunity and Cardiovascular Disease, University of Sheffield, Sheffield, S10 2JF, UK.
Phone: 00 44 (0)114 2712423
Email: c.d.bingle@sheffield.ac.uk

Key words: Otitis media, middle ear epithelium, *Bpifa1,* air liquid interface, *NTHi*

Summary statement: Development and systematic characterisation of an *in vitro* otopathogenic infection model of the murine middle ear epithelium as a tool to better understand the complex pathophysiology of Otitis media.

Abstract

Otitis media (OM) or middle ear inflammation is the most common pediatric disease and leads to significant morbitity. Although understanding of underlying disease mechanisms is hampered by complex pathophysiology it is clear that epithelial abnormalities underpin the disease. There is currently a lack of a well characterised *in vitro* model of the middle ear (ME) epithelium that replicates the complex cellular composition of the middle ear. Here we report the development of a novel *in vitro* model of mouse middle ear epithelial cells (mMECs) at air liquid interface (ALI) that recapitulates the characteristics of the native murine ME epithelium. We demonstrate that mMECs undergo differentiation into the varied cell populations seen within the native middle ear. Proteomic analysis confirmed that the cultures secrete a multitude of innate defence proteins from their apical surface. We could show that the mMECs supported the growth of the otopathogen, *NTHi*, suggesting that the model can be succesfully utilised to study host pathogen interactions in the middle ear. Overall, our mMEC culture system can help better understand the cell biology of the middle ear and improve our understanding of the pathophysiology of OM. The model also has the potential to serve as a platform for validation of treatments designed to reverse aspects of epithelial remodelling underpinning OM development.

Introduction:

Otitis Media (OM) or inflammation of the middle ear is the most prevalent childhood disease, a leading cause of surgery in developed countries, and a significant reason for pediatric mortality in developing countries. Eighty percent of children suffer from at least one episode of OM by three years of age (Bakaletz 2010, Woodfield & Dugdale 2008).

The middle ear epithelium, and its secretions, are involved in maintaining homeostasis and sterility within the middle ear cavity (MEC). Epithelial remodelling, characterised by mucociliary metaplasia and infiltration of the MEC with inflammatory cells, is a common feature of OM (Straetemans et al 2001). In most animals, the middle ear is a relatively inaccessible organ lined by a thin mucociliary epithelium and sampling of the mucosa is a terminal procedure. Human middle ear tissue can be acquired only during surgical procedures and this limits the amount of sample

available for study of OM. Culturing of middle ear cells *in vitro* enables maximisation of the available material, allows the effect of modifying culture conditions to be studied more easily and also allows functional studies to be performed. Previously, attempts have been made to culture middle ear epithelial cells from a number of organisms including rats (Toyama et al 2004, Ueyama et al 2001, Vanblitterswijk et al 1986), mice (Tsuchiya et al 2005), chinchillas (Amesara et al 1992, Nakamura et al 1991), gerbils (Herman et al 1992, Portier et al 2005, Takeno 1990), rabbits (Schousboe et al 1995) and humans (Choi et al 2002, Chun et al 2002, Moon et al 2000). These studies have included organ and explant cultures, primary cell cultures and development of middle ear cell lines.

However, there remains a lack of a robust *in vitro* middle ear epithelial model that differentiates into the different epithelial cell types of the middle ear and is free of fibroblast contamination. This has greatly restricted the ability to identify the function of different cell types and their products within the middle ear and limits our understanding of the pathophysiology of OM development.

We report here the development of a novel *in vitro* primary model of the mouse middle ear epithelium using air liquid interface (ALI) culture and systematically characterise the different cell types present in the middle ear. We also demonstrate, that this culture system can be utilised to study host pathogen interactions within the middle ear and thus has the potential to allow investigatation of the mechanisms of OM pathogenesis.

Results:

We established an air liquid interface (ALI) culture system to model the mouse middle ear epithelium *in vitro* (Fig. 1A*)*. We performed a morphological analysis and systemactically characterised the various epithelial cell types expressed by our model in comparison to the native mouse middle ear epithelium.

Cell culture characteristics

The average number of epithelial cells isolated was 74,667±10,621 cells per MEC (n=12 batches). Primary culture of mMECs proceeded in two phases – a proliferative phase in submerged culture and a differentiation phase at air liquid interface (Fig. 1B-H). mMECs were seeded at a density of $1x10^4$ cells/ membrane and 3 days after

seeding 16.8±2.6% adhered to the membrane and had started forming small epithelial islands (Fig. 1B). The attached cells began to elongate to establish contact with neighbouring cells and began to proliferate rapidly from day 5 to day 7 (Fig. 1C, D). Cells formed a confluent monolayer of flat, polygonal cells within 9 to 10 days in submerged culture (ALI Day 0) in the presence of ROCKi (Fig. 1E). The morphology of the cells became more complex when transferred to ALI. At ALI Day 3, cells started changing in size and shape (Fig. 1F) and by ALI Day 7 two distinct sub populations of cells could be observed, the majority of which were flat polygonal cells, intersected with clusters of slightly elevated, more compactly arranged cells (Fig. 1G). Around ALI Day 9, ciliary beating could be seen in these clusters under phase contrast microscope. ALI Day 14 cells ($1.2x10^5$cells/membrane) displayed a cobble-stone appearance with well-defined cell boundaries; and were a combination of flat polygonal cells and compactly clustered elevated cells with actively beating ciliated cells. (Fig. 1H, Movie S1). No cells with fibroblast-like morphology were seen in the mMEC ALI cultures. However, fibroblasts were isolated through differential adherence to plastic during the cell isolation process. (Fig. 1I).

Cell morphology

Electron microscopy analysis during ALI culture revealed the development of a mucociliary epithelium (Fig. 2). At ALI Day 0 (undifferentiated cells), scanning electron microscopy showed uniformly flat, large cells with microvilli on the apical surfaces (Fig. 2A). At ALI Day14, the cells exhibited a dome shaped appearance (Fig. 2B), areas of flatter polygonal and secretory cells with microvilli on the apical surfaces and areas abundant in ciliated cells (Fig. 2C). The morphology of the ALI Day 14 mMEC cultures resembled the *in vivo* middle ear epithelium (Fig. 2D). Transmission electron microscopy revealed that ALI Day 14 cells were polarized with desmosomes on the baso-lateral surfaces suggesting the formation of tight junctions, another feature of epithelial cells (Fig. 2E). The formation of tight junctions was further confirmed by uniform expression of ZO-1 in the cell membrane (Fig. 2F)

Expression of epithelial markers by mMEC cultures

The expression of a selected panel of genes, known to be expressed by the middle ear epithelium and upper airways, was analysed by RT- PCR of RNA from the original mMECs before seeding and compared to ALI Days 0 and 14 cells.

Fibroblasts isolated by differential adherence were used as a negative control for epithelial markers (Fig. 3A). *Bpifa1 and Bpifb1* are secreted, putative innate immune molecules expressed in the upper airways. *Bpifa1* was expressed strongly in the original and ALI Day 14 cells, but lower in the undifferentated ALI Day 0 cells. *Bpifb1* was detected only in the original cells, not in cultured cells. *Tekt1* (a marker of ciliated cells) was detected at ALI Day 14. Analysis of *Muc5ac* and *Muc5b* expression, markers of goblet cells, suggested that *Muc5ac* was weakly expressed in mMEC original cells but was not detectable in the cultured cells, whereas Muc5b was expressed more strongly in the original cells and maintained this expression to ALI Day 14. We also studied the mucosal innate immune genes *Lactotransferrin, Surfactant protein D (Stfpd)* and *Regenerating islet-derived protein 3 gamma* (*Reg3γ)*. *Lactotransferrin* and *Reg3γ* were detected in the mMEC original cells and at ALI Days 0 and 14, whereas expression of *Stfpd* was seen in the cells during ALI differentiation. As expected, the expression of *Keratin5*, a marker of basal cells, was reduced as cells differentiated from ALI Day 0 to Day 14. The expression of these epithelial markers in the mMEC cultures indicates that the cells differentiate in culture from ALI Day 0 to ALI Day 14 and the pattern of expression in the differentiated cells is in line with that seen in the mMEC original cells isolated from the middle ear. The absence of *Vimentin* in ALI Day 14 cultures indicates that our mMEC cultures are devoid of fibroblast contamination. *Oaz1* was used as a housekeeping gene for all RT-PCR experiments.

MS analysis of the apical secretome of mMECs

To complement our gene expression studies, we also performed a global proteomic analysis of apical ALI Day 14 secretions of mMEC cells by Orbitrap mass spectrometry (MS). Table 1 lists the most abundant secreted proteins identified classified according to their emPAI score. The most abundant secreted protein was Lactotransferrin, with Serotransferrin, Reg3γ, Lipocalin2, Ceruloplasmin and Bpifa1 also being found at high levels. Multiple anti-proteinase and proteinase proteins were also found in the secretions including members of the WFDC family, WFDC2, WFDC18 (EXPI) and SLPI (WFDC4), as well as multiple cathepsins. We validated the secretion of Bpifa1, Lactotransferrin and Reg3γ in the apical washes from the differentiating mMEC cells using western blotting (Fig. 3B,C). The full list of proteins identifeid is given in Table S1.

Localisation of epithelial markers in mMEC cultures.

We used immunofluorescence confocal (IFC) microscopy to study the localisation of epithelial markers in ALI Day 0 and ALI Day 14 cultures, in order confirm the differentiation process at the protein level. ALI Day 0 cultures showed abundant staining of P63 (basal cell marker), scanty staining of Bpifa1 (Fig. 4A) and no staining of FoxJ1 (ciliated cells) and Muc5B (goblet cells) (Fig. 4C). However by ALI Day 14, the cells had differentiated into multiple cell types. These stained strongly for Bpifa1, had reduced levels of p63 (Fig. 4B) and were populated with ciliated and goblet cells (Fig. 4D). Bpifa1 was localised the non ciliated population in differentiated mMECs, consistent with that seen in the *in vivo* middle ear epithelium (Fig. S1). In keeping with proteomic and expression data, we also detected abundant cytosolic levels of Lactotransferrin and Reg3γ in the ALI Day 14 cultures (Fig. 4E, F). Staining of nuclei with DAPI and Z-slice imaging using confocal microscopy also demonstrated that the cells formed a flat monolayer at ALI Day 0, but showed a more complex reorganisation by ALI Day14 with a combination of flat and elevated cells showing 2 or 3 different layers, with nuclei further away from the base of the membrane (Fig. 4G, H).

Relative abundance of secretory and ciliated cells

As noted above, phase contrast microscopy and SEM of mMEC cultures demonstrated that the ALI Day 14 cultures were composed of distinct anatomical areas of flat polygonal cells and patches of more elevated pseudostratified cells (Fig. 1H, Fig. 2B). To study this in more detail, we used IFC to determine the localisation of different epithelial markers within the two regions of cellular morphology. FoxJ1 positive ciliated cells and Muc5B positive goblet cells, were restricted to the elevated pseudostratified cell clusters, whilst Bpifa1 was more commonly seen in the flatter cells, although some staining was seen in the elevated cells, especially near the periphery (Fig. 5). This was consistent with our observation that ciliated cells could be seen beating in the elevated clusters of cells under light microscopy. We also confirmed Bpifa1 and Muc5B positive cells were not ciliated (Fig. 5A, B). Again this alaysis confirmed the existence of elevated pseudostratified cells within the cultures (Fig. 5C,D).

mMEC ALI cultures as an otopathogenic infection model

Having established a novel mMEC culture model, we wanted to evaluate its utility as a model system for the study of host pathogen interactions in the middle ear. We infected differentiated ALI Day 14 cells with a GFP-tagged *NTHI 375*^{SR}. IFC microscopy indicated that only a few cells were infected 24 hpi but by 48 hpi the infection rate had increased and the bacteria continued to spread laterally in culture infecting the majority of cells by 72 hpi (Fig. 6A-C). We confirmed this observation by quantifying the amount of green fluorescence using image analysis and observed that in every batch the amount of bacterial infection increased in a time dependent manner (Fig. 6E, Fig. S2).

We also studied the expression of the pro-inflammatory chemokine *Cxcl2/MIP2α* during the progression of infection. *Cxcl2* was significantly upregulated post infection at 24hpi (131 fold) and 48hpi (36 fold) compared to the 24hpi MOCK sample set as the reference (Fig. 6F). This data confirms that our mMEC model is capable of eliciting an inflammatory response.

Discussion:

We have developed a novel *in vitro* model for the culture and differentiation of primary mouse middle ear epithelial cells (mMECs) cultured at an air liquid interface. The ALI system has previously been used to culture respiratory epithelial cells (TBE) from several species (Clarke et al 1992, Davidson et al 2000, Yamaya et al 1992, You et al 2002) and more recently, it has been applied to the culture of murine nasal epithelial cells (Woodworth et al 2007). The exposure of apical cell surfaces to air and the supply of nutrients from the basal compartment mimics the *in vivo* upper airway epithelium and promotes differentiation. As the middle ear epithelium can be considered to be an extension of the upper airways and exhibits physiological similarities to the upper respiratory tract, we reasoned that we could extend the use of the ALI system for the successful culture of primary mMECs.

Our mMEC cultures can be used to study both proliferation and differentiation of middle ear cells. The addition of ROCKi to the culture medium has been shown to enhance basal cell proliferation in airway epithelial cultures (Horani et al 2013). Using ROCKi, we could maximise the number of transwell-cultures established from the limited number of cells isolated from the thin middle ear epithelium without

altering differentiation (Fig. S3); an observation that has been made in both human and mouse airway cells (Horani et al 2013) and thus reduce the number of animals required for each batch of cells cultured.

An important and common problem identified in a number of previous attempts to grow middle ear epithelial cells was the contamination and overgrowth of fibroblasts in the cultures (Nakamura et al 1991, Tsuchiya et al 2005, Vanblitterswijk et al 1986). By adding a differential adherence step, in which fibroblasts adhere to plastic in preference to the epithelial cells, we were able to eliminate fibroblasts from our mMEC cultures, generating a pure epithelial population, as shown by a lack of expression of the fibroblast marker, *Vimentin*, in ALI Day 14 cultures.

The mMEC cultures model the native middle ear epithelium as the cells exhibit characteristic epithelial features such as a cobble-stoned morphology, formation of tight junctions, apical-basal polarised, presence of desmosomes and apical microvilli. The cultures contained a combination of single layers of flatter polygonal cells and clusters of pseudostratified, dome shaped, elevated cells, with some of these having beating cilia. The dome shaped appearance of cells can be attributed to an active ion transport mechanism (Chun et al 2002, Nakamura et al 1991).

A major limitation of previous middle ear epithelial cultures has been the lack of differentiation into distinct epithelial cell types. The middle ear epithelium, like the upper airway epithelium, is composed of ciliated cells, basal cells, goblet cells and other secretory cells. Previous studies outlined difficulties in maintaining ciliated cells in culture (Nakamura et al 1991, Ueyama et al 2001). To our knowledge, the development of ciliated cells has only been described in one study of human middle ear cultures (Choi et al 2002), also grown at the ALI. Our cultures clearly show the presence of actively beating cilia and also stain for nuclear FoxJ1 protein. We found that the distribution of cilia in our cultures partially mimics that seen in the native middle ear epithelium by SEM (Fig. S4). Parts of the middle ear epithelium are populated with tracts of dense cilia, parts with interspersed ciliated and non-ciliated cells and some parts with a simple epithelium composed of flat non-ciliated polygonal cells. This distribution of cell types within the middle ear cavity is supported by the study (Thompson & Tucker 2013) who also found that the native middle ear epithelium is a combination of densely packed cilitaed zones, intermittent ciliated and non ciliated zones and areas of flat polygonal cells. On this basis, we

believe that our mMECs closely model the morphology of the native middle ear epithelium.

Mucins are products of goblet cells, unique to the mucosal epithelia, and are essential in the maintenance of mucosal innate defence. A number of attempts have been described to utilise the available middle ear models to study mucin gene expression at the transcriptional level (Kerschner et al 2010, Liu et al 2016, Moon et al 2000, Tsuchiya et al 2005). However, these studies were limited by the lack of production and localisation of detectable amounts of mucins at the protein level. Goblet cells (as shown by Muc5b positivity) were seen in our ALI Day 14 mMEC cells. The lack of Muc5ac or Muc5b detection in our MS analysis could be because of the loss of these high molecular weight glycoproteins during the sample preparation process. MUC5B is the predominant mucin in COM effusions (Preciado et al 2010). It has been shown to be indispensible for airway mucocilary clearance and maintainence of mucosal homeostasis and *Muc5b*$^{-/-}$ mice develop OM (Roy et al 2014) Expression of Muc5b at proteomically detectable levels as demonstrated by IFC enables our model to be potentially utilised for further study of the role of mucins in the middle ear epithelium. Moreover, treating primary tracheal and bronchial epithelial cells grown at ALI with IL-13 has been shown to induce goblet cell hyperplasia(Atherton et al 2003, Kondo et al 2002). Our model provides a platform to study middle ear mucous hypersecretory phenotypes *in vitro*.

In addition to ciliated and goblet cells, our cultures also produce a range of other secretory cell products. Bpifa1 is the most widely studied member of the BPI fold (BPIF) containing family of putative host defence proteins (Bingle et al 2011) and we have previously shown it to be an abundant product of the murine upper respiratory tract and nasopharynx (Musa et al 2012). *BPIFA1* was identified as a candidate for OM in a recent GWAS study (Rye et al 2012) and loss of the protein has been implicated in the development of OM in aged mice (Bartlett et al 2015). Bpifa1 was readily detectable in mMEC cultures and apical secretions from the cells. Bpifa1 was localised to non-ciliated cells in the cultures, which is consistent with studies from the respiratory tract (Barnes et al 2008, Kim et al 2006, Musa et al 2012). *Bpifb1*, on the other hand, was detectable in the original cells, but not in the ALI Day 14 cultures and was absent from the list of proteins identified in the proteomic analysis performed using mass spectrometry. Bpifb1 protein is localised to goblet cells and minor glands associated with the Eustaschian tube (ET), but its expression is limited

in the middle ear epithelium (data not shown). This observation suggests that our mMEC cultures model the middle ear epithelium rather than the ET epithelium.

Proteomic analysis by MS identified a number of secretory proteins in the apical washes from the cells. The most abundant proteins comprised a variety of secretory host defence proteins with anti-microbial roles, proteins involved in cellular proliferation, wound repair, stress response, compliment activity and maintenance of cellular homeostasis. It is notable that our MS data contains a number of proteins also identified in a proteomic analysis of ear exudates from Chronic OM patients such as Lactotransferrin, Bpifa1, Lipocalin, Lysozyme and various cathespins and complement proteins (Val et al 2016). Lactotransferrin was the most abundant protein identified in our study. It is an innate immune protein secreted by airway mucosal surfaces that has been shown to play a role in maintenance of middle ear immunity (Bernstei.Jm et al 1974, Lim et al 2000, Moon et al 2002). It prevents colonisation of mucosal surfaces by scavenging environmental iron, thus limiting its availability for bacterial growth. Human milk Lactotransferrin has been shown to attenuate the pathogenic potential of *Haemophilus influenzae* by proteolytically cleaving two important colonisation factors found on the bacterial surface (Hendrixson et al 2003) and the administration of Apolactoferrin has been shown to reduce bacterial counts in chinchilla middle ears with pneumococcal induced OM (Schachern et al 2010). Surfactant protein D was originally identified as a lung surfactant associated protein but is also expressed in the ME and the ET and has a suggested role in enhancing opsonisation and phagocytosis of bacteria (Lim et al 2000, van Rozendaal et al 2001, Wright 1997). Reg3γ is C-type lectin produced by Paneth cells and secreted into the intestinal lumen with a suggested bactericidal activity against gram-positive bacteria by binding to peptidoglycan in the bacterial cell wall (Cash et al 2006). It has been shown to spatially regulate the separation of microbiota from the host small intestinal epithelium (Vaishnava et al 2011). *Reg3γ*$^{-/-}$ mice have an altered mucosal distribution and increased inflammatory response in the small intestine (Loonen et al 2014). *Reg3γ* has also been shown to be involved in pulmonary innate immunity as it is induced by *Stat3* during methicillin resistant *Staphalococcus aureus (MRSA)* infection in lung and inhibits *MRSA* growth *in vitro* (Choi et al 2013). This is the first study reporting the expression of this protein in the ME and it is possible that Reg3γ performs a similar function in the middle ear.

It was noticeable that the proteomic data unexpectedly contained many intracellular proteins. We also detected the presence of the membrane tethered mucins Muc1, Muc4 and Muc18. (Table S1). This can be reasoned to be the content of secreted exosomes. Exosomes are small membrane bound units released by the fusion of endosomal micro vesicular bodies with the apical plasma membrane. They have been suggested to be involved in stimulating immune responses, modulating secretory activities and engaging in cell communication by packaging and delivering microRNAs to other cells (Keller et al 2006, Valadi et al 2007). Exosomes are released by epithelial cells (Kapsogeorgou et al 2005, van Niel et al 2001), found in BAL fluids (Admyre et al 2003) and also in the apical secretions from human tracheobronchial epithelial (HBE) cultures (Kesimer et al 2009, Pillai et al 2014). . The presence of exosome asssociated proteins in our mMEC secretome further adds to the potential utility of this model to study the role of exosomes in middle ear biology and OM pathogenesis.

Infection of mMECs using the human otopathogen, *NTHi* demonstrates that our culture system can be effectively utilised for the study of host pathogen interactions within the middle ear. Our studies show that, *NTHi* initially infected a small number of cells in culture and the infection spread laterally over time. Since the advent of pneumococcal vaccines, *NTHi* is the most common pathogen in OM (Casey & Pichichero 2004). Epithelial remodelling, one of the most common features of OM, is characterised by mucous metaplasia. The chemokine Cxcl2/MIP2α is the murine homologue of IL-8 and is a key mediator of overproduction of mucin (Juhn et al 2008). *NTHi* infection is known to stimulate *Cxcl2* upregulation in several murine tissues including the middle ear, lungs and the inner ear (Gaschler et al 2009, Lim et al 2007, Woo et al 2012). Moreover, *Cxcl2* was identified as the most upregulated gene when mice were trans-tympanically injected with NTHi and on infection of the mouse middle ear epithelial cell line (mMEEC) with NTHi (Preciado et al 2013). Our data shows that *Cxcl2* was significantly upregulated on NTHi infection at 24 and 48 hours post infection, suggesting that our mMECs respond to bacterial infection in a manner similar to the native middle ear epithelium. This opens up a new avenue to utilise this system to study the response of middle ear cells to different insults, injuries and infections. Our mMEC cultures can potentially be utilised to study the interaction of host middle ear epithelial cells with a variety of bacterial as well as viral otopathogens.

It is known that primary cells cultured from cystic fibrosis and asthma patients maintain the disease phenotype in culture (Davies et al 2003, Matsui et al 1998). A number of mouse models are available for the study of OM. These include mice deficient in innate immunity genes such as *Evi1*, *Fbxo11, TLRs* and *Myd88,* cilliary development genes such as *Dnahc5* (Rye et al 2011) and goblet cells (Roy et al 2014). It will be interesting to see if our mMEC culture system can be utilised to reproduce the OM phenotype of these mouse mutants *in vitro* and enable comparative studies between unaffected and diseased cultures. OM often involves complex responses involving the middle ear epithelium, sub-epithelial mesenchyme, inflammatory cells and middle ear effusion, making it challenging to identify epithelial cell-specific responses. The mMEC culture system will provide us with the ability to isolate and assay responses of specific sub poupulations of epithelial cells. Our cell isolation method eliminates the influence of explants and excludes fibroblasts from culture, which were two of the most important confounding factors showin in previous studies of primary middle ear epithelial cells. It is a 3-dimentional model of the middle ear epithelium and hence mimics the in vivo physiology more closely compared to cell lines. The possibility of replicating the phenotype of the genetic models of OM, the capacity to easily manipulate differentiation of cells by modifying culture conditions and the ability to infect cells with various ototpathogens makes our model widely applicable to the wider OM community. The availability of such a well-characterised model of the middle ear epithelium can help better understand the cell biology of the middle ear and improve our understanding of the pathogenesis of OM.

Materials and Methods

Ethics statement

Humane care and animal procedures were carried out in accordance to the appropriate UK Home Office Project licence. Randomised male and female 8-10 week old C57BL/6 and C3H/HeH mice, housed in individually ventilated cages (Techniplast UK Ltd) under specific pathogen free (SPF) conditions were obtained from MRC Harwell, UK.

Dissection of the middle ear cavity

406 The detailed protocol used for dissection is outlined in Fig S5. Mice were euthanized
407 by terminal intra-peritoneal injection of 100µL pentobarbital (50mg/ml, Henry
408 Schein®) and exsanguinated by cutting the inferior vana cava. Mice were
409 decapitated, the skin at the nape of the neck was incised, bisected anteriorly and
410 removed entirely to expose the bony surface of the skull and the lower jaw was
411 detached under direct visualization. Under a dissecting microscope (Olympus
412 SZx10), the skullcap was gently opened with a pair of fine forceps and the brain was
413 removed. The head was bisected at midline and oriented with the opening of the ear
414 facing upwards. Any muscle, soft tissue and remnant hair surrounding the ear were
415 removed using fine dissecting scissors and forceps, leaving the MEC (bulla), still
416 attached to the outer ear canal (OEC) and the inner ear (IE). The bony shell of the
417 bulla was further cleaned free of any attached extraneous tissue. The OEC, which
418 appears a shade lighter than the MEC, was gently broken away from the MEC using
419 stork bill forceps. The tympanic membrane and the ossicles usually detached from
420 the MEC along with the OEC. Alternatively, they were physically removed using fine
421 stork bill forceps. Lastly, the cup-shaped MEC was carefully lifted away from the
422 inner ear.
423
424 *Isolation and differentiation of middle ear epithelial cells at air liquid interface*
425 The protocol for primary culture and differentiation of mouse middle ear epithelial
426 cells (mMECs) was adapted from a previously described method for mouse tracheal
427 epithelial cells (mTECs; (You & Brody 2013, You et al 2002). For each batch of cells,
428 bullae from approximately six mice (12 bullae) were pooled in a tube containing
429 pronase (1.5 mg/ml) in *'mMEC basic media'*: DMEM/F-12 HAMs media (Life
430 Technology, Cat No- 31330-038) supplemented with penicillin (100 µg /ml) and
431 streptomycin (100 µg/ml) (Life Technology, Cat No- 15070-063) and subjected to
432 overnight proteolysis at 4°C. The pronase was neutralised by the addition of 10%
433 foetal bovine serum (FBS) and the bullae were gently agitated by inverting the tube
434 25 times. The bullae were then transferred to 2ml of fresh *mMEC basic 10% FBS*
435 *media*, the tube was inverted again 25 times and this process was repeated 3 times.
436 The combined proteolytic and mechanical actions led to dissociation of the middle
437 ear cells from the bullae (Fig. S6). Media from the three tubes was combined and
438 centrifuged at 500g for 10 minutes at 10°C. The pelleted cells were re-suspended in
439 1ml of media containing 1 mg/ml bovine serum albumin (BSA) and 0.5 mg/ml DNase

I (Sigma-Aldrich, Cat No- DN25). Cell viability and number were assessed using trypan blue staining and a haemocytometer. Cells were centrifuged at 500g for 5 minutes at 10°C and the pellet re-suspended in 5ml of *mMEC basic 10% FBS media*. In order to seperate contaminating fibroblasts from epithelial cells a differential adherence step was performed by plating the cells on 60mm surface treated tissue culture dishes at 37°C in a 5% CO2 incubator for 3-4 hours. Fibroblasts attached to the plastic whilst the non-adherent epithelial cells were collected, centrifuged at 500 xg for 5 minutes at 10°C and re-suspended in 1ml of '*mMEC plus' media*: mMEC basic media supplemented with 5% FBS, 30 µg/ml bovine pituitary extract (Life Technology, Cat No- 13028-014), 10 µg/ml of insulin (Sigma-Aldrich, Cat No- I1882), 25 ng/ml of mouse epidermal growth factor (BD Biosciences, Cat No- 354001), 5 µg/ml of transferrin (Sigma-Aldrich, Cat No- T1147), 0.1 µg/ml of cholera toxin (Sigma-Aldrich, Cat No- C8052) and 0.01 µM of freshly added retinoic acid (Sigma-Aldrich, Cat No- R2625).

For optimisation of culture conditions, cells were plated on either tissue culture plastic or sterile, 0.4µm pore sized transparent PET (Polyethylene Terephthalate) membranes coated with 150µL (50µg/ml) of rat-tail collagen type I (BD Biosciences, Cat No- 354236) in a 24-well supported transwell format (Falcon, Cat No-353095). mMECs were seeded at an initial density of 1 x 10^4 and 2 x 10^4 cells/well in the presence or absence of 10 µM of Rho Kinase inhibitor, Y-27632 dihydrochloride (ROCKi, Tocris bioscience, Cat- 1254) and 5 x 10^4 cells/well without ROCKi. A seeding density of 1 x 10^4 cells/well with ROCKi on transwell membranes was identified as optimum and therefore used for culturing all following batches of cells (Fig. S3A-G).

Cells were initally cultured, submerged, in '*mMEC plus-proliferation media*' with 300 µL of media in the top chamber and 700 µL in the bottom chamber. Media was changed every 48 hours, until the cells were completely confluent, thereafter media from the apical chamber was removed and media in the basal chamber was replaced with *'mMEC SF- differentiation media'*: DMEM/F-12 media supplemented with 1 mg/ml BSA (Life Technology, Cat No- 31330-038), 5 µg/ml insulin, 30 µg/ml bovine pituitary extract, 5 µg/ml transferrin, 5 ng/ml mouse epidermal growth factor, 0.025 µg/ml cholera toxin and freshly added 0.01 µM retinoic acid to induce ALI culture. This system of culture promotes differentiation of cells by mimicking the *in vivo* situation. Cells were differentiated at ALI for 14 days and media was changed

every 48 hours. Cells were lysed in 250 µL of Trizol reagent (Sigma- Aldrich, Cat No- T2494) for RNA extraction and apical washes were collected in 200 µL of sterile HBSS at ALI Day 0 (submerged Day 10), Day 3, Day 7 and Day 14. Figure 2A gives a brief overview of the complete cell culture system. Doubling time for cells seeded at 5 x 10^4 cells/well in *mMEC- Plus media* without ROCKi was determined by trypsinizing the cells and using the formula: PD = t x Log2/(LogC2-LogC1) [PD = Population doubling, t = 48 hours, Log = 10 based Log, C1 = initial cell count, C2 = final cell count].

Immunoflorescence microscopy

Transwell membranes at ALI Day 0 and Day 14 were fixed with 10% phosphate buffered formalin at 37^0C for 30 minutes. Cells were permeabilised using 0.5% Triton X-100. Non-specific binding was blocked using 10% goat serum in PBS and incubation for 1 hour at 80rpm on an orbital shaker at room temperature. The membranes were washed 3 times with PBS for 5 minutes at 150 rpm and incubated with the following primary antibodies: anti-Bpifa1 (1:200), anti-Foxj1 (1:300), anti-p63 (1:100), anti-MUC5B (1:100), anti-ZO1 (1:200), anti-lacto transferrin (1:200) or anti-Reg3γ (1:200), overnight at 4^0C at 80rpm on the shaker. All antibody details are given in Table S2. The following day, membranes were washed 3 times with PBS for 5 minutes at 150 rpm and bound primary antibodies detected using 1:200 dilution of the appropriate fluorophore-tagged secondary antibody (Alexa-Fluor 568 Goat anti-rabbit antibody (Cat No- A11011) or Alexa Fluor 488 Goat anti-mouse antibody (Cat No- A11001)) incubated for 1 hour at room temperature at 80 rpm in the dark. Membranes were washed 3 times as above, detached carefully from their transwell support with a fine scalpel and placed on a glass microscope slide with the cells facing upwards. Nuclei were counterstained using Vectashield DAPI mounting medium (Vector laboratories) and the cells imaged using an Olympus Fluoview 1000 Confocal microscope.

Scanning Electron Microscopy

ALI Day 0 and Day 14 cell membranes were washed free of culture media with sterile, warm HBSS and fixed in 3% Glutaraldehyde in 0.1M Sodium Cacodylate buffer overnight at 4^0C. The membranes were washed 2 times with 0.1M Cacodylate buffer for 5 minutes each, detached from their transwell support as described above

and postfixed in 2% aqueous Osmium tetroxide. The specimens were washed briefly in water, dehydrated in a graded ethanol series, dried in a 1:1 mixture of 100% ethanol: Hexamethyldisilazane (HEX) before final drying in 100% HEX. The membranes were placed overnight in a fume hood, mounted onto a pin-stub using a Leit-C sticky tab, (gold sputter coated) and examined using a Philips XL-20 SEM at 15kV.

Transmission Electron Microscopy

ALI Day 14 cell membranes were fixed with 3% Glutaraldehyde in 0.1M Sodium Cacodylate buffer, washed and post fixed in 2% Osmium Tetroxide as mentioned above. The detached membranes were washed briefly in water and dehydrated through graded ethanols, cleared in Epoxy-propane (EPP) and infiltrated in 1:1 mixture of araldite resin: EPP mixture overnight on a rotor. This mixture was replaced in two changes with fresh araldite resin mixture over an 8-hour period, before being embedded and cured at 60^0C in an oven for 48-72 hours. Ultrathin sections (approximately 85nm thick) were cut on a Leica UC 6 ultra-microtome onto 200 mesh copper grids, stained for 30 minutes with saturated aqueous Uranyl Acetate followed by Reynold's Lead Citrate for 5minutes. Sections were examined using a FEI Tecnai Transmission Electron Microscope at an accelerating voltage of 80Kv. Electron micrographs were recorded using a Gatan Orius 1000 digital camera and Digital Micrograph software.

Non-typeable Haemophilus influenzae infections

mMECs were cultured in antibiotic-free media for 48 hours prior to infection. A GFP tagged, streptomycin resistant strain of the clinical OM isolate, *NTHi-375 (NTHi 375^{SR})*, derived from a Finnish pneumococcal vaccine study on children undergoing tympanocentesis in 1994-95 was used for all bacterial challenge experiments (Cody et al 2003). *NTHi 375^{SR}* was grown from glycerol stocks on brain heart infusion (BHI) agar plates supplemented with 2µg/ml Nicotinamide adenine dinucleotide hydrate (NAD, Sigma Aldrich, Cat No- N7004), 2µg/ml hemin (Sigma Aldrich, Cat No- H9039) and 200µg/ml streptomycin sulphate (Melford Laboratories, Cat No- S0148) at 37^0C, 5% CO_2 overnight. The following day colonies were transferred into BHI broth supplemented with NAD and hemin and incubated for 3 hr at 37^0C, 5% CO_2, 250rpm. The optical density (OD_{490}) of 1ml of liquid culture was

spectrophotometrically determined (Jenway 6300) and the culture diluted with PBS to give a concentration of $1x10^9$ bacteria/ml. An appropriate amount of culture in antibiotic-free mMEC-SF media was added to the apical chamber of ALI Day 14 mMEC cultures such that the membranes were infected at a multiplicity of infection (MOI) of 1:100 (mMECs: bacteria). An equal volume of sterile PBS was added to generate MOCK infected controls. The membranes were incubated at 37^0C, 5% CO_2 for 1 hr and washed 3 times with sterile HBSS to remove non-adherent bacteria. Media was replaced in the basal chamber and cultures were incubated for 4, 24, 48 and 72 hours post infection (hpi). At each time point apical washes were collected, cells were lysed in Trizol reagent for RNA extraction and membranes were fixed for IFC as described. Membranes were visualized using confocal microscopy and infection was quantified by measuring the mean integrated fluorescence intensity of four central 10x fields at each time point, in each batch, using Image J software.

Reverse transcription PCR (RT-PCR)

For end-point RT- PCR, total RNA was extracted from at least 3 batches of freshly isolated mMECs before seeding (mMEC original) and mMECS at ALI days 0 and 14 lysed in Trizol. RNA yield was determined using NanoDrop-1000 (Thermoscientific). Residual genomic DNA was digested by DNase I treatment (Promega, Cat No- M6101) and 200ng of RNA was reverse transcribed using AMV Reverse Transcriptase (Promega, Cat No- M9004). RT-PCR was performed with 1µl of template cDNA and Maxima Hot Start Green PCR Master Mix (ThermoFisher Scientific, Cat No- K1061). The cycling conditions were: 95°C for 5 minutes; denaturation: 94°C for 1 minute (25-35 cycles); annealing: 60°C for 1 minute; extension: 72°C for 1 minute; final extension: 72°C for 7 minutes (MJ Research PTC-200). The primer pairs used are described in Table S3. The amplified PCR products were run on a 2% agarose gel containing 0.5µg/ml ethidium bromide (Dutscher scientific, Cat No- 4905006) and bands visualised using a Biorad ChemiDoc™ XRS+.

Real time quantitative PCR (RT-qPCR)

For RT-qPCR, total RNA was extracted from at least three independent batches of ALI Day 14 cultures infected with NTHi-375^{SR} for 24 and 48 hours and their corresponding MOCK infected cultures. Residual genomic DNA was removed using

the DNA-*free*™ kit (Life technologies, Cat No- AM1906), RNA quantified using NanoDrop-8000 (Thermoscientific) and integrity checked on an Agilent Bioanalyzer 2100 instrument using RNA 6000 Nano kit. 400ng of total RNA was reverse transcribed into cDNA in a 20µL reaction volume using a Superscript™ III First Strand Synthesis kit (Invitrogen, cat No- 11752-050), in accordance with manufacturer's instructions. RT-qPCR was performed using an Applied Biosystems TaqMan gene expression assay for Cxcl2 (Mm00436450_m1) on a 7500 Fast Real Time PCR system (Applied Biosystems), with 2x Taqman Fast Universal Master Mix (Applied Biosystems, Cat No- 4352042). 10ng cDNA was added to each reaction and three technical replicates were performed for each assay in each batch. Genetic expression levels of Cxcl2 were normalized to three endogenous controls: ATP5B, CyC1 (Primerdesign geNorm^{TM} Reference Gene Selection Kit) and Ppia (TaqMan assay (Mm02342429_g1) and analysed using ABI 7500 software v2.0.1 using the $2^{-\Delta\Delta Ct}$ method. Data is presented as mean Relative quantification (RQ) and error bars represent standard error of mean.

Western Blotting

Standard western blotting technique was used to detect secreted proteins in apical HBSS washes collected at ALI D0, D3, D7 and D14 from the mMEC cultures. An equal volume of 2x SDS loading buffer (20% SDS, 1M DTT, Glycerol, Tris-HCl 0.5M pH6.8, 0.2% bromophenol blue, protease inhibitors) was added to the wash and denatured at 95°C for 5 minutes. 40 µL of total sample was resolved on a 12% polyacrylamide gel, transferred to a PVDF membrane using a semi dry blotting system (Biorad Trans-blot turbo) and probed with primary antibodies (anti-Bpifa1 (1:200), anti-lacto transferrin (1:2000), and anti-REG3γ (1:5000) overnight at 4°C. The primary antibody was detected using a polyclonal goat anti-rabbit secondary antibody (Dako P0448) conjugated with HRP (1:2000). Primary antibody details are described in Table S1. Protein bands were visualised using the EZ system (Geneflow, Cat No- 30500500B).

Immunohistochemistry

Formalin fixed, paraffin embedded serial sections of the mouse head passing through the middle ear cavity were deparaffinised and dewaxed in a 100% Xylene (Sigma, UK) and rehydrated in 100% Ethanol (Fischer Scientific, UK). Endogenous

peroxidase activity was blocked using 0.3 % H_2O_2- Methanol (Fischer Scientific, UK). Non-specific binding was blocked by incubating the sections in 100% goat serum for 30 minutes at room temperature. Sections were washed and incubated in anti-Bpifa1 primary antibody (1:750) overnight in a humified chamber at 4°C. The following day, sections were washed twice in PBS, incubated in 0.5% biotinylated polyclonal goat anti-rabbit secondary antibody (Vectastain^R Elite^R ABC kit, Cat No- PK-6101) for 30 minutes at room temperature, followed by incubation with the ABC reagent for signal amplification for 30 minutes. NovaRed mixture (Vector, Cat No- SK 4800) was used for colour development. Sections were counterstained using Harris's Haematoxylin (Thermo Scientific), differentiated in acid alcohol, treated with Scott's tap water, dehydrated in 95% to absolute ethanol, cleared using Xylene (Leica, Cat No- ST 4020), mounted in DPX (Leica Biosystems) and visualized and imaged using a light microscope (Olympus BX61).

Sample preparation for Mass Spectrometry

Apical wash secretions from 6 batches of ALI Day 14 mMEC cultures were pooled. TCA precipitation was performed (30% TCA in acetone) at -20°C for 2 hours to precipitate soluble proteins (50 µg). Proteins were pelleted at 12,000 g for 10 minutes (4°C) and pellets washed three times with ice-cold acetone, air dried and. re-suspended in 50 mM ammonium bicarbonate, 0.1 % RapiGest SF (waters). Samples were heated at 80°C for 10 minutes, reduced with 3 mM DTT at 60°C for 10 minutes, cooled and then alkylated with 9 mM iodoacetamide (Sigma) for 30 minutes. All steps were performed with intermittent vortexing. Proteomic-grade trypsin (Sigma) was added at a protein: trypsin ratio of 50:1 and incubated at 37°C overnight. The samples were precipitated using 1% TFA at 37°C for 2 hr and centrifuged at 12,000 g for 1 hr (4°C) to remove RapiGest SF. The peptide supernatant was desalted using C_{18} reverse-phase stage tips (Thermo Scientific Pierce) according to the manufacturer's instructions, dried and re-suspended in 3% (v/v) acetonitrile, 0.1% (v/v) TFA for analysis by Mass Spectrometry (MS).

NanoLC-MS ESI MS/MS analysis

Peptides were analysed by on-line nanoflow LC using the Thermo EASY-nLC 1000 LC system (Thermo Fisher Scientific) coupled with Q-Exactive mass spectrometer (Thermo Fisher Scientific). Samples were loaded onto an Easy-Spray C_{18} column

(50cm, i.d. 75 µm), fused to a silica nano-electrospray emitter (Thermo Fisher Scientific). Chromatography was performed at 35°C with a buffer system consisting of 0.1% formic acid (buffer A) and 80% acetonitrile in 0.1% formic acid (buffer B). The peptides were separated over a 97 minute linear gradient of 3.8 – 50% buffer B at a flow rate of 300 nL/min. The Q-Exactive was operated in data-dependent mode with dynamic exclusion and survey scans acquired at a resolution of 70,000. The 10 most abundant isotope patterns with charge states +2, +3 and/or +4 from the survey scan were selected with an isolation window of 2.0Th and fragmented by higher energy collisional dissociation with normalized collision energies of 30. The maximum ion injection times for the survey scan and the MS/MS scans were 250 and 100ms, respectively, and the ion target value was set to 1E6 for survey scans and 1E4 for the MS/MS scans.

Protein Identification and Quantification

Thermo RAW files were imported into Progenesis LC–MS (version 4.1, Nonlinear Dynamics) and only peaks with a charge state between +2 and +7 were picked. Spectral data were exported for peptide identification using the Mascot (version 2.3.02, Matrix Science) search engine. Tandem MS data were searched against translated ORFs from the mouse genome (Uniprot release 2015_02; 16,868 sequences; 9,451,355 residues). The search parameters were as follows: precursor mass tolerance was set to 10 ppm and fragment mass tolerance was set to 0.8 or 0.01Da and two missed tryptic cleavages were permitted. Carbamidomethylation (cysteine) was set as a fixed modification and oxidation (methionine) set as variable modification. Mascot search results were further validated using the machine-learning algorithm Percolator embedded within Mascot. The Mascot decoy database function was utilised and the false discovery rate was <1%, while individual percolator ion scores> 13 indicated identities or extensive homology ($p < 0.05$). Mascot search results were imported into Progenesis LC–MS for relative quantification using non- conflicting peptides.

Statistics

A paired two tailed Students t-test was used to compare relative Cxcl2 expression between the MOCK infected and *NTHi* infected samples at each time point. Data was presented using GraphPad Prism version 6.0.

Acknowledgements:

We acknowledege Professor Michael Cheeseman (University of Edinburgh) for valuable insights into middle ear biology, Christopher Jill (University of Sheffield) for Electron Microscopy, Lynne Williams and Dr. Helen Marriot (University of Sheffield) for culling mice and the staff of Ward 4 at the Mary Lyon Centre (MRC Harwell) for animal husbandry.

Competing interests

The authors declare that they have no competing or financial interests.

Author contributions

A.M.and C.D.B. concieved and designed the experiments and interpreted results.
A.M. and C.D.B. wrote the paper.
A.M. performed majority of the experiments and analysed data.
K.M.A. and L.B. provided technical expertise on cell culture work.
D.W. helped with design and analysis of qPCR experiments.
H.A. performed RT-PCRs on differentiation samples and western blots for LTF and REG3γ.
C.R. performed IHC for Bpifa1 on Wt middle ear sections.
S.A. and J.P.S. performed and analysed the proteomics data.
D.H. provided the NTHi strain and helped concieve infection experiments.
K.M.A., S.D.M.B. and L.B. assisted critical evaluation and drafting of the manuscript.

Funding

AM was supported by a University of Sheffield PhD Studentship (supervised by LB and CDB) and funds from MRC Harwell. HA was supported by a University of Sheffield hearing research Summer Studentship. The proteomic work and confocal microscopy was supported by Biotechnology and Biological Sciences Research Council (UK) grants BB/K009664/1 to JPS and BB/K009737/1 to CDB and LB.

References

Admyre C, Grunewald J, Thyberg J, Gripenback S, Tornling G, et al. 2003. Exosomes with major histocompatibility complex class II and co-stimulatory molecules are present in human BAL fluid. *European Respiratory Journal* 22: 578-83

Amesara R, Kim Y, Sano S, Harada T, Juhn SK. 1992. Primary cultures of middle-ear epithelial-cells from chinchillas. *European Archives of Oto-Rhino-Laryngology* 249: 164-67

Atherton HC, Jones G, Danahay H. 2003. IL-13-induced changes in the goblet cell density of human bronchial epithelial cell cultures: MAP kinase and phosphatidylinositol 3-kinase regulation. *American Journal of Physiology-Lung Cellular and Molecular Physiology* 285: L730-L39

Bakaletz LO. 2010. Immunopathogenesis of polymicrobial otitis media. *J Leukoc Biol* 87: 213-22

Barnes FA, Bingle L, Bingle CD. 2008. Pulmonary Genomics, Proteomics, and PLUNCs. *Am J Respir Cell Mol Biol* 38: 377-9

Bartlett JA, Meyerholz DK, Wohlford-Lenane CL, Naumann PW, Salzman NH, McCray PB. 2015. Increased susceptibility to otitis media in a Splunc1-deficient mouse model. *Disease Models & Mechanisms* 8: 501-08

Bernstei.Jm, Tomasi TB, Ogra P. 1974. Immunochemistry of middle-ear effusions. *Archives of Otolaryngology-Head & Neck Surgery* 99: 320-26

Bingle CD, Bingle L, Craven CJ. 2011. Distant cousins: genomic and sequence diversity within the BPI fold-containing (BPIF)/PLUNC protein family. *Biochemical Society Transactions* 39: 961-65

Casey JR, Pichichero ME. 2004. Changes in frequency and pathogens causing acute otitis media in 1995-2003. *Pediatric Infectious Disease Journal* 23: 824-28

Cash HL, Whitham CV, Behrendt CL, Hooper LV. 2006. Symbiotic bacteria direct expression of an intestinal bactericidal lectin. *Science* 313: 1126-30

Choi JY, Kim CH, Lee WS, Kim HN, Song KS, Yoon JH. 2002. Ciliary and secretory differentiation of normal human middle ear epithelial cells. *Acta Oto-Laryngologica* 122: 270-75

Choi SM, McAleer JP, Zheng MQ, Pociask DA, Kaplan MH, et al. 2013. Innate Stat3-mediated induction of the antimicrobial protein Reg3 gamma is required for host defense against MRSA pneumonia. *Journal of Experimental Medicine* 210: 551-61

Chun YM, Moon SK, Lee HY, Webster P, Brackmann DE, et al. 2002. Immortalization of normal adult human middle ear epithelial cells using a retrovirus containing the E6/E7 genes of human papillomavirus type 16. *Annals of Otology Rhinology and Laryngology* 111: 507-17

Clarke LL, Burns KA, Bayle JY, Boucher RC, Vanscott MR. 1992. Sodium-conductive and chloride-conductive pathways in cultured mouse tracheal epithelium. *American Journal of Physiology* 263: L519-L25

Cody AJ, Field D, Feil EJ, Stringer S, Deadman ME, et al. 2003. High rates of recombination in otitis media isolates of non-typeable Haemophilus influenzae. *Infection Genetics and Evolution* 3: 57-66

Davidson DJ, Kilanowski FM, Randell SH, Sheppard DN, Dorin JR. 2000. A primary culture model of differentiated murine tracheal epithelium. *American Journal of Physiology-Lung Cellular and Molecular Physiology* 279: L766-L78

Davies DE, Wicks J, Powell RM, Puddicombe SM, Holgate ST. 2003. Airway remodeling in asthma: New insights. *Journal of Allergy and Clinical Immunology* 111: 215-25

Gaschler GJ, Skrtic M, Zavitz CCJ, Linclahl M, Onnervik PO, et al. 2009. Bacteria Challenge in Smoke-exposed Mice Exacerbates Inflammation and Skews the Inflammatory Profile. *American Journal of Respiratory and Critical Care Medicine* 179: 666-75

Hendrixson DR, Qiu J, Shewry SC, Fink DL, Petty S, et al. 2003. Human milk lactoferrin is a serine protease that cleaves Haemophilus surface proteins at arginine-rich sites. *Molecular Microbiology* 47: 607-17

Herman P, Friedlander G, Huy PTB, Amiel C. 1992. Ion-transport by primary cultures of mongolian gerbil middle-ear epithelium. *American journal of physiology* 262: F373-F80

Horani A, Nath A, Wasserman MG, Huang T, Brody SL. 2013. Rho-Associated Protein Kinase Inhibition Enhances Airway Epithelial Basal-Cell Proliferation and Lentivirus Transduction. *American Journal of Respiratory Cell and Molecular Biology* 49: 341-47

Juhn SK, Jung MK, Hoffman MD, Drew BR, Preciado DA, et al. 2008. The Role of Inflammatory Mediators in the Pathogenesis of Otitis Media and Sequelae. *Clinical and Experimental Otorhinolaryngology* 1: 117-38

Kapsogeorgou EK, Abu-Helu RF, Moutsopoulos HM, Manoussakis MN. 2005. Salivary gland epithelial cell exosomes - A source of autoantigenic ribonucleoproteins. *Arthritis and Rheumatism* 52: 1517-21

Keller S, Sanderson MP, Stoeck A, Altevogt P. 2006. Exosomes: From biogenesis and secretion to biological function. *Immunology Letters* 107: 102-08

Kerschner JE, Li JZ, Tsushiya K, Khampang P. 2010. Mucin gene expression and mouse middle ear epithelium. *International Journal of Pediatric Otorhinolaryngology* 74: 864-68

Kesimer M, Scull M, Brighton B, DeMaria G, Burns K, et al. 2009. Characterization of exosome-like vesicles released from human tracheobronchial ciliated epithelium: a possible role in innate defense. *Faseb Journal* 23: 1858-68

Kim CH, Kim K, Jik Kim H, Kook Kim J, Lee JG, Yoon JH. 2006. Expression and regulation of PLUNC in human nasal epithelium. *Acta Otolaryngol* 126: 1073-8

Kondo M, Tamaoki J, Takeyama K, Nakata J, Nagai A. 2002. Interleukin-13 induces goblet cell differentiation in primary cell culture from guinea pig tracheal epithelium. *American Journal of Respiratory Cell and Molecular Biology* 27: 536-41

Lim DJ, Chun YM, Lee HY, Moon SK, Chang KH, et al. 2000. Cell biology of tubotympanum in relation to pathogenesis of otitis media - a review. *Vaccine* 19: S17-S25

Lim JH, Jono H, Koga T, Woo CH, Ishinaga H, et al. 2007. Tumor Suppressor CYLD Acts as a Negative Regulator for Non-Typeable Haemophilus influenza-Induced Inflammation in the Middle Ear and Lung of Mice. *Plos One* 2: 10

Liu X, Sheng HB, Ma R, Yang JM, Luo WW, et al. 2016. Notch signaling is active in normal mouse middle ear epithelial cells. *Experimental and Therapeutic Medicine* 11: 1661-67

Loonen LMP, Stolte EH, Jaklofsky MTJ, Meijerink M, Dekker J, et al. 2014. REG3 gamma-deficient mice have altered mucus distribution and increased mucosal inflammatory responses to the microbiota and enteric pathogens in the ileum. *Mucosal Immunology* 7: 939-47

805 Matsui H, Grubb BR, Tarran R, Randell SH, Gatzy JT, et al. 1998. Evidence for periciliary
806 liquid layer depletion, not abnormal ion composition, in the pathogenesis of
807 cystic fibrosis airways disease. *Cell* 95: 1005-15
808 Moon SK, Lee HY, Li JD, Nagura M, Kang SH, et al. 2002. Activation of a Src-dependent
809 Raf-MEK1/2-ERK signaling pathway is required for IL-1 alpha-induced
810 upregulation of beta-defensin 2 in human middle ear epithelial cells. *Biochimica*
811 *Et Biophysica Acta-Molecular Cell Research* 1590: 41-51
812 Moon SK, Lim DJ, Lee HK, Kim HN, Yoon JH. 2000. Mucin gene expression in cultured
813 human middle ear epithelial cells. *Acta Oto-Laryngologica* 120: 933-39
814 Musa M, Wilson K, Sun L, Mulay A, Bingle L, et al. 2012. Differential localisation of
815 BPIFA1 (SPLUNC1) and BPIFB1 (LPLUNC1) in the nasal and oral cavities of mice.
816 *Cell and Tissue Research* 350
817 Nakamura A, Demaria TF, Arya G, Lim DJ, Vanblitterswijk C. 1991. Serial culture and
818 characterization of the chinchilla middle-ear epithelium. *Annals of Otology*
819 *Rhinology and Laryngology* 100: 1024-31
820 Pillai DK, Sankoorikal BJV, Johnson E, Seneviratne AN, Zurko J, et al. 2014. Directional
821 Secretomes Reflect Polarity-Specific Functions in an In Vitro Model of Human
822 Bronchial Epithelium. *American Journal of Respiratory Cell and Molecular Biology*
823 50: 292-300
824 Portier F, Kania R, Planes C, Hsu WC, Couette S, et al. 2005. Enhanced sodium absorption
825 in middle ear epithelial cells cultured at air-liquid interface. *Acta Oto-*
826 *Laryngologica* 125: 16-22
827 Preciado D, Burgett K, Ghimbovschi S, Rose M. 2013. NTHi Induction of Cxcl2 and
828 Middle Ear Mucosal Metaplasia in Mice. *Laryngoscope* 123: E66-E71
829 Preciado D, Goyal S, Rahimi M, Watson AM, Brown KJ, et al. 2010. MUC5B Is the
830 predominant mucin glycoprotein in chronic otitis media fluid. *Pediatr Res* 68:
831 231-6
832 Roy MG, Livraghi-Butrico A, Fletcher AA, McElwee MM, Evans SE, et al. 2014. Muc5b is
833 required for airway defence. *Nature* 505: 412-+
834 Rye MS, Bhutta MF, Cheeseman MT, Burgner D, Blackwell JM, et al. 2011. Unraveling the
835 genetics of otitis media: from mouse to human and back again. *Mamm Genome*
836 22: 66-82
837 Rye MS, Warrington NM, Scaman ESH, Vijayasekaran S, Coates HL, et al. 2012. Genome-
838 Wide Association Study to Identify the Genetic Determinants of Otitis Media
839 Susceptibility in Childhood. *Plos One* 7
840 Schachern PA, Tsuprun V, Cureoglu S, Ferrieri PA, Briles DE, et al. 2010. Effect of
841 Apolactoferrin on Experimental Pneumococcal Otitis Media. *Archives of*
842 *Otolaryngology-Head & Neck Surgery* 136: 1127-31
843 Schousboe LP, Ovesen T, Ottosen PD, Ledet T, Elbrond O. 1995. Culture of rabbit middle-
844 ear epithelial-cells - a method for primary culture and subculture with
845 identification, characterization and growth specification. *Acta Oto-Laryngologica*
846 115: 787-95
847 Straetemans M, van Heerbeek N, Tonnaer E, Ingels KJ, Rijkers GT, Zielhuis GA. 2001. A
848 comprehensive model for the aetiology of otitis media with effusion. *Med*
849 *Hypotheses* 57: 784-91
850 Takeno S. 1990. Tissue culture of middle ear epithelium of the guinea pig--differences of
851 the cellular growth activity in the middle ear cavity using collagen gel culture
852 method. *Nihon Jibiinkoka Gakkai kaiho* 93: 2038-46

Thompson H, Tucker AS. 2013. Dual Origin of the Epithelium of the Mammalian Middle Ear. *Science* 339: 1453-56

Toyama K, Kim Y, Paparella MM, Lin JZ. 2004. Temperature-sensitive SV40-immortalized rat middle ear epithelial cells. *Annals of Otology Rhinology and Laryngology* 113: 967-+

Tsuchiya K, Kim Y, Ondrey FG, Lin JZ. 2005. Characterization of a temperature-sensitive mouse middle ear epithelial cell line. *Acta Oto-Laryngologica* 125: 823-29

Ueyama S, Jin SJ, Rhim JS, Ueyama T, Lim DJ. 2001. Immortalization of rat middle ear epithelial cells by adeno 12-SV40 hybrid virus. *Annals of Otology Rhinology and Laryngology* 110: 132-41

Vaishnava S, Yamamoto M, Severson KM, Ruhn KA, Yu XF, et al. 2011. The Antibacterial Lectin RegIII gamma Promotes the Spatial Segregation of Microbiota and Host in the Intestine. *Science* 334: 255-58

Val S, Poley M, Brown K, Choi R, Jeong S, et al. 2016. Proteomic Characterization of Middle Ear Fluid Confirms Neutrophil Extracellular Traps as a Predominant Innate Immune Response in Chronic Otitis Media. *Plos One* 11

Valadi H, Ekstrom K, Bossios A, Sjostrand M, Lee JJ, Lotvall JO. 2007. Exosome-mediated transfer of mRNAs and microRNAs is a novel mechanism of genetic exchange between cells. *Nature Cell Biology* 9: 654-U72

van Niel G, Raposo G, Candalh C, Boussac M, Hershberg R, et al. 2001. Intestinal epithelial cells secrete exosome-like vesicles. *Gastroenterology* 121: 337-49

van Rozendaal BAWM, van Golde LMG, Haagsman HP. 2001. Localization and functions of SP-A and SP-D at mucosal surfaces. *Pediatric Pathology and Molecular Medicine* 20: 319-39

Vanblitterswijk CA, Ponec M, Vanmuijen GNP, Wijsman MC, Koerten HK, Grote JJ. 1986. CULTURE AND CHARACTERIZATION OF RAT MIDDLE-EAR EPITHELIUM. *Acta Oto-Laryngologica* 101: 453-66

Woo JI, Oh S, Lim D, Moon S. 2012. ERK2-dependent activation of c-Jun is required for nontypeable H. influenzae-induced Cxcl2 up-regulation in the inner ear fibrocytes. *Faseb Journal* 26: 1

Woodfield G, Dugdale A. 2008. Evidence behind the WHO guidelines: Hospital care for children: What is the most effective antibiotic regime for chronic suppurative otitis media in children. *J. Trop. Pediatr.* 54: 151-56

Woodworth BA, Antunes MB, Bhargave G, Palmer JN, Cohen NA. 2007. Murine tracheal and nasal septal epithelium for air-liquid interface cultures: A comparative study. *American Journal of Rhinology* 21: 533-37

Wright JR. 1997. Immunomodulatory functions of surfactant. *Physiological Reviews* 77: 931-62

Yamaya M, Finkbeiner WE, Chun SY, Widdicombe JH. 1992. DIFFERENTIATED STRUCTURE AND FUNCTION OF CULTURES FROM HUMAN TRACHEAL EPITHELIUM. *American Journal of Physiology* 262: L713-L24

You Y, Brody SL. 2013. Culture and differentiation of mouse tracheal epithelial cells. *Methods in molecular biology (Clifton, N.J.)* 945: 123-43

You YJ, Richer EJ, Huang T, Brody SL. 2002. Growth and differentiation of mouse tracheal epithelial cells: selection of a proliferative population. *American Journal of Physiology-Lung Cellular and Molecular Physiology* 283: L1315-L21

Figures

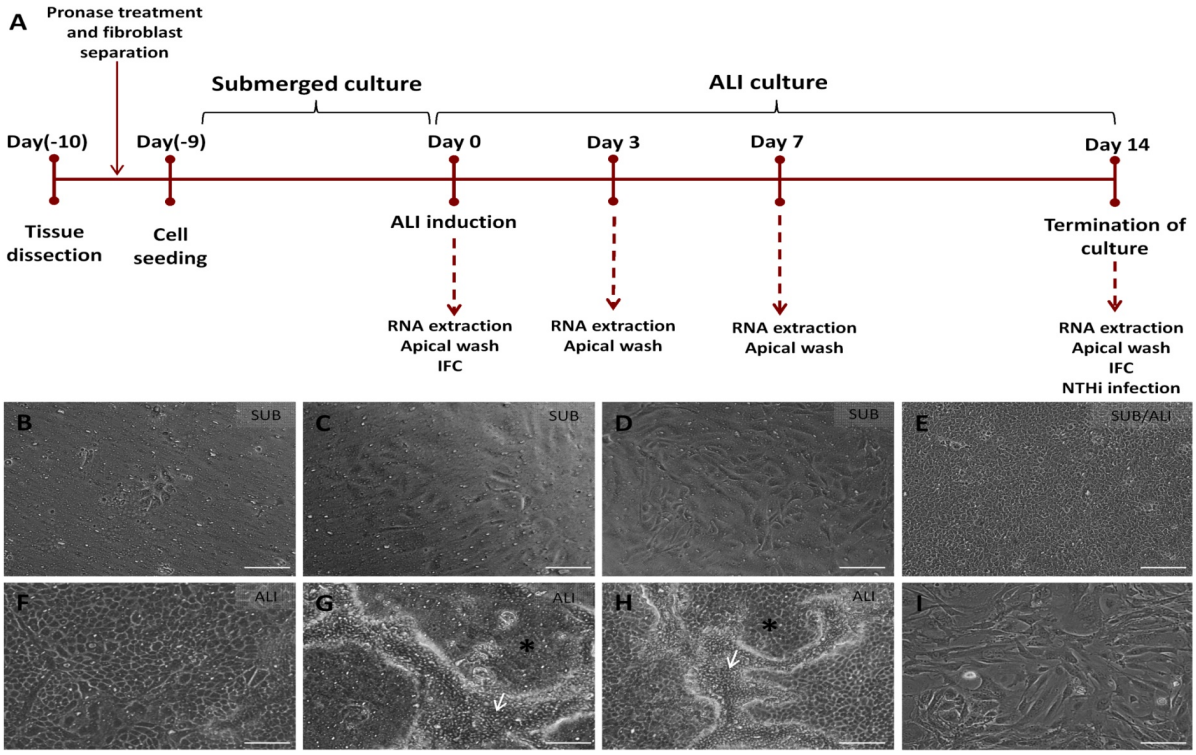

Fig. 1: Primary culture of mouse middle ear epithelial cells. Timeline for culture of mMECs is shown above (A). Bullae were dissected, treated with pronase for dissociation of the middle ear epithelial cells and fibroblasts were excluded from culture by differential adherence to plastic. Epithelial cells were grown in submerged culture till confluence, before ALI was induced. Samples for transcriptional and proteomic analysis were collected at regular time points. Phase contrast images showing cells in culture under 10x magnification (B-I). In the proliferative submerged conditions, a small number of cells attached to form epithelial islands 3 days after seeding (B) The cells proliferated faster from day 5 (C) through day 7 (D) and formed a confluent monolayer at day 9. This was termed as ALI Day 0 (E) Morphology of cells changed from ALI Day 3 (F) and clusters of compactly arranged cells started forming at ALI Day 7 (G). ALI Day 14 cultures were composed of flat polygonal and compactly clustered pseudo stratified cells with active cilia. White arrowheads mark

920 elevated ciliated cells and asterisk mark flatter polygonal cells. (H). Fibroblasts
921 cultured on plastic plates through differential adhesion method (I)
922

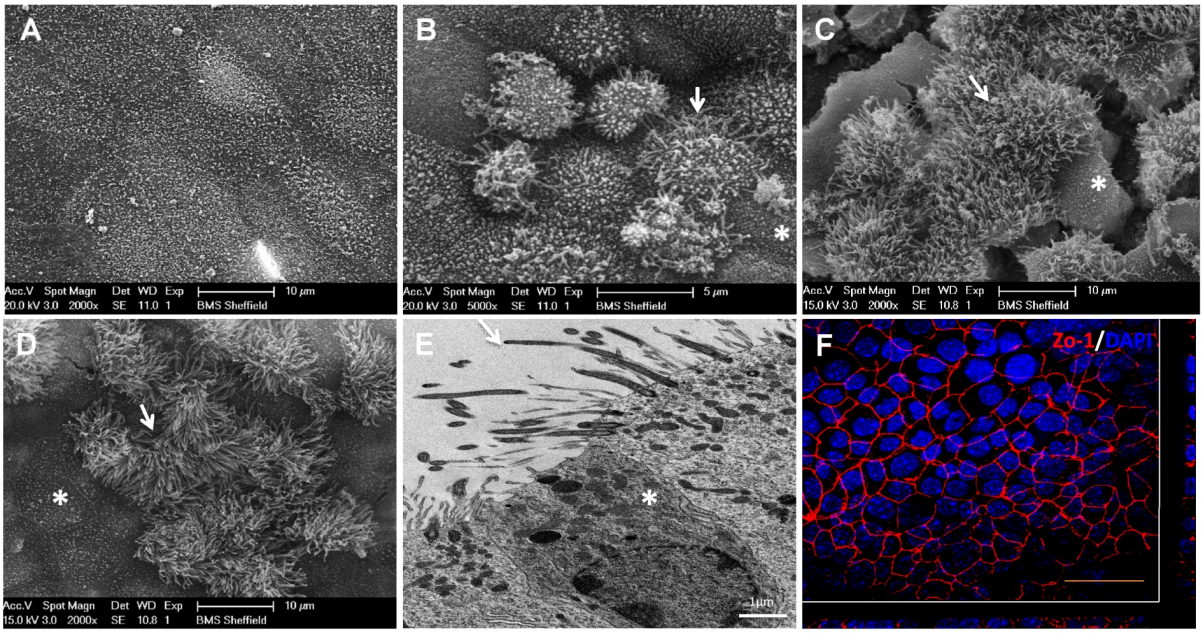

Fig. 2: Electron microscopy of mMEC cultures. Scanning electron microscopy of ALI Day 0 mMEC cultures showing large flat polygonal cells with apical microvilli (A) ALI Day 14 cultures showing dome shaped cells at higher magnification (B) and combination of interspersed flat polygonal and densely ciliated cell populations a lower magnification (C) resembling the morphology of native middle ear epithelium (D). Cracks developed in the membrane are due to processing of samples for SEM. White arrowheads mark elevated ciliated cells and asterix mark flatter polygonal cells. Transmission electron microscopy of ALI Day 14 mMEC cultures showing adjacent ciliated and secretory cells and formation of tight junctions demonstrated by presence of desmosomes (asterisk) (E) Immunoconfocal microscopy image showing formation of tight junctions marked by ZO1 positive staining. (n=3) Scale bar = 50 µm (F).

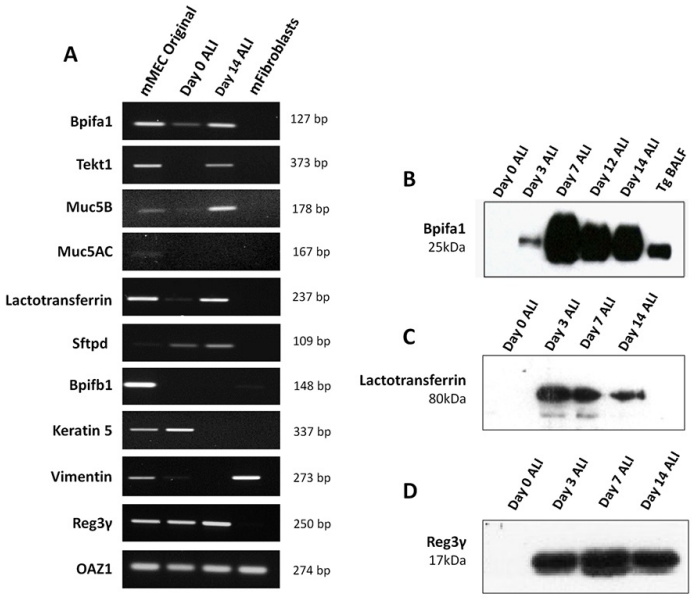

939

940

941 **Fig. 3: Expression of epithelial markers in mMEC cultures.** End-point RT-PCR
942 showing expression of a selected panel of upper airway associated genes in mMEC
943 original cells isolated from the middle ear cavity, ALI D0 cells and ALI D14 cells.
944 Expression profile of ALI Day 14 cells was similar to mMEC original cells isolated
945 from the middle ear for most genes (A). Detection of Bpifa1 (B), Lactotransferrin (C)
946 and Reg3Ɣ (D) in the apical washes from differentiating cells using Western blotting
947 technique. Data is representative of three independent cultures.

948

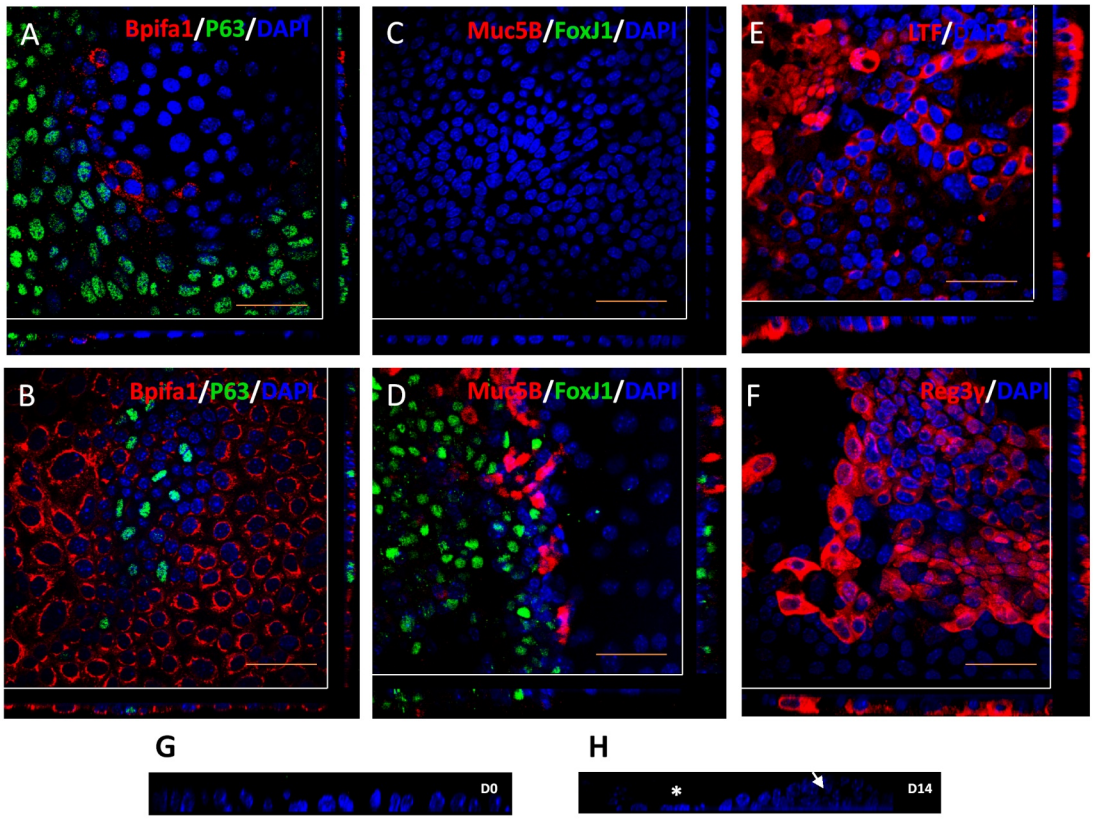

Fig. 4: Localisation of epithelial markers in mMEC cultures. Immunofluorescence confocal images (representative of three independent batches) showing abundant expression of the basal cell marker, P63; limited expression of the secretory protein, Bpifa1 (A), no expression of goblet cell marker, Muc5B and the ciliated marker, FoxJ1 (D) in undifferentiated ALI Day 0 mMEC cultures (A and C). Differentiated mMEC ALI Day 14 (B, D, E, F) cultures showing expression of secretory cells positive for Bpifa1 (B), Lactotransferrin (E), Reg3γ (F), goblet cells positive for Muc5B and ciliated cells positive for FoxJ1 (D.Z-stack images showing a cross sections of nuclei stained with DAPI shows that ALI Day 0 cells form a flat monolayer (G) whereas ALI Day 14 cells are a combination of pseudostratified elevated cells (arrowheads) and flatter cells (asterisk) (H). Scale bar =50µm.

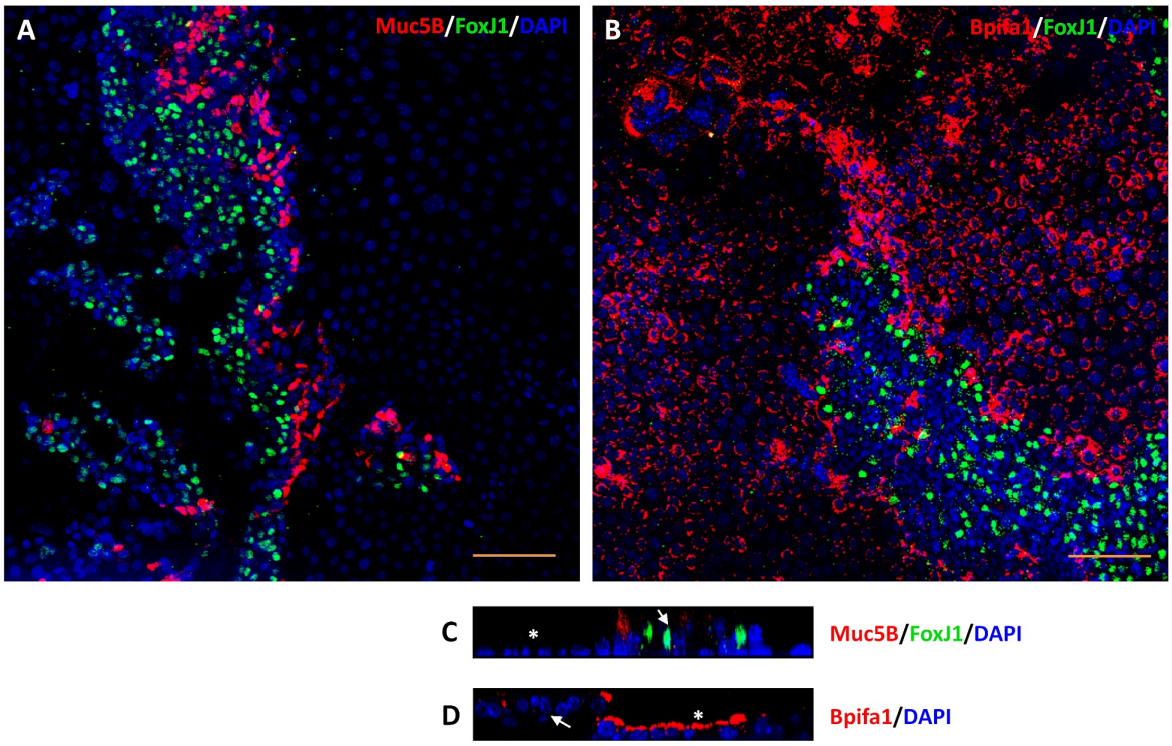

963
964

965 **Fig. 5: Distribution of cell types in mMEC cultures.** Low powered (20x)
966 immunofluorescence confocal images representative of 3 independent batches of
967 ALI Day 14 mMEC cultures showing a combination of flat cells and clusters of
968 elevated cells at slightly different foci. Ciliated cells (FoxJ1) do not co-localise with
969 and goblet cells (Muc5B) (A) and Bpifa1 expressing cells (B) Scale bar =100μm.
970 High magnification (60x) cross section Z-stack confocal images showing that FoxJ1
971 and Muc5B expression is mostly restricted to the elevated cell types (arrowheads)
972 (C) and Bpifa1 is predominantly expressed by flatter cells (asterisk) (D) Scale bar =
973 50μm (C,D).
974

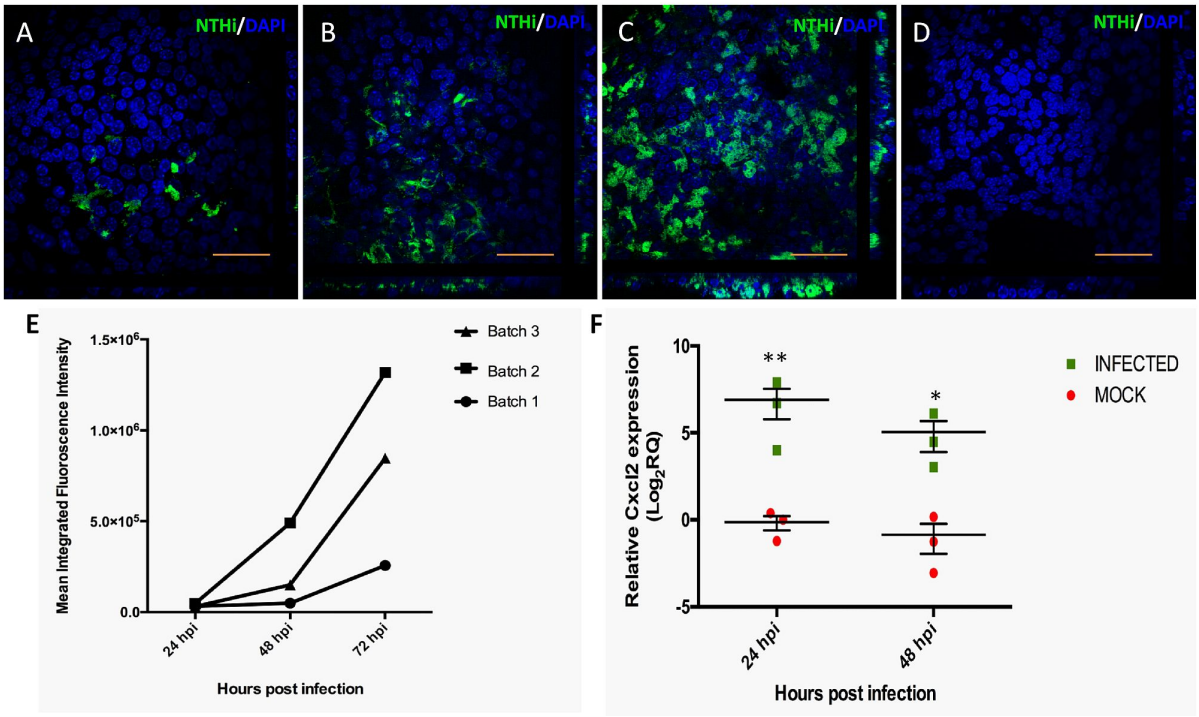

Fig. 6: mMEC cultures serve as an otopathogenic infection model. High magnification (60x) confocal images representative of n=3 independent batches of ALI Day 14 mMECs infected with GFP tagged NTHi-375SR for 24 hours (A), 48 hours (B) and 72 hours (C) showing a time dependent increase in bacterial infection. Control ALI Day 14 mMECs mock infected for 72 hrs (D) Scale bar =50μm. Increase in mean green fluorescence intensity from 24hpi to 72hpi quantified from lower magnification (10x) images from three independent batches, suggesting demonstrating an increase is the amount of bacteria infecting the cultures with time (E). Relative gene expression of Cxcl2 (F) in infected mMEC cultures compared with MOCK infected cultures at 24 and 48 hours post infection. Expression of target gene Cxcl2 was normalized to 3 endogenous controls: ATP5B, CyC1 and Ppia and plotted relative to the 24hpi MOCK sample. Data is analysed using two tailed student's t-test and represented as mean relative quantification (RQ) ± SEM for three independent batches of cultures. *: $p<0.05$ **$p<0.01$ ***$p<0.005$.

992

993 **Table 1: Most abundant secreted proteins identified in apical ALI Day 14**
994 **washes from mMEC cultures**

Accession Number	Protein	Peptide count	emPAI Score	Biological reference
P08071	Lactotransferrin	47	202.53	Anti-microbial iron chelation
Q921I1	Serotransferrin	40	29.58	Iron chelation, cell proliferation
O09049	Regenerating islet-derived protein 3-gamma	8	11.38	Anti-microbial
P11672	Neutrophil gelatinase-associated lipocalin	9	10.45	Iron trafficking, innate immunity
Q61147	Ceruloplasmin	55	10.1	Copper transport, antioxidant defence
P97361	BPI fold-containing family A member 1	9	4.74	Suggested role in innate immunity
P01027	Complement C3	111	4.68	Activates complement system
P06797	Cathepsin L1	12	3.11	Lysosomal protein degradation
Q61805	Lipopolysaccharide-binding protein	19	2.96	Antimicrobial activity through bacterial LPS binding
P10605	Cathepsin B	15	2.47	Intracellular protein degradation and turnover
Q61362	Chitinase-3-like protein 1	22	2.16	Tissue remodelling in response to environmental stress, activation of NfκB signalling pathway
P25785	Metalloproteinase inhibitor 2	14	2.08	Inactivates metalloenzymes
Q9CQV3	Serpin B11	24	1.97	Serine protease inhibitor
P18242	Cathepsin D	20	1.67	Intracellular protein breakdown
O88312	Anterior gradient protein 2 homolog	10	1.53	Regulates giblet cell differentiation and mucous secretion.
P50404	Pulmonary surfactant-associated protein D	23	1.5	Innate immunity response, respiratory gaseous exchange and homeostasis
P10810	Monocyte differentiation antigen CD14	16	1.41	TLR2 mediated innate immune and inflammatory response to bacterial LPS in concert with LBP
Q62426	Cystatin-B	6	1.24	Proteinase inhibitor
Q9ER10	Brain-specific serine protease 4	15	1.11	Protease activity
P08905	Lysozyme	10	1.05	Bacteriolytic activity
Q9DAU7	WAP four-disulfide core domain protein 2	6	0.91	Protease inhibitor
P11214	Tissue-type plasminogen activator	31	0.89	Tissue remodelling, cell migration
Q9WUU7	Cathepsin Z	14	0.89	Peptidase activity
O88593	Peptidoglycan recognition protein 1	10	0.81	Triggers apoptosis of Gram positive bacteria
Q60854	Serpin B6	23	0.81	Regulation of serine proteases
P34884	Macrophage migration inhibitory factor	5	0.61	Pro inflammatory cytokine involved in regulation o macrophage activity
Q9R118	Serine protease HTRA1	21	0.54	Cell proliferation and viral response

P12032	Metalloproteinase inhibitor 1	12	0.49	Cell differentiation and wound healing
P97430	Antileukoproteinase	11	0.49	Anti microbial host defence
P61939	Thyroxine-binding globulin	22	0.4	Thyroid hormone transport
P25085	Interleukin-1 receptor antagonist protein	7	0.35	Inhibits IL-1 activity
P70124	Serpin B5	22	0.35	Morphogenesis of epithelium
Q61703	Inter-alpha-trypsin inhibitor heavy chain H2	48	0.24	Hyaluronan metabolic process
P97290	Plasma protease C1 inhibitor	25	0.12	Blood coagulation, complement activation.

995 NB- Acession numbers and biological functions from the UniProt database

996

Supplementary Data for

An *in vitro* model of murine middle ear epithelium

Apoorva Mulay[a], Khondoker Akram[a], Debbie Williams[b], Hannah Armes[a,c], Catherine Russell[a], Derek Hood[b] Stuart Armstrong[d], James P Stewart[d], Steve DM Brown[b], Lynne Bingle[c], Colin D Bingle [a].

[a]Academic Unit of Respiratory Medicine, Department of Infection, Immunity and Cardiovascular Disease, University of Sheffield, Sheffield, UK.

[b]MRC Mammalian Genetics Unit, Harwell, UK

[c]Oral and Maxillofacial Pathology, Department of Clinical Dentistry, University of Sheffield, Sheffield, UK

[d]Institute of Infection and Global Health, University of Liverpool, Liverpool, UK.

Corresponding author: Colin Bingle PhD, Academic Unit of Respiratory Medicine, Department of Infection, Immunity and Cardiovascular Disease, University of Sheffield, Sheffield, S10 2JF, UK.
Phone: 00 44 (0)114 2712423
Email: c.d.bingle@sheffield.ac.uk

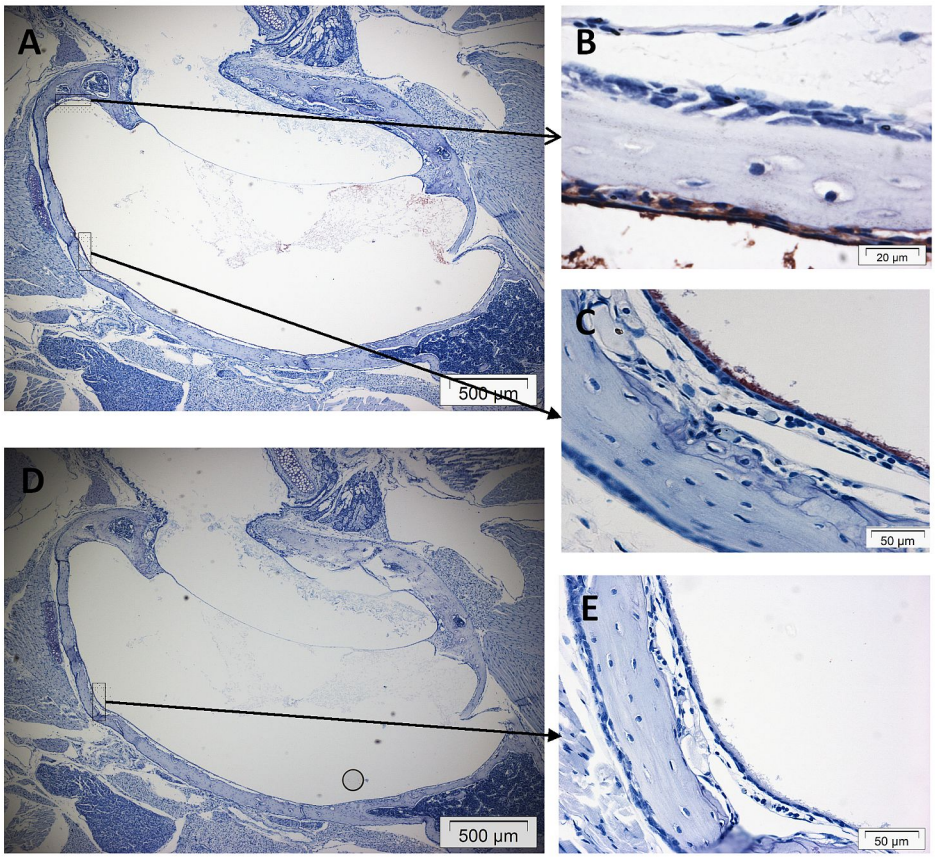

Fig. S1: Expression of Bpifa1 in WT middle ear epithelium

Bpifa1 expression was detected in the Wt mouse middle ear using immunohistochemistry. Low magnification image showing expression of Bpifa1 all along the middle ear epithelium (A). Bpifa1 is secreted by non-ciliated cells of the middle ear epithelium (B), but it coats the surface of the cilia (C). Negative controls showed absence of staining (D, E).

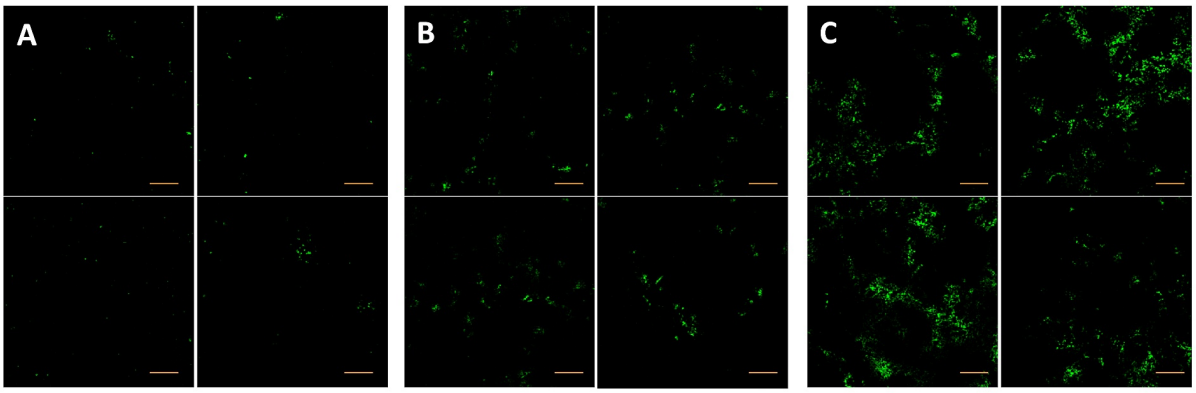

Fig. S2: Progression of NTHi infection in mMEC cultures

Low power confocal images of ALI Day 14 mMEC cells infected with GFP tagged NTHI-375^{SR} at 24 hpi (A), 48hpi (B) and 72 hpi (C). Each panel represents 4 central fields at 10x magnification spanning approximately 50% of the membrane. The amount of infection at each time point was quantified as a measure of the mean integrated intensity for green fluorescence in these panels from 3 independent batches of infections. Scale bar = 200 μm

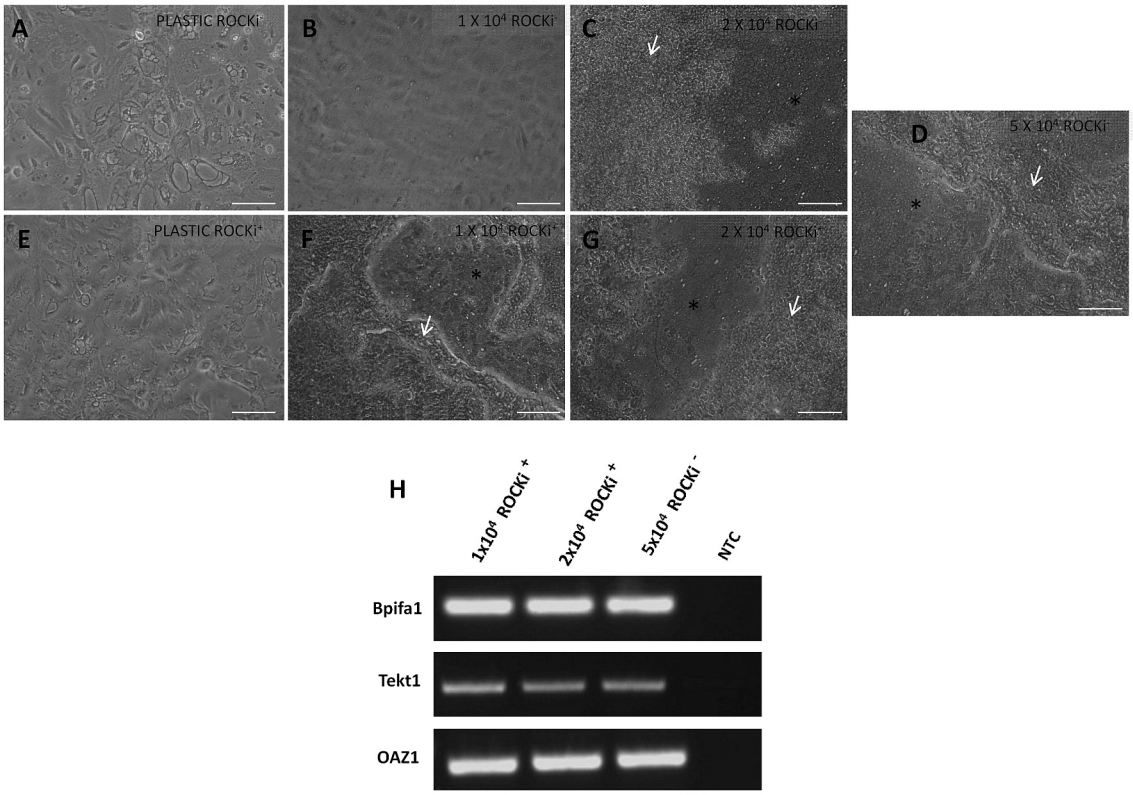

Fig. S3: Optimisation of seeding density for mMEC culture

Phase contrast images of ALI Day 14 mMEC cells in culture seeded at various densities in absence and presence of ROCKi (A- G). When grown on plastic, both in absence (A) and presence (E) of ROCKi, cells did not exhibit the typical epithelial morphology, started forming vacuoles, detached from the surface and did not achieve confluence. In absence of ROCKi, at 1 x10^4 cells/ well (B) cells grew in small epithelial clusters but did not form a confluent monolayer, at 2 x10^4 cells/ well (C) a proportion of wells formed a confluent monolayer at submerged Day 15 and at 5 x10^4 cells (D), cells formed a confluent monolayer around submerged Day 9. The cells differentiated on ALI and demonstrated a typical cobbled stone appearance. In presence of ROCKi, both at 1 x10^4 cells/ well (F) and 2 x10^4 cells/ well (G), the cells formed a confluent monolayer in submerged culture by day 9-10. By ALI Day 14, the cells differentiated into various cell types and exhibited cobbled stone appearance typical of epithelial cells. Scale bar = 200 µm. White arrowheads indicate elevated clusters of cells with actively beating cilia and asterisk denote flatter polygonal cells. RT PCR of ALI Day 14 samples (H) demonstrating that adding ROCKi to the culture medium did not affect differentiation into secretory and ciliated cell types. Seeding

density of 1 x10^4 cells/ well with ROCKi was selected in order to maximize the utility of the isolated cells.

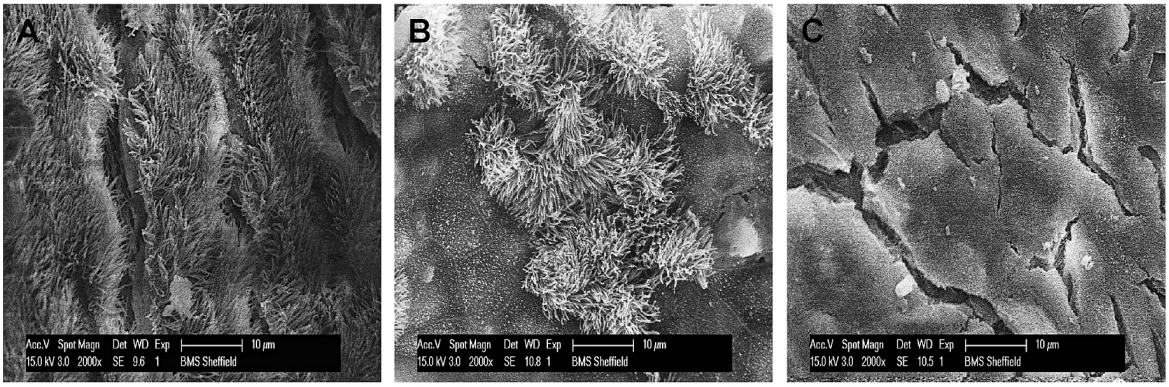

Fig. S4: Distribution of ciliated cells in WT native mouse middle ear cavity

Scanning electron microscopy images showing the distribution of ciliated cells in various parts of the native WT middle ear cavity. Areas near the Eustachian tube were lined with tracts of dense ciliated cells (A). The central part of the middle consists of flat polygonal cells interspersed with clusters of short and long ciliated cells (B), similar to what is seen in our mMEC cultures. Areas towards the tympanic membrane exhibit patches similar to central part of the middle ear as well as larger patches of flat polygonal cells with apical microvilli (C).

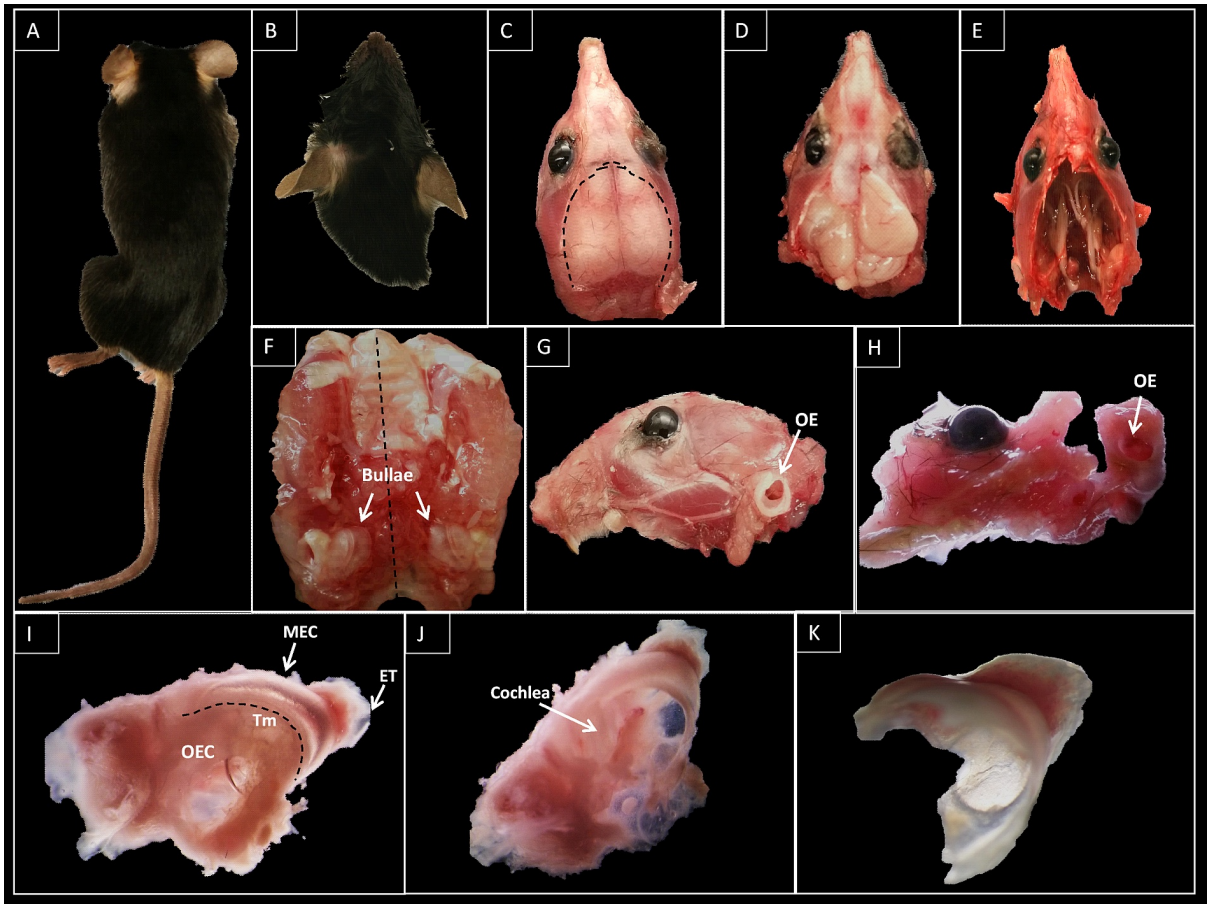

Fig. S5: Dissection and isolation of the mouse middle ear cavity

Wild type C57Bl/6J or C3HeH mice (A) were decapitated (B). The head was skinned (C) and skull cap removed (D). Dorsal (E) and ventral (F) view of the head after removing the brain, showing the bullae or middle ear cavities, MECs. Bisected head showing the outer ear, OE (G). Under dissecting microscope the bullae were separated from surrounding tissue (H). The MEC is attached to the outer ear cavity (OEC) at the tympanic membrane (Tm) and tapers towards the opening of the Eustachian tube (ET) near its posterior end (I). Removal of the OEC and the Tm reveals the cochlea of the inner ear on the ventral side of the MEC (J) The cup shaped MEC was detached from the inner ear (K) Tissue was dissected along the dotted lines.

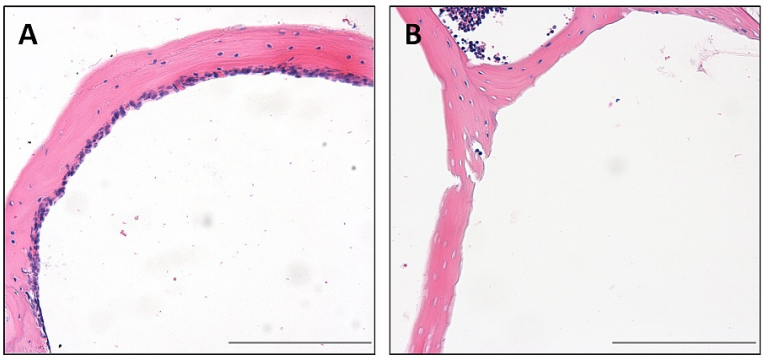

Fig. S6: Effect of Pronase treatment on the middle ear epithelial cells

Haematoxylin and eosin staining of dissected middle ear cavities showing intact middle ear epithelium before proteolytic treatment with pronase (A) and loss of the epithelial lining after treatment with pronase and mechanical agitation (B) during the cell isolation process suggesting that our isolation protocol successfully dissociates middle ear epithelial cells for culture. Scale bar = 200µm

Table S1: Proteins identified by MS analysis of ALI Day 14 mMEC apical washes

Accession Number	Protein Name	Gene name	Peptide count	emPAI
P08071	Lactotransferrin	TRFL_MOUSE	47	202.53
Q921I1	Serotransferrin	TRFE_MOUSE	40	29.58
O09131	Glutathione S-transferase omega-1	GSTO1_MOUSE	17	28.64
P60710	Actin, cytoplasmic 1	ACTB_MOUSE	23	24.63
P50446	Keratin, type II cytoskeletal 6A	K2C6A_MOUSE	35	19.14
P08074	Carbonyl reductase [NADPH] 2	CBR2_MOUSE	16	19.04
Q9Z331	Keratin, type II cytoskeletal 6B	K2C6B_MOUSE	36	18.18
P62806	Histone H4	H4_MOUSE	6	17.1
P10107	Annexin A1	ANXA1_MOUSE	24	14.87
P11679	Keratin, type II cytoskeletal 8	K2C8_MOUSE	33	14.67
P19001	Keratin, type I cytoskeletal 19	K1C19_MOUSE	35	14.07
Q61781	Keratin, type I cytoskeletal 14	K1C14_MOUSE	35	13
O09049	Regenerating islet-derived protein 3-gamma	REG3G_MOUSE	8	11.38
P35700	Peroxiredoxin-1	PRDX1_MOUSE	14	11.13
Q06890	Clusterin	CLUS_MOUSE	22	10.47
P11672	Neutrophil gelatinase-associated lipocalin	NGAL_MOUSE	9	10.45
Q61147	Ceruloplasmin	CERU_MOUSE	55	10.1
Q61414	Keratin, type I cytoskeletal 15	K1C15_MOUSE	32	9.92
P17742	Peptidyl-prolyl cis-trans isomerase A	PPIA_MOUSE	14	9.81
Q922U2	Keratin, type II cytoskeletal 5	K2C5_MOUSE	34	8.7
Q9QWL7	Keratin, type I cytoskeletal 17	K1C17_MOUSE	33	7.76
O08709	Peroxiredoxin-6	PRDX6_MOUSE	15	7.38
P10649	Glutathione S-transferase Mu 1	GSTM1_MOUSE	18	6.68
P07356	Annexin A2	ANXA2_MOUSE	23	6.63
P52480	Pyruvate kinase PKM	KPYM_MOUSE	36	6.57
P68372	Tubulin beta-4B chain	TBB4B_MOUSE	21	6.13
Q6ZWY9	Histone H2B type 1-C/E/G	H2B1C_MOUSE	11	6.12
Q8BND5	Sulfhydryl oxidase 1	QSOX1_MOUSE	43	6.1
Q9DCV7	Keratin, type II cytoskeletal 7	K2C7_MOUSE	35	6.01
P16858	Glyceraldehyde-3-phosphate dehydrogenase	G3P_MOUSE	21	5.87
Q61398	Procollagen C-	PCOC1_MOUSE	23	5.56

	endopeptidase enhancer 1			
P07744	Keratin, type II cytoskeletal 4	K2C4_MOUSE	31	5.43
O35639	Annexin A3	ANXA3_MOUSE	24	5.16
P68033	Actin, alpha cardiac muscle 1	ACTC_MOUSE	23	5.06
P26040	Ezrin	EZRI_MOUSE	39	5.04
P99024	Tubulin beta-5 chain	TBB5_MOUSE	21	4.94
Q05816	Fatty acid-binding protein, epidermal	FABP5_MOUSE	9	4.92
P08249	Malate dehydrogenase, mitochondrial	MDHM_MOUSE	24	4.77
P97361	BPI fold-containing family A member 1	BPIA1_MOUSE	9	4.74
P01027	Complement C3	CO3_MOUSE	111	4.68
Q8BGZ7	Keratin, type II cytoskeletal 75	K2C75_MOUSE	36	4.22
P56480	ATP synthase subunit beta, mitochondrial	ATPB_MOUSE	30	4.18
P62830	60S ribosomal protein L23	RL23_MOUSE	10	4.08
P05784	Keratin, type I cytoskeletal 18	K1C18_MOUSE	32	3.99
P50543	Protein S100-A11	S10AB_MOUSE	5	3.92
P28654	Decorin	PGS2_MOUSE	23	3.86
P40142	Transketolase	TKT_MOUSE	34	3.7
Q9QUI0	Transforming protein RhoA	RHOA_MOUSE	13	3.7
Q8VCT4	Carboxylesterase 1D	CES1D_MOUSE	27	3.69
Q9Z2K1	Keratin, type I cytoskeletal 16	K1C16_MOUSE	35	3.64
P57780	Alpha-actinin-4	ACTN4_MOUSE	61	3.61
P17563	Selenium-binding protein 1	SBP1_MOUSE	31	3.49
P17182	Alpha-enolase	ENOA_MOUSE	28	3.36
P11499	Heat shock protein HSP 90-beta	HS90B_MOUSE	40	3.31
P08730	Keratin, type I cytoskeletal 13	K1C13_MOUSE	31	3.29
P14211	Calreticulin	CALR_MOUSE	27	3.28
Q9D379	Epoxide hydrolase 1	HYEP_MOUSE	29	3.27
P63017	Heat shock cognate 71 kDa protein	HSP7C_MOUSE	37	3.24
Q00493	Carboxypeptidase E	CBPE_MOUSE	28	3.17
P06797	Cathepsin L1	CATL1_MOUSE	12	3.11
P62962	Profilin-1	PROF1_MOUSE	9	3.1
P27773	Protein disulfide-isomerase A3	PDIA3_MOUSE	35	3.05
P62908	40S ribosomal protein S3	RS3_MOUSE	19	3.05
Q7TMM9	Tubulin beta-2A chain	TBB2A_MOUSE	21	3.03
Q8VDD5	Myosin-9	MYH9_MOUSE	127	3.03
P09103	Protein disulfide-isomerase	PDIA1_MOUSE	39	3.02
P68368	Tubulin alpha-4A chain	TBA4A_MOUSE	22	2.99
P68373	Tubulin alpha-1C chain	TBA1C_MOUSE	22	2.99

Q8VED5	Keratin, type II cytoskeletal 79	K2C79_MOUSE	32	2.98
Q61805	Lipopolysaccharide-binding protein	LBP_MOUSE	19	2.96
Q9Z1Q5	Chloride intracellular channel protein 1	CLIC1_MOUSE	17	2.96
Q07797	Galectin-3-binding protein	LG3BP_MOUSE	26	2.94
Q61646	Haptoglobin	HPT_MOUSE	20	2.94
Q7TPR4	Alpha-actinin-1	ACTN1_MOUSE	60	2.92
P62821	Ras-related protein Rab-1A	RAB1A_MOUSE	18	2.9
O88844	Isocitrate dehydrogenase [NADP] cytoplasmic	IDHC_MOUSE	30	2.87
P08228	Superoxide dismutase [Cu-Zn]	SODC_MOUSE	11	2.78
P18760	Cofilin-1	COF1_MOUSE	12	2.72
P19157	Glutathione S-transferase P 1	GSTP1_MOUSE	10	2.71
Q9R0P5	Destrin	DEST_MOUSE	13	2.7
P06151	L-lactate dehydrogenase A chain	LDHA_MOUSE	23	2.62
P20029	78 kDa glucose-regulated protein	GRP78_MOUSE	39	2.61
P10126	Elongation factor 1-alpha 1	EF1A1_MOUSE	23	2.54
Q60605	Myosin light polypeptide 6	MYL6_MOUSE	11	2.51
Q62159	Rho-related GTP-binding protein RhoC	RHOC_MOUSE	11	2.5
Q9D1G1	Ras-related protein Rab-1B	RAB1B_MOUSE	17	2.5
P07901	Heat shock protein HSP 90-alpha	HS90A_MOUSE	39	2.47
P10605	Cathepsin B	CATB_MOUSE	15	2.47
P68040	Guanine nucleotide-binding protein subunit beta-2-like 1	GBLP_MOUSE	22	2.47
P97429	Annexin A4	ANXA4_MOUSE	22	2.4
Q64669	NAD(P)H dehydrogenase [quinone] 1	NQO1_MOUSE	15	2.38
O54974	Galectin-7	LEG7_MOUSE	10	2.33
P33267	Cytochrome P450 2F2	CP2F2_MOUSE	29	2.3
P47739	Aldehyde dehydrogenase, dimeric NADP-preferring	AL3A1_MOUSE	25	2.29
Q61508	Extracellular matrix protein 1	ECM1_MOUSE	37	2.29
Q9R0P3	S-formylglutathione hydrolase	ESTD_MOUSE	16	2.28
P47738	Aldehyde dehydrogenase, mitochondrial	ALDH2_MOUSE	26	2.24
P17751	Triosephosphate isomerase	TPIS_MOUSE	18	2.19
P63038	60 kDa heat shock protein, mitochondrial	CH60_MOUSE	36	2.16
Q61362	Chitinase-3-like protein 1	CH3L1_MOUSE	22	2.16
P25785	Metalloproteinase inhibitor 2	TIMP2_MOUSE	14	2.08
Q8BFZ3	Beta-actin-like protein 2	ACTBL_MOUSE	24	2.08

Q9DCW4	Electron transfer flavoprotein subunit beta	ETFB_MOUSE	14	2.08
P63101	14-3-3 protein zeta/delta	1433Z_MOUSE	19	2.07
Q03265	ATP synthase subunit alpha, mitochondrial	ATPA_MOUSE	36	2.07
Q62266	Cornifin-A	SPR1A_MOUSE	13	2.01
P21956	Lactadherin	MFGM_MOUSE	23	1.99
P15626	Glutathione S-transferase Mu 2	GSTM2_MOUSE	18	1.97
Q9CQV3	Serpin B11	SPB11_MOUSE	24	1.97
P63242	Eukaryotic translation initiation factor 5A-1	IF5A1_MOUSE	8	1.93
P11276	Fibronectin	FINC_MOUSE	108	1.84
P51881	ADP/ATP translocase 2	ADT2_MOUSE	21	1.84
P05064	Fructose-bisphosphate aldolase A	ALDOA_MOUSE	23	1.82
Q01853	Transitional endoplasmic reticulum ATPase	TERA_MOUSE	45	1.82
P70296	Phosphatidylethanolamine-binding protein 1	PEBP1_MOUSE	9	1.81
P21981	Protein-glutamine gamma-glutamyltransferase 2	TGM2_MOUSE	36	1.79
P26043	Radixin	RADI_MOUSE	39	1.79
P62245	40S ribosomal protein S15a	RS15A_MOUSE	11	1.76
Q6IFX2	Keratin, type I cytoskeletal 42	K1C42_MOUSE	33	1.75
Q9DCD0	6-phosphogluconate dehydrogenase, decarboxylating	6PGD_MOUSE	29	1.74
P54116	Erythrocyte band 7 integral membrane protein	STOM_MOUSE	17	1.71
P26041	Moesin	MOES_MOUSE	40	1.7
P18242	Cathepsin D	CATD_MOUSE	20	1.67
Q923D2	Flavin reductase (NADPH)	BLVRB_MOUSE	13	1.65
Q9R0Q7	Prostaglandin E synthase 3	TEBP_MOUSE	9	1.65
P23492	Purine nucleoside phosphorylase	PNPH_MOUSE	19	1.64
Q60932	Voltage-dependent anion-selective channel protein 1	VDAC1_MOUSE	18	1.64
Q9D051	Pyruvate dehydrogenase E1 component subunit beta, mitochondrial	ODPB_MOUSE	18	1.63
Q9WVA4	Transgelin-2	TAGL2_MOUSE	14	1.63
P37040	NADPH--cytochrome P450 reductase	NCPR_MOUSE	35	1.6
P61027	Ras-related protein Rab-10	RAB10_MOUSE	17	1.6
P67778	Prohibitin	PHB_MOUSE	18	1.58
P56382	ATP synthase subunit epsilon, mitochondrial	ATP5E_MOUSE	4	1.56
O88312	Anterior gradient protein 2 homolog	AGR2_MOUSE	10	1.53
P24369	Peptidyl-prolyl cis-trans isomerase B	PPIB_MOUSE	15	1.51

P50404	Pulmonary surfactant-associated protein D	SFTPD_MOUSE	23	1.5
P48678	Prelamin-A/C	LMNA_MOUSE	46	1.47
P61750	ADP-ribosylation factor 4	ARF4_MOUSE	12	1.47
Q61176	Arginase-1	ARGI1_MOUSE	18	1.47
Q8BSL7	ADP-ribosylation factor 2	ARF2_MOUSE	12	1.45
P62827	GTP-binding nuclear protein Ran	RAN_MOUSE	11	1.44
P10810	Monocyte differentiation antigen CD14	CD14_MOUSE	16	1.41
Q9CRB3	5-hydroxyisourate hydrolase	HIUH_MOUSE	7	1.41
Q61598	Rab GDP dissociation inhibitor beta	GDIB_MOUSE	28	1.4
P24549	Retinal dehydrogenase 1	AL1A1_MOUSE	23	1.39
P38647	Stress-70 protein, mitochondrial	GRP75_MOUSE	43	1.39
Q61468	Mesothelin	MSLN_MOUSE	29	1.38
Q9QYB1	Chloride intracellular channel protein 4	CLIC4_MOUSE	17	1.38
P24472	Glutathione S-transferase A4	GSTA4_MOUSE	12	1.36
Q8BFU2	Histone H2A type 3	H2A3_MOUSE	7	1.36
O35129	Prohibitin-2	PHB2_MOUSE	26	1.35
O88569	Heterogeneous nuclear ribonucleoproteins A2/B1	ROA2_MOUSE	19	1.33
P47911	60S ribosomal protein L6	RL6_MOUSE	19	1.33
Q9CPV4	Glyoxalase domain-containing protein 4	GLOD4_MOUSE	22	1.33
Q9WV54	Acid ceramidase	ASAH1_MOUSE	21	1.33
Q8BPB5	EGF-containing fibulin-like extracellular matrix protein 1	FBLN3_MOUSE	27	1.31
Q8VDN2	Sodium/potassium-transporting ATPase subunit alpha-1	AT1A1_MOUSE	53	1.27
P97461	40S ribosomal protein S5	RS5_MOUSE	10	1.25
Q60931	Voltage-dependent anion-selective channel protein 3	VDAC3_MOUSE	17	1.25
Q64433	10 kDa heat shock protein, mitochondrial	CH10_MOUSE	10	1.25
Q62426	Cystatin-B	CYTB_MOUSE	6	1.24
Q99LC5	Electron transfer flavoprotein subunit alpha, mitochondrial	ETFA_MOUSE	23	1.24
P47757	F-actin-capping protein subunit beta	CAPZB_MOUSE	20	1.22
P51174	Long-chain specific acyl-CoA dehydrogenase, mitochondrial	ACADL_MOUSE	24	1.21
P08207	Protein S100-A10	S10AA_MOUSE	5	1.2
P84228	Histone H3.2	H32_MOUSE	6	1.2
Q9CR57	60S ribosomal protein L14	RL14_MOUSE	12	1.2
P09411	Phosphoglycerate kinase 1	PGK1_MOUSE	29	1.18

Q6IFZ6	Keratin, type II cytoskeletal 1b	K2C1B_MOUSE	39	1.18
P62267	40S ribosomal protein S23	RS23_MOUSE	8	1.15
Q91VR2	ATP synthase subunit gamma, mitochondrial	ATPG_MOUSE	17	1.15
Q9CQI6	Coactosin-like protein	COTL1_MOUSE	10	1.14
Q9D8N0	Elongation factor 1-gamma	EF1G_MOUSE	27	1.14
P10639	Thioredoxin	THIO_MOUSE	7	1.12
P84084	ADP-ribosylation factor 5	ARF5_MOUSE	13	1.12
P62264	40S ribosomal protein S14	RS14_MOUSE	6	1.11
Q9ER10	Brain-specific serine protease 4	BSSP4_MOUSE	15	1.11
Q91VI7	Ribonuclease inhibitor	RINI_MOUSE	27	1.1
P62702	40S ribosomal protein S4, X isoform	RS4X_MOUSE	20	1.09
P62717	60S ribosomal protein L18a	RL18A_MOUSE	14	1.09
P97351	40S ribosomal protein S3a	RS3A_MOUSE	19	1.08
Q99JY9	Actin-related protein 3	ARP3_MOUSE	21	1.08
P17879	Heat shock 70 kDa protein 1B	HS71B_MOUSE	37	1.07
P60766	Cell division control protein 42 homolog	CDC42_MOUSE	9	1.06
O88342	WD repeat-containing protein 1	WDR1_MOUSE	37	1.05
P08905	Lysozyme C-2	LYZ2_MOUSE	10	1.05
P29758	Ornithine aminotransferase, mitochondrial	OAT_MOUSE	23	1.05
P15532	Nucleoside diphosphate kinase A	NDKA_MOUSE	12	1.03
P48036	Annexin A5	ANXA5_MOUSE	25	1.03
P51410	60S ribosomal protein L9	RL9_MOUSE	11	1.03
Q61171	Peroxiredoxin-2	PRDX2_MOUSE	10	1.03
Q01768	Nucleoside diphosphate kinase B	NDKB_MOUSE	12	1.02
Q8K354	Carbonyl reductase [NADPH] 3	CBR3_MOUSE	20	1.02
Q91XV3	Brain acid soluble protein 1	BASP1_MOUSE	10	1.02
P62889	60S ribosomal protein L30	RL30_MOUSE	8	1.01
P99029	Peroxiredoxin-5, mitochondrial	PRDX5_MOUSE	15	1.01
Q00612	Glucose-6-phosphate 1-dehydrogenase X	G6PD1_MOUSE	35	1.01
P14152	Malate dehydrogenase, cytoplasmic	MDHC_MOUSE	21	1
Q68FD5	Clathrin heavy chain 1	CLH1_MOUSE	95	0.99
Q6ZWN5	40S ribosomal protein S9	RS9_MOUSE	14	0.99
P60843	Eukaryotic initiation factor 4A-I	IF4A1_MOUSE	23	0.98
Q60930	Voltage-dependent anion-selective channel protein 2	VDAC2_MOUSE	16	0.98
Q9WV32	Actin-related protein 2/3 complex subunit 1B	ARC1B_MOUSE	19	0.98

P16110	Galectin-3	LEG3_MOUSE	10	0.97
P35441	Thrombospondin-1	TSP1_MOUSE	70	0.97
P05202	Aspartate aminotransferase, mitochondrial	AATM_MOUSE	29	0.95
P48962	ADP/ATP translocase 1	ADT1_MOUSE	22	0.95
P58252	Elongation factor 2	EF2_MOUSE	52	0.95
P62281	40S ribosomal protein S11	RS11_MOUSE	10	0.94
P62874	Guanine nucleotide-binding protein G(I)/G(S)/G(T) subunit beta-1	GBB1_MOUSE	13	0.94
Q9WTY4	Aquaporin-5	AQP5_MOUSE	8	0.94
Q9Z0K8	Pantetheinase	VNN1_MOUSE	23	0.94
O70435	Proteasome subunit alpha type-3	PSA3_MOUSE	14	0.93
P53994	Ras-related protein Rab-2A	RAB2A_MOUSE	15	0.93
Q3UV17	Keratin, type II cytoskeletal 2 oral	K22O_MOUSE	39	0.93
P35486	Pyruvate dehydrogenase E1 component subunit alpha, somatic form, mitochondrial	ODPA_MOUSE	25	0.92
P47791	Glutathione reductase, mitochondrial	GSHR_MOUSE	25	0.91
Q9DAU7	WAP four-disulfide core domain protein 2	WFDC2_MOUSE	6	0.91
P24452	Macrophage-capping protein	CAPG_MOUSE	14	0.9
P62259	14-3-3 protein epsilon	1433E_MOUSE	18	0.9
Q9CZM2	60S ribosomal protein L15	RL15_MOUSE	14	0.9
P11214	Tissue-type plasminogen activator	TPA_MOUSE	31	0.89
P62242	40S ribosomal protein S8	RS8_MOUSE	10	0.89
Q8BG05	Heterogeneous nuclear ribonucleoprotein A3	ROA3_MOUSE	20	0.89
Q9WUU7	Cathepsin Z	CATZ_MOUSE	14	0.89
P04104	Keratin, type II cytoskeletal 1	K2C1_MOUSE	35	0.88
Q61581	Insulin-like growth factor-binding protein 7	IBP7_MOUSE	18	0.88
P08113	Endoplasmin	ENPL_MOUSE	47	0.87
Q3THE2	Myosin regulatory light chain 12B	ML12B_MOUSE	11	0.86
Q6ZWV3	60S ribosomal protein L10	RL10_MOUSE	13	0.86
P27659	60S ribosomal protein L3	RL3_MOUSE	22	0.85
P62331	ADP-ribosylation factor 6	ARF6_MOUSE	9	0.85
P63323	40S ribosomal protein S12	RS12_MOUSE	7	0.85
P67984	60S ribosomal protein L22	RL22_MOUSE	6	0.85
Q80X90	Filamin-B	FLNB_MOUSE	146	0.85
Q99LX0	Protein DJ-1	PARK7_MOUSE	13	0.85
P06745	Glucose-6-phosphate isomerase	G6PI_MOUSE	32	0.84

P16460	Argininosuccinate synthase	ASSY_MOUSE	25	0.84
P48758	Carbonyl reductase [NADPH] 1	CBR1_MOUSE	19	0.84
Q6ZWU9	40S ribosomal protein S27	RS27_MOUSE	5	0.83
Q91YQ5	Dolichyl-diphosphooligosaccharide--protein glycosyltransferase subunit 1	RPN1_MOUSE	40	0.83
Q9CXW4	60S ribosomal protein L11	RL11_MOUSE	9	0.83
O35640	Annexin A8	ANXA8_MOUSE	23	0.82
P56395	Cytochrome b5	CYB5_MOUSE	8	0.82
Q9CZ13	Cytochrome b-c1 complex subunit 1, mitochondrial	QCR1_MOUSE	22	0.82
O88593	Peptidoglycan recognition protein 1	PGRP1_MOUSE	10	0.81
Q60854	Serpin B6	SPB6_MOUSE	23	0.81
P14069	Protein S100-A6	S10A6_MOUSE	5	0.79
P61358	60S ribosomal protein L27	RL27_MOUSE	6	0.79
P62835	Ras-related protein Rap-1A	RAP1A_MOUSE	10	0.79
P62880	Guanine nucleotide-binding protein G(I)/G(S)/G(T) subunit beta-2	GBB2_MOUSE	13	0.79
Q9QXC1	Fetuin-B	FETUB_MOUSE	17	0.79
P11983	T-complex protein 1 subunit alpha	TCPA_MOUSE	35	0.78
P14206	40S ribosomal protein SA	RSSA_MOUSE	15	0.78
P62137	Serine/threonine-protein phosphatase PP1-alpha catalytic subunit	PP1A_MOUSE	19	0.78
P62911	60S ribosomal protein L32	RL32_MOUSE	8	0.77
P70441	Na(+)/H(+) exchange regulatory cofactor NHE-RF1	NHRF1_MOUSE	27	0.77
P61514	60S ribosomal protein L37a	RL37A_MOUSE	6	0.75
P61979	Heterogeneous nuclear ribonucleoprotein K	HNRPK_MOUSE	27	0.75
P63168	Dynein light chain 1, cytoplasmic	DYL1_MOUSE	5	0.75
P68254	14-3-3 protein theta	1433T_MOUSE	18	0.75
P0CG49	Polyubiquitin-B	UBB_MOUSE	28	0.74
P40124	Adenylyl cyclase-associated protein 1	CAP1_MOUSE	30	0.74
P62196	26S protease regulatory subunit 8	PRS8_MOUSE	28	0.74
Q9CQV8	14-3-3 protein beta/alpha	1433B_MOUSE	17	0.74
Q9Z2X1	Heterogeneous nuclear ribonucleoprotein F	HNRPF_MOUSE	22	0.74
O55234	Proteasome subunit beta type-5	PSB5_MOUSE	16	0.73
P10630	Eukaryotic initiation factor 4A-II	IF4A2_MOUSE	23	0.73
P47962	60S ribosomal protein L5	RL5_MOUSE	17	0.73
P08752	Guanine nucleotide-binding protein G(i) subunit alpha-2	GNAI2_MOUSE	20	0.72

Q9CQQ7	ATP synthase F(0) complex subunit B1, mitochondrial	AT5F1_MOUSE	18	0.72
Q9DBH5	Vesicular integral-membrane protein VIP36	LMAN2_MOUSE	21	0.72
P14602	Heat shock protein beta-1	HSPB1_MOUSE	12	0.71
P99026	Proteasome subunit beta type-4	PSB4_MOUSE	11	0.71
P80316	T-complex protein 1 subunit epsilon	TCPE_MOUSE	36	0.7
P12970	60S ribosomal protein L7a	RL7A_MOUSE	16	0.69
P51150	Ras-related protein Rab-7a	RAB7A_MOUSE	17	0.69
P63330	Serine/threonine-protein phosphatase 2A catalytic subunit alpha isoform	PP2AA_MOUSE	18	0.69
P97494	Glutamate--cysteine ligase catalytic subunit	GSH1_MOUSE	34	0.69
Q8BTM8	Filamin-A	FLNA_MOUSE	143	0.69
Q99KI0	Aconitate hydratase, mitochondrial	ACON_MOUSE	41	0.69
O54734	Dolichyl-diphosphooligosaccharide--protein glycosyltransferase 48 kDa subunit	OST48_MOUSE	22	0.68
O70570	Polymeric immunoglobulin receptor	PIGR_MOUSE	38	0.68
P47955	60S acidic ribosomal protein P1	RLA1_MOUSE	4	0.68
Q8BP67	60S ribosomal protein L24	RL24_MOUSE	10	0.68
Q91V41	Ras-related protein Rab-14	RAB14_MOUSE	15	0.68
Q9D154	Leukocyte elastase inhibitor A	ILEUA_MOUSE	23	0.68
Q9JII6	Alcohol dehydrogenase [NADP(+)]	AK1A1_MOUSE	23	0.68
P60122	RuvB-like 1	RUVB1_MOUSE	22	0.66
Q93092	Transaldolase	TALDO_MOUSE	23	0.66
Q99020	Heterogeneous nuclear ribonucleoprotein A/B	ROAA_MOUSE	14	0.66
Q9D2Q8	Protein S100-A14	S10AE_MOUSE	8	0.66
P09405	Nucleolin	NUCL_MOUSE	48	0.65
P25444	40S ribosomal protein S2	RS2_MOUSE	22	0.65
Q61503	5~-nucleotidase	5NTD_MOUSE	32	0.65
Q6IME9	Keratin, type II cytoskeletal 72	K2C72_MOUSE	34	0.65
Q9D1D4	Transmembrane emp24 domain-containing protein 10	TMEDA_MOUSE	10	0.65
P30115	Glutathione S-transferase A3	GSTA3_MOUSE	14	0.64
P54071	Isocitrate dehydrogenase [NADP], mitochondrial	IDHP_MOUSE	31	0.64
P80317	T-complex protein 1 subunit zeta	TCPZ_MOUSE	29	0.64
Q64727	Vinculin	VINC_MOUSE	84	0.64
Q9WTM5	RuvB-like 2	RUVB2_MOUSE	28	0.64

Q9CZU6	Citrate synthase, mitochondrial	CISY_MOUSE	21	0.63
P00405	Cytochrome c oxidase subunit 2	COX2_MOUSE	6	0.62
Q61937	Nucleophosmin	NPM_MOUSE	16	0.62
Q62186	Translocon-associated protein subunit delta	SSRD_MOUSE	8	0.62
Q69ZN7	Myoferlin	MYOF_MOUSE	131	0.62
O55142	60S ribosomal protein L35a	RL35A_MOUSE	9	0.61
P21107	Tropomyosin alpha-3 chain	TPM3_MOUSE	24	0.61
P34884	Macrophage migration inhibitory factor	MIF_MOUSE	5	0.61
Q8VEM8	Phosphate carrier protein, mitochondrial	MPCP_MOUSE	21	0.61
Q9Z2U1	Proteasome subunit alpha type-5	PSA5_MOUSE	11	0.6
Q8BMS1	Trifunctional enzyme subunit alpha, mitochondrial	ECHA_MOUSE	40	0.59
O08756	3-hydroxyacyl-CoA dehydrogenase type-2	HCD2_MOUSE	16	0.58
P35550	rRNA 2~-O-methyltransferase fibrillarin	FBRL_MOUSE	24	0.58
P49312	Heterogeneous nuclear ribonucleoprotein A1	ROA1_MOUSE	19	0.58
O35737	Heterogeneous nuclear ribonucleoprotein H	HNRH1_MOUSE	25	0.57
O70456	14-3-3 protein sigma	1433S_MOUSE	19	0.57
P60867	40S ribosomal protein S20	RS20_MOUSE	6	0.57
P62315	Small nuclear ribonucleoprotein Sm D1	SMD1_MOUSE	5	0.57
P62855	40S ribosomal protein S26	RS26_MOUSE	6	0.57
Q9QUM9	Proteasome subunit alpha type-6	PSA6_MOUSE	13	0.57
P08003	Protein disulfide-isomerase A4	PDIA4_MOUSE	43	0.56
P0C0S6	Histone H2A.Z	H2AZ_MOUSE	6	0.56
P61982	14-3-3 protein gamma	1433G_MOUSE	18	0.56
P68510	14-3-3 protein eta	1433F_MOUSE	18	0.56
Q8BP47	Asparagine--tRNA ligase, cytoplasmic	SYNC_MOUSE	30	0.56
Q9JM76	Actin-related protein 2/3 complex subunit 3	ARPC3_MOUSE	12	0.56
P45376	Aldose reductase	ALDR_MOUSE	20	0.55
P50396	Rab GDP dissociation inhibitor alpha	GDIA_MOUSE	26	0.55
P62754	40S ribosomal protein S6	RS6_MOUSE	13	0.55
P62852	40S ribosomal protein S25	RS25_MOUSE	6	0.55
Q78IK2	Up-regulated during skeletal muscle growth protein 5	USMG5_MOUSE	3	0.55
P12265	Beta-glucuronidase	BGLR_MOUSE	33	0.54
P35980	60S ribosomal protein L18	RL18_MOUSE	9	0.54
P50580	Proliferation-associated	PA2G4_MOUSE	24	0.54

	protein 2G4			
Q9R118	Serine protease HTRA1	HTRA1_MOUSE	21	0.54
O54990	Prominin-1	PROM1_MOUSE	41	0.53
P09803	Cadherin-1	CADH1_MOUSE	33	0.53
P63001	Ras-related C3 botulinum toxin substrate 1	RAC1_MOUSE	9	0.53
Q921F2	TAR DNA-binding protein 43	TADBP_MOUSE	17	0.53
P14685	26S proteasome non-ATPase regulatory subunit 3	PSMD3_MOUSE	39	0.52
P62082	40S ribosomal protein S7	RS7_MOUSE	11	0.52
Q8BFZ9	Erlin-2	ERLN2_MOUSE	24	0.52
Q8BHN3	Neutral alpha-glucosidase AB	GANAB_MOUSE	51	0.52
Q9D8W5	26S proteasome non-ATPase regulatory subunit 12	PSD12_MOUSE	34	0.52
O55143	Sarcoplasmic/endoplasmic reticulum calcium ATPase 2	AT2A2_MOUSE	54	0.51
Q60668	Heterogeneous nuclear ribonucleoprotein D0	HNRPD_MOUSE	15	0.51
Q9R0Q3	Transmembrane emp24 domain-containing protein 2	TMED2_MOUSE	11	0.51
O08807	Peroxiredoxin-4	PRDX4_MOUSE	16	0.5
P29341	Polyadenylate-binding protein 1	PABP1_MOUSE	38	0.5
P30412	Peptidyl-prolyl cis-trans isomerase C	PPIC_MOUSE	11	0.5
Q99K51	Plastin-3	PLST_MOUSE	40	0.5
Q9CYN9	Renin receptor	RENR_MOUSE	17	0.5
P12032	Metalloproteinase inhibitor 1	TIMP1_MOUSE	12	0.49
P14148	60S ribosomal protein L7	RL7_MOUSE	18	0.49
P57776	Elongation factor 1-delta	EF1D_MOUSE	20	0.49
P97430	Antileukoproteinase	SLPI_MOUSE	11	0.49
Q99PT1	Rho GDP-dissociation inhibitor 1	GDIR1_MOUSE	14	0.49
Q9DB20	ATP synthase subunit O, mitochondrial	ATPO_MOUSE	14	0.49
Q9WU78	Programmed cell death 6-interacting protein	PDC6I_MOUSE	52	0.49
P10493	Nidogen-1	NID1_MOUSE	46	0.48
P17225	Polypyrimidine tract-binding protein 1	PTBP1_MOUSE	22	0.48
P28474	Alcohol dehydrogenase class-3	ADHX_MOUSE	20	0.48
P62814	V-type proton ATPase subunit B, brain isoform	VATB2_MOUSE	29	0.48
P62849	40S ribosomal protein S24	RS24_MOUSE	7	0.48
P14733	Lamin-B1	LMNB1_MOUSE	39	0.47
P41105	60S ribosomal protein L28	RL28_MOUSE	11	0.47

P47963	60S ribosomal protein L13	RL13_MOUSE	14	0.47
P80315	T-complex protein 1 subunit delta	TCPD_MOUSE	37	0.47
Q8BFR5	Elongation factor Tu, mitochondrial	EFTU_MOUSE	31	0.47
Q9DC16	Endoplasmic reticulum-Golgi intermediate compartment protein 1	ERGI1_MOUSE	13	0.47
O70251	Elongation factor 1-beta	EF1B_MOUSE	14	0.46
P14824	Annexin A6	ANXA6_MOUSE	49	0.46
P14131	40S ribosomal protein S16	RS16_MOUSE	12	0.45
P24270	Catalase	CATA_MOUSE	35	0.45
P24527	Leukotriene A-4 hydrolase	LKHA4_MOUSE	39	0.45
P42932	T-complex protein 1 subunit theta	TCPQ_MOUSE	39	0.45
P53026	60S ribosomal protein L10a	RL10A_MOUSE	15	0.45
Q791V5	Mitochondrial carrier homolog 2	MTCH2_MOUSE	14	0.45
Q9CQX2	Cytochrome b5 type B	CYB5B_MOUSE	8	0.45
Q9DBG6	Dolichyl-diphosphooligosaccharide--protein glycosyltransferase subunit 2	RPN2_MOUSE	26	0.45
Q9WTP7	GTP:AMP phosphotransferase AK3, mitochondrial	KAD3_MOUSE	19	0.45
P13745	Glutathione S-transferase A1	GSTA1_MOUSE	14	0.44
P14869	60S acidic ribosomal protein P0	RLA0_MOUSE	18	0.44
P49722	Proteasome subunit alpha type-2	PSA2_MOUSE	13	0.44
P61079	Ubiquitin-conjugating enzyme E2 D3	UB2D3_MOUSE	5	0.44
Q61206	Platelet-activating factor acetylhydrolase IB subunit beta	PA1B2_MOUSE	10	0.44
Q9CVB6	Actin-related protein 2/3 complex subunit 2	ARPC2_MOUSE	22	0.44
P14094	Sodium/potassium-transporting ATPase subunit beta-1	AT1B1_MOUSE	16	0.43
P61089	Ubiquitin-conjugating enzyme E2 N	UBE2N_MOUSE	11	0.43
P61255	60S ribosomal protein L26	RL26_MOUSE	9	0.43
P62334	26S protease regulatory subunit 10B	PRS10_MOUSE	27	0.43
Q8K183	Pyridoxal kinase	PDXK_MOUSE	16	0.43
Q921H8	3-ketoacyl-CoA thiolase A, peroxisomal	THIKA_MOUSE	22	0.43
Q9D0S9	Histidine triad nucleotide-binding protein 2, mitochondrial	HINT2_MOUSE	11	0.43
P06801	NADP-dependent malic enzyme	MAOX_MOUSE	32	0.42
P16675	Lysosomal protective	PPGB_MOUSE	22	0.42

	protein			
Q62267	Cornifin-B	SPR1B_MOUSE	15	0.42
Q8K2B3	Succinate dehydrogenase [ubiquinone] flavoprotein subunit, mitochondrial	SDHA_MOUSE	36	0.42
Q9JJI8	60S ribosomal protein L38	RL38_MOUSE	3	0.42
P35979	60S ribosomal protein L12	RL12_MOUSE	11	0.41
P62270	40S ribosomal protein S18	RS18_MOUSE	12	0.41
Q8R081	Heterogeneous nuclear ribonucleoprotein L	HNRPL_MOUSE	24	0.41
Q9JJ00	Phospholipid scramblase 1	PLS1_MOUSE	13	0.41
P45952	Medium-chain specific acyl-CoA dehydrogenase, mitochondrial	ACADM_MOUSE	22	0.4
P60335	Poly(rC)-binding protein 1	PCBP1_MOUSE	20	0.4
P61939	Thyroxine-binding globulin	THBG_MOUSE	22	0.4
Q08761	Vitamin K-dependent protein S	PROS_MOUSE	37	0.4
Q61753	D-3-phosphoglycerate dehydrogenase	SERA_MOUSE	22	0.4
Q9D8E6	60S ribosomal protein L4	RL4_MOUSE	27	0.4
Q9WV55	Vesicle-associated membrane protein-associated protein A	VAPA_MOUSE	15	0.4
Q9Z2U0	Proteasome subunit alpha type-7	PSA7_MOUSE	16	0.4
O09167	60S ribosomal protein L21	RL21_MOUSE	9	0.39
P63325	40S ribosomal protein S10	RS10_MOUSE	13	0.39
Q8VEK3	Heterogeneous nuclear ribonucleoprotein U	HNRPU_MOUSE	43	0.39
Q922R8	Protein disulfide-isomerase A6	PDIA6_MOUSE	25	0.39
Q9DB77	Cytochrome b-c1 complex subunit 2, mitochondrial	QCR2_MOUSE	22	0.39
P13597	Intercellular adhesion molecule 1	ICAM1_MOUSE	26	0.38
P17710	Hexokinase-1	HXK1_MOUSE	57	0.38
P70333	Heterogeneous nuclear ribonucleoprotein H2	HNRH2_MOUSE	25	0.38
Q02053	Ubiquitin-like modifier-activating enzyme 1	UBA1_MOUSE	55	0.38
Q6URW6	Myosin-14	MYH14_MOUSE	126	0.38
Q9DBJ1	Phosphoglycerate mutase 1	PGAM1_MOUSE	15	0.38
P26443	Glutamate dehydrogenase 1, mitochondrial	DHE3_MOUSE	35	0.37
P48771	Cytochrome c oxidase subunit 7A2, mitochondrial	CX7A2_MOUSE	5	0.37
P59999	Actin-related protein 2/3 complex subunit 4	ARPC4_MOUSE	13	0.37
P70195	Proteasome subunit beta type-7	PSB7_MOUSE	12	0.37
Q62425	Cytochrome c oxidase subunit NDUFA4	NDUA4_MOUSE	6	0.37
Q9D6R2	Isocitrate dehydrogenase	IDH3A_MOUSE	21	0.37

	[NAD] subunit alpha, mitochondrial			
Q9R1P0	Proteasome subunit alpha type-4	PSA4_MOUSE	14	0.37
O55023	Inositol monophosphatase 1	IMPA1_MOUSE	17	0.36
P42208	Septin-2	SEPT2_MOUSE	21	0.36
Q8CAQ8	MICOS complex subunit Mic60	MIC60_MOUSE	55	0.36
Q99JY0	Trifunctional enzyme subunit beta, mitochondrial	ECHB_MOUSE	28	0.36
P04186	Complement factor B	CFAB_MOUSE	42	0.35
P13020	Gelsolin	GELS_MOUSE	34	0.35
P25085	Interleukin-1 receptor antagonist protein	IL1RA_MOUSE	7	0.35
P61211	ADP-ribosylation factor-like protein 1	ARL1_MOUSE	10	0.35
P70124	Serpin B5	SPB5_MOUSE	22	0.35
Q9QZ88	Vacuolar protein sorting-associated protein 29	VPS29_MOUSE	11	0.35
O08749	Dihydrolipoyl dehydrogenase, mitochondrial	DLDH_MOUSE	26	0.34
P47740	Fatty aldehyde dehydrogenase	AL3A2_MOUSE	21	0.34
P97384	Annexin A11	ANX11_MOUSE	22	0.34
P97449	Aminopeptidase N	AMPN_MOUSE	51	0.34
P97807	Fumarate hydratase, mitochondrial	FUMH_MOUSE	32	0.34
Q62465	Synaptic vesicle membrane protein VAT-1 homolog	VAT1_MOUSE	18	0.34
Q99K48	Non-POU domain-containing octamer-binding protein	NONO_MOUSE	23	0.34
Q9CQS8	Protein transport protein Sec61 subunit beta	SC61B_MOUSE	6	0.34
Q9DC53	Copine-8	CPNE8_MOUSE	33	0.34
Q9JKR6	Hypoxia up-regulated protein 1	HYOU1_MOUSE	58	0.34
O55022	Membrane-associated progesterone receptor component 1	PGRC1_MOUSE	10	0.33
Q07813	Apoptosis regulator BAX	BAX_MOUSE	10	0.33
Q9CQW2	ADP-ribosylation factor-like protein 8B	ARL8B_MOUSE	12	0.33
Q9DBS1	Transmembrane protein 43	TMM43_MOUSE	21	0.33
P36536	GTP-binding protein SAR1a	SAR1A_MOUSE	11	0.32
P46978	Dolichyl-diphosphooligosaccharide--protein glycosyltransferase subunit STT3A	STT3A_MOUSE	36	0.32
P80314	T-complex protein 1 subunit beta	TCPB_MOUSE	36	0.32
Q7TMK9	Heterogeneous nuclear ribonucleoprotein Q	HNRPQ_MOUSE	39	0.32

Q8BMF4	Dihydrolipoyllysine-residue acetyltransferase component of pyruvate dehydrogenase complex, mitochondrial	ODP2_MOUSE	33	0.32
Q8JZU2	Tricarboxylate transport protein, mitochondrial	TXTP_MOUSE	17	0.32
Q922B2	Aspartate--tRNA ligase, cytoplasmic	SYDC_MOUSE	38	0.32
Q9CQN1	Heat shock protein 75 kDa, mitochondrial	TRAP1_MOUSE	50	0.32
Q9DCN2	NADH-cytochrome b5 reductase 3	NB5R3_MOUSE	17	0.32
O70503	Estradiol 17-beta-dehydrogenase 12	DHB12_MOUSE	18	0.31
O88310	Intelectin-1a	ITL1A_MOUSE	17	0.31
P05201	Aspartate aminotransferase, cytoplasmic	AATC_MOUSE	27	0.31
P42669	Transcriptional activator protein Pur-alpha	PURA_MOUSE	15	0.31
P62305	Small nuclear ribonucleoprotein E	RUXE_MOUSE	4	0.31
Q02257	Junction plakoglobin	PLAK_MOUSE	44	0.31
Q9D1Q6	Endoplasmic reticulum resident protein 44	ERP44_MOUSE	24	0.31
Q9JKF1	Ras GTPase-activating-like protein IQGAP1	IQGA1_MOUSE	93	0.31
Q9QWR8	Alpha-N-acetylgalactosaminidase	NAGAB_MOUSE	27	0.31
Q9R1P1	Proteasome subunit beta type-3	PSB3_MOUSE	9	0.31
P19253	60S ribosomal protein L13a	RL13A_MOUSE	17	0.3
P27048	Small nuclear ribonucleoprotein-associated protein B	RSMB_MOUSE	14	0.3
P35279	Ras-related protein Rab-6A	RAB6A_MOUSE	17	0.3
P80313	T-complex protein 1 subunit eta	TCPH_MOUSE	33	0.3
P80318	T-complex protein 1 subunit gamma	TCPG_MOUSE	38	0.3
P97467	Peptidyl-glycine alpha-amidating monooxygenase	AMD_MOUSE	51	0.3
Q62167	ATP-dependent RNA helicase DDX3X	DDX3X_MOUSE	40	0.3
Q8K3J9	G-protein coupled receptor family C group 5 member C	GPC5C_MOUSE	11	0.3
Q9CQD1	Ras-related protein Rab-5A	RAB5A_MOUSE	14	0.3
Q9ESW8	Pyroglutamyl-peptidase 1	PGPI_MOUSE	10	0.3
Q9JIW9	Ras-related protein Ral-B	RALB_MOUSE	10	0.3
Q9WUM5	Succinyl-CoA ligase [ADP/GDP-forming] subunit alpha, mitochondrial	SUCA_MOUSE	15	0.3
Q9Z0L8	Gamma-glutamyl hydrolase	GGH_MOUSE	17	0.3
O08547	Vesicle-trafficking protein SEC22b	SC22B_MOUSE	13	0.29

O70554	Small proline-rich protein 2B	SPR2B_MOUSE	5	0.29
P00493	Hypoxanthine-guanine phosphoribosyltransferase	HPRT_MOUSE	13	0.29
P46638	Ras-related protein Rab-11B	RB11B_MOUSE	16	0.29
Q07076	Annexin A7	ANXA7_MOUSE	23	0.29
Q61879	Myosin-10	MYH10_MOUSE	125	0.29
Q8K353	Cysteine-rich and transmembrane domain-containing protein 1	CYTM1_MOUSE	2	0.29
Q8VDW0	ATP-dependent RNA helicase DDX39A	DX39A_MOUSE	26	0.29
Q9CYH2	Redox-regulatory protein FAM213A	F213A_MOUSE	14	0.29
Q9D103	Interferon-induced transmembrane protein 1	IFM1_MOUSE	2	0.29
Q9R112	Sulfide:quinone oxidoreductase, mitochondrial	SQRD_MOUSE	32	0.29
O54782	Epididymis-specific alpha-mannosidase	MA2B2_MOUSE	44	0.28
P30416	Peptidyl-prolyl cis-trans isomerase FKBP4	FKBP4_MOUSE	30	0.28
P47964	60S ribosomal protein L36	RL36_MOUSE	7	0.28
P63158	High mobility group protein B1	HMGB1_MOUSE	11	0.28
Q3UQ28	Peroxidasin homolog	PXDN_MOUSE	86	0.28
Q60692	Proteasome subunit beta type-6	PSB6_MOUSE	11	0.28
Q62093	Serine/arginine-rich splicing factor 2	SRSF2_MOUSE	11	0.28
Q6IRU5	Clathrin light chain B	CLCB_MOUSE	10	0.28
Q78IS1	Transmembrane emp24 domain-containing protein 3	TMED3_MOUSE	13	0.28
Q91WS0	CDGSH iron-sulfur domain-containing protein 1	CISD1_MOUSE	6	0.28
Q9CWJ9	Bifunctional purine biosynthesis protein PURH	PUR9_MOUSE	35	0.28
Q9ERI2	Ras-related protein Rab-27A	RB27A_MOUSE	13	0.28
Q9WVJ9	EGF-containing fibulin-like extracellular matrix protein 2	FBLN4_MOUSE	23	0.28
O09061	Proteasome subunit beta type-1	PSB1_MOUSE	14	0.27
P51807	Dynein light chain Tctex-type 1	DYLT1_MOUSE	7	0.27
P61804	Dolichyl-diphosphooligosaccharide--protein glycosyltransferase subunit DAD1	DAD1_MOUSE	5	0.27
P83882	60S ribosomal protein L36a	RL36A_MOUSE	6	0.27
Q8R3G9	Tetraspanin-8	TSN8_MOUSE	8	0.27
Q91X52	L-xylulose reductase	DCXR_MOUSE	15	0.27

Q9WUA2	Phenylalanine--tRNA ligase beta subunit	SYFB_MOUSE	41	0.27
Q9Z2W0	Aspartyl aminopeptidase	DNPEP_MOUSE	24	0.27
O35215	D-dopachrome decarboxylase	DOPD_MOUSE	9	0.26
P62869	Transcription elongation factor B polypeptide 2	ELOB_MOUSE	9	0.26
Q61656	Probable ATP-dependent RNA helicase DDX5	DDX5_MOUSE	35	0.26
Q64437	Alcohol dehydrogenase class 4 mu/sigma chain	ADH7_MOUSE	23	0.26
Q6PCW6	Cornifelin	CNFN_MOUSE	2	0.26
Q8CG76	Aflatoxin B1 aldehyde reductase member 2	ARK72_MOUSE	17	0.26
Q8CI94	Glycogen phosphorylase, brain form	PYGB_MOUSE	53	0.26
Q91VR5	ATP-dependent RNA helicase DDX1	DDX1_MOUSE	46	0.26
Q91YD6	Villin-like protein	VILL_MOUSE	51	0.26
Q9D8Y0	EF-hand domain-containing protein D2	EFHD2_MOUSE	16	0.26
P12023	Amyloid beta A4 protein	A4_MOUSE	39	0.25
P20108	Thioredoxin-dependent peroxide reductase, mitochondrial	PRDX3_MOUSE	15	0.25
P46735	Unconventional myosin-Ib	MYO1B_MOUSE	70	0.25
Q02248	Catenin beta-1	CTNB1_MOUSE	42	0.25
Q571E4	N-acetylgalactosamine-6-sulfatase	GALNS_MOUSE	25	0.25
Q8BK67	Protein RCC2	RCC2_MOUSE	32	0.25
Q8K2I4	Beta-mannosidase	MANBA_MOUSE	49	0.25
Q8VDM4	26S proteasome non-ATPase regulatory subunit 2	PSMD2_MOUSE	56	0.25
Q91V12	Cytosolic acyl coenzyme A thioester hydrolase	BACH_MOUSE	20	0.25
Q9D0F3	Protein ERGIC-53	LMAN1_MOUSE	25	0.25
Q9D1R9	60S ribosomal protein L34	RL34_MOUSE	6	0.25
Q9JIF0	Protein arginine N-methyltransferase 1	ANM1_MOUSE	20	0.25
P10852	4F2 cell-surface antigen heavy chain	4F2_MOUSE	30	0.24
P62320	Small nuclear ribonucleoprotein Sm D3	SMD3_MOUSE	9	0.24
P70349	Histidine triad nucleotide-binding protein 1	HINT1_MOUSE	8	0.24
Q07417	Short-chain specific acyl-CoA dehydrogenase, mitochondrial	ACADS_MOUSE	21	0.24
Q61703	Inter-alpha-trypsin inhibitor heavy chain H2	ITIH2_MOUSE	48	0.24
Q8BKX1	Brain-specific angiogenesis inhibitor 1-associated protein 2	BAIP2_MOUSE	42	0.24
Q8BT60	Copine-3	CPNE3_MOUSE	26	0.24

Q9CQM5	Thioredoxin domain-containing protein 17	TXD17_MOUSE	8	0.24
Q9DCV5	Transmembrane protein 254	TM254_MOUSE	4	0.24
O09172	Glutamate--cysteine ligase regulatory subunit	GSH0_MOUSE	12	0.23
P23953	Carboxylesterase 1C	EST1C_MOUSE	25	0.23
P28656	Nucleosome assembly protein 1-like 1	NP1L1_MOUSE	13	0.23
P62900	60S ribosomal protein L31	RL31_MOUSE	7	0.23
Q61316	Heat shock 70 kDa protein 4	HSP74_MOUSE	57	0.23
Q64310	Surfeit locus protein 4	SURF4_MOUSE	9	0.23
Q64435	UDP-glucuronosyltransferase 1-6	UD16_MOUSE	25	0.23
Q9CX86	Heterogeneous nuclear ribonucleoprotein A0	ROA0_MOUSE	15	0.23
Q9D0T1	NHP2-like protein 1	NH2L1_MOUSE	9	0.23
Q9QYJ0	DnaJ homolog subfamily A member 2	DNJA2_MOUSE	23	0.23
P16045	Galectin-1	LEG1_MOUSE	9	0.22
P24668	Cation-dependent mannose-6-phosphate receptor	MPRD_MOUSE	18	0.22
P50247	Adenosylhomocysteinase	SAHH_MOUSE	27	0.22
P63276	40S ribosomal protein S17	RS17_MOUSE	6	0.22
Q02496	Mucin-1	MUC1_MOUSE	11	0.22
Q7TQI3	Ubiquitin thioesterase OTUB1	OTUB1_MOUSE	15	0.22
Q8BH95	Enoyl-CoA hydratase, mitochondrial	ECHM_MOUSE	18	0.22
Q8VC85	U6 snRNA-associated Sm-like protein LSm1	LSM1_MOUSE	11	0.22
Q99JZ0	Syntenin-2	SDCB2_MOUSE	16	0.22
Q9CQR4	Acyl-coenzyme A thioesterase 13	ACO13_MOUSE	10	0.22
Q9CQW9	Interferon-induced transmembrane protein 3	IFM3_MOUSE	4	0.22
Q9DCL9	Multifunctional protein ADE2	PUR6_MOUSE	27	0.22
Q9EQK5	Major vault protein	MVP_MOUSE	51	0.22
Q9EST5	Acidic leucine-rich nuclear phosphoprotein 32 family member B	AN32B_MOUSE	12	0.22
Q9QZD8	Mitochondrial dicarboxylate carrier	DIC_MOUSE	17	0.22
Q9WUZ9	Ectonucleoside triphosphate diphosphohydrolase 5	ENTP5_MOUSE	24	0.22
O08992	Syntenin-1	SDCB1_MOUSE	15	0.21
O55131	Septin-7	SEPT7_MOUSE	26	0.21
O88685	26S protease regulatory subunit 6A	PRS6A_MOUSE	26	0.21
P10923	Osteopontin	OSTP_MOUSE	12	0.21

P12787	Cytochrome c oxidase subunit 5A, mitochondrial	COX5A_MOUSE	10	0.21
P16546	Spectrin alpha chain, non-erythrocytic 1	SPTN1_MOUSE	189	0.21
P20352	Tissue factor	TF_MOUSE	17	0.21
P21460	Cystatin-C	CYTC_MOUSE	10	0.21
P35564	Calnexin	CALX_MOUSE	27	0.21
P42125	Enoyl-CoA delta isomerase 1, mitochondrial	ECI1_MOUSE	18	0.21
P47753	F-actin-capping protein subunit alpha-1	CAZA1_MOUSE	17	0.21
P47754	F-actin-capping protein subunit alpha-2	CAZA2_MOUSE	15	0.21
P50516	V-type proton ATPase catalytic subunit A	VATA_MOUSE	37	0.21
P52196	Thiosulfate sulfurtransferase	THTR_MOUSE	18	0.21
P63082	V-type proton ATPase 16 kDa proteolipid subunit	VATL_MOUSE	3	0.21
Q00915	Retinol-binding protein 1	RET1_MOUSE	12	0.21
Q60597	2-oxoglutarate dehydrogenase, mitochondrial	ODO1_MOUSE	52	0.21
Q6ZQI3	Malectin	MLEC_MOUSE	18	0.21
Q8C1B7	Septin-11	SEP11_MOUSE	25	0.21
Q8R164	Valacyclovir hydrolase	BPHL_MOUSE	23	0.21
Q99K30	Epidermal growth factor receptor kinase substrate 8-like protein 2	ES8L2_MOUSE	40	0.21
Q9D2G2	Dihydrolipoyllysine-residue succinyltransferase component of 2-oxoglutarate dehydrogenase complex, mitochondrial	ODO2_MOUSE	23	0.21
Q9EQU5	Protein SET	SET_MOUSE	12	0.21
Q9R0X4	Acyl-coenzyme A thioesterase 9, mitochondrial	ACOT9_MOUSE	30	0.21
Q9Z2I9	Succinyl-CoA ligase [ADP-forming] subunit beta, mitochondrial	SUCB1_MOUSE	31	0.21
P62204	Calmodulin	CALM_MOUSE	9	0.2
P97326	Cadherin-6	CADH6_MOUSE	40	0.2
Q02819	Nucleobindin-1	NUCB1_MOUSE	29	0.2
Q61425	Hydroxyacyl-coenzyme A dehydrogenase, mitochondrial	HCDH_MOUSE	19	0.2
Q7TNG5	Echinoderm microtubule-associated protein-like 2	EMAL2_MOUSE	31	0.2
Q80UW2	F-box only protein 2	FBX2_MOUSE	14	0.2
Q80VQ0	Aldehyde dehydrogenase family 3 member B1	AL3B1_MOUSE	24	0.2
Q80Y14	Glutaredoxin-related protein 5, mitochondrial	GLRX5_MOUSE	8	0.2

Q8BMD8	Calcium-binding mitochondrial carrier protein SCaMC-1	SCMC1_MOUSE	29	0.2
Q9ERS2	NADH dehydrogenase [ubiquinone] 1 alpha subcomplex subunit 13	NDUAD_MOUSE	10	0.2
Q9WVJ3	Carboxypeptidase Q	CBPQ_MOUSE	21	0.2
Q9Z0N1	Eukaryotic translation initiation factor 2 subunit 3, X-linked	IF2G_MOUSE	24	0.2
Q9Z1Q9	Valine--tRNA ligase	SYVC_MOUSE	66	0.2
P16125	L-lactate dehydrogenase B chain	LDHB_MOUSE	21	0.19
P27046	Alpha-mannosidase 2	MA2A1_MOUSE	63	0.19
P70372	ELAV-like protein 1	ELAV1_MOUSE	17	0.19
Q91VS7	Microsomal glutathione S-transferase 1	MGST1_MOUSE	6	0.19
Q99JW5	Epithelial cell adhesion molecule	EPCAM_MOUSE	14	0.19
Q9CZ42	ATP-dependent (S)-NAD(P)H-hydrate dehydratase	NNRD_MOUSE	18	0.19
Q9D1M0	Protein SEC13 homolog	SEC13_MOUSE	13	0.19
Q9D3D9	ATP synthase subunit delta, mitochondrial	ATPD_MOUSE	5	0.19
Q9DAW9	Calponin-3	CNN3_MOUSE	18	0.19
Q9QZD9	Eukaryotic translation initiation factor 3 subunit I	EIF3I_MOUSE	22	0.19
O35685	Nuclear migration protein nudC	NUDC_MOUSE	23	0.18
O70492	Sorting nexin-3	SNX3_MOUSE	10	0.18
Q61990	Poly(rC)-binding protein 2	PCBP2_MOUSE	18	0.18
Q7TQ65	Transmembrane channel-like protein 4	TMC4_MOUSE	33	0.18
Q80YX1	Tenascin	TENA_MOUSE	105	0.18
Q8JZM8	Mucin-4	MUC4_MOUSE	115	0.18
Q8K023	Aldo-keto reductase family 1 member C18	AKC1H_MOUSE	22	0.18
Q91YW3	DnaJ homolog subfamily C member 3	DNJC3_MOUSE	32	0.18
Q9CRB6	Tubulin polymerization-promoting protein family member 3	TPPP3_MOUSE	14	0.18
Q9D0E1	Heterogeneous nuclear ribonucleoprotein M	HNRPM_MOUSE	52	0.18
Q9DCX2	ATP synthase subunit d, mitochondrial	ATP5H_MOUSE	11	0.18
Q9QXD1	Peroxisomal acyl-coenzyme A oxidase 2	ACOX2_MOUSE	41	0.18
Q9QYA2	Mitochondrial import receptor subunit TOM40 homolog	TOM40_MOUSE	12	0.18
B2RWJ3	Transmembrane protein 240	TM240_MOUSE	6	0.17
P20060	Beta-hexosaminidase subunit beta	HEXB_MOUSE	30	0.17

P26231	Catenin alpha-1	CTNA1_MOUSE	56	0.17
P29268	Connective tissue growth factor	CTGF_MOUSE	24	0.17
P51660	Peroxisomal multifunctional enzyme type 2	DHB4_MOUSE	40	0.17
P63028	Translationally-controlled tumor protein	TCTP_MOUSE	7	0.17
P84104	Serine/arginine-rich splicing factor 3	SRSF3_MOUSE	10	0.17
Q64176	Carboxylesterase 1E	EST1E_MOUSE	26	0.17
Q8BHL4	Retinoic acid-induced protein 3	RAI3_MOUSE	13	0.17
Q8BI08	Protein MAL2	MAL2_MOUSE	2	0.17
Q99K85	Phosphoserine aminotransferase	SERC_MOUSE	27	0.17
Q99KK7	Dipeptidyl peptidase 3	DPP3_MOUSE	46	0.17
Q9CX00	IST1 homolog	IST1_MOUSE	12	0.17
Q9EQP2	EH domain-containing protein 4	EHD4_MOUSE	32	0.17
Q9QUR6	Prolyl endopeptidase	PPCE_MOUSE	47	0.17
Q9QZQ8	Core histone macro-H2A.1	H2AY_MOUSE	19	0.17
P15864	Histone H1.2	H12_MOUSE	12	0.16
P23198	Chromobox protein homolog 3	CBX3_MOUSE	10	0.16
P70404	Isocitrate dehydrogenase [NAD] subunit gamma 1, mitochondrial	IDHG1_MOUSE	17	0.16
P97315	Cysteine and glycine-rich protein 1	CSRP1_MOUSE	14	0.16
Q63844	Mitogen-activated protein kinase 3	MK03_MOUSE	22	0.16
Q76MZ3	Serine/threonine-protein phosphatase 2A 65 kDa regulatory subunit A alpha isoform	2AAA_MOUSE	39	0.16
Q8BMK4	Cytoskeleton-associated protein 4	CKAP4_MOUSE	40	0.16
Q8BWT1	3-ketoacyl-CoA thiolase, mitochondrial	THIM_MOUSE	24	0.16
Q8VCC2	Liver carboxylesterase 1	EST1_MOUSE	23	0.16
Q9R0P6	Signal peptidase complex catalytic subunit SEC11A	SC11A_MOUSE	12	0.16
Q9R0Q6	Actin-related protein 2/3 complex subunit 1A	ARC1A_MOUSE	23	0.16
O35286	Putative pre-mRNA-splicing factor ATP-dependent RNA helicase DHX15	DHX15_MOUSE	43	0.15
P11438	Lysosome-associated membrane glycoprotein 1	LAMP1_MOUSE	18	0.15
P12815	Programmed cell death protein 6	PDCD6_MOUSE	10	0.15
P15535	Beta-1,4-galactosyltransferase 1	B4GT1_MOUSE	19	0.15
P61161	Actin-related protein 2	ARP2_MOUSE	21	0.15
Q61187	Tumor susceptibility gene 101 protein	TS101_MOUSE	18	0.15

Q62261	Spectrin beta chain, non-erythrocytic 1	SPTB2_MOUSE	161	0.15
Q62470	Integrin alpha-3	ITA3_MOUSE	40	0.15
Q64324	Syntaxin-binding protein 2	STXB2_MOUSE	40	0.15
Q8K211	High affinity copper uptake protein 1	COPT1_MOUSE	3	0.15
Q8R2S8	CD177 antigen	CD177_MOUSE	37	0.15
Q8VCF1	Soluble calcium-activated nucleotidase 1	CANT1_MOUSE	27	0.15
Q9CZ30	Obg-like ATPase 1	OLA1_MOUSE	26	0.15
Q9DBP5	UMP-CMP kinase	KCY_MOUSE	11	0.15
Q9DCS2	UPF0585 protein C16orf13 homolog	CP013_MOUSE		0.15
Q9JHI5	Isovaleryl-CoA dehydrogenase, mitochondrial	IVD_MOUSE	24	0.15
Q9Z0F4	Calcium and integrin-binding protein 1	CIB1_MOUSE	15	0.15
Q9Z261	Claudin-7	CLD7_MOUSE	4	0.15
O88668	Protein CREG1	CREG1_MOUSE	11	0.14
P06869	Urokinase-type plasminogen activator	UROK_MOUSE	25	0.14
P10833	Ras-related protein R-Ras	RRAS_MOUSE	16	0.14
P28301	Protein-lysine 6-oxidase	LYOX_MOUSE	20	0.14
P30275	Creatine kinase U-type, mitochondrial	KCRU_MOUSE	26	0.14
P35282	Ras-related protein Rab-21	RAB21_MOUSE	15	0.14
P35293	Ras-related protein Rab-18	RAB18_MOUSE	14	0.14
P45700	Mannosyl-oligosaccharide 1,2-alpha-mannosidase IA	MA1A1_MOUSE	37	0.14
P46467	Vacuolar protein sorting-associated protein 4B	VPS4B_MOUSE	27	0.14
P46471	26S protease regulatory subunit 7	PRS7_MOUSE	31	0.14
P54775	26S protease regulatory subunit 6B	PRS6B_MOUSE	22	0.14
P84099	60S ribosomal protein L19	RL19_MOUSE	9	0.14
Q501J6	Probable ATP-dependent RNA helicase DDX17	DDX17_MOUSE	35	0.14
Q60963	Platelet-activating factor acetylhydrolase	PAFA_MOUSE	23	0.14
Q62165	Dystroglycan	DAG1_MOUSE	42	0.14
Q78IQ7	Zinc transporter ZIP4	S39A4_MOUSE	18	0.14
Q8BG32	26S proteasome non-ATPase regulatory subunit 11	PSD11_MOUSE	32	0.14
Q8R2Y2	Cell surface glycoprotein MUC18	MUC18_MOUSE	34	0.14
Q8VDP6	CDP-diacylglycerol--inositol 3-phosphatidyltransferase	CDIPT_MOUSE	10	0.14
Q8VIJ6	Splicing factor, proline- and glutamine-rich	SFPQ_MOUSE	31	0.14
Q91VC3	Eukaryotic initiation factor 4A-III	IF4A3_MOUSE	25	0.14

Q91W90	Thioredoxin domain-containing protein 5	TXND5_MOUSE	23	0.14
Q99LP6	GrpE protein homolog 1, mitochondrial	GRPE1_MOUSE	17	0.14
Q9DCT8	Cysteine-rich protein 2	CRIP2_MOUSE	11	0.14
Q9JM14	5~(3~)-deoxyribonucleotidase, cytosolic type	NT5C_MOUSE	11	0.14
Q9WTI7	Unconventional myosin-Ic	MYO1C_MOUSE	66	0.14
Q9WTL2	Ras-related protein Rab-25	RAB25_MOUSE	14	0.14
Q9Z2I8	Succinyl-CoA ligase [GDP-forming] subunit beta, mitochondrial	SUCB2_MOUSE	30	0.14
P09671	Superoxide dismutase [Mn], mitochondrial	SODM_MOUSE	13	0.13
P35762	CD81 antigen	CD81_MOUSE	7	0.13
P40240	CD9 antigen	CD9_MOUSE	6	0.13
P51855	Glutathione synthetase	GSHB_MOUSE	29	0.13
P51859	Hepatoma-derived growth factor	HDGF_MOUSE	16	0.13
P63073	Eukaryotic translation initiation factor 4E	IF4E_MOUSE	14	0.13
P70202	Latexin	LXN_MOUSE	6	0.13
Q3TXS7	26S proteasome non-ATPase regulatory subunit 1	PSMD1_MOUSE	50	0.13
Q61205	Platelet-activating factor acetylhydrolase IB subunit gamma	PA1B3_MOUSE	17	0.13
Q64521	Glycerol-3-phosphate dehydrogenase, mitochondrial	GPDM_MOUSE	48	0.13
Q8BHH8	Clarin-3	CLRN3_MOUSE	6	0.13
Q8R016	Bleomycin hydrolase	BLMH_MOUSE	28	0.13
Q8R5F8	Epidermal growth factor receptor kinase substrate 8-like protein 1	ES8L1_MOUSE	41	0.13
Q8VCR9	Occludin/ELL domain-containing protein 1	OCEL1_MOUSE	14	0.13
Q8VEN2	Placenta-expressed transcript 1 protein	PLET1_MOUSE	4	0.13
Q91VT4	Carbonyl reductase family member 4	CBR4_MOUSE	14	0.13
Q91VU0	Protein FAM3C	FAM3C_MOUSE	16	0.13
Q99JR5	Tubulointerstitial nephritis antigen-like	TINAL_MOUSE	22	0.13
Q99LJ1	Tissue alpha-L-fucosidase	FUCO_MOUSE	25	0.13
Q9D8T0	Protein FAM3A	FAM3A_MOUSE	15	0.13
Q9JKB1	Ubiquitin carboxyl-terminal hydrolase isozyme L3	UCHL3_MOUSE	13	0.13
O09159	Lysosomal alpha-mannosidase	MA2B1_MOUSE	47	0.12
O55135	Eukaryotic translation initiation factor 6	IF6_MOUSE	10	0.12
P12382	ATP-dependent 6-	PFKAL_MOUSE	38	0.12

	phosphofructokinase, liver type			
P29533	Vascular cell adhesion protein 1	VCAM1_MOUSE	39	0.12
P31809	Carcinoembryonic antigen-related cell adhesion molecule 1	CEAM1_MOUSE	18	0.12
P32921	Tryptophan--tRNA ligase, cytoplasmic	SYWC_MOUSE	33	0.12
P62918	60S ribosomal protein L8	RL8_MOUSE	14	0.12
P97290	Plasma protease C1 inhibitor	IC1_MOUSE	25	0.12
Q5SYD0	Unconventional myosin-Id	MYO1D_MOUSE	74	0.12
Q61553	Fascin	FSCN1_MOUSE	29	0.12
Q6IRU2	Tropomyosin alpha-4 chain	TPM4_MOUSE	20	0.12
Q6PDM2	Serine/arginine-rich splicing factor 1	SRSF1_MOUSE	15	0.12
Q91ZJ5	UTP--glucose-1-phosphate uridylyltransferase	UGPA_MOUSE	30	0.12
Q99KC8	von Willebrand factor A domain-containing protein 5A	VMA5A_MOUSE	45	0.12
Q99KP6	Pre-mRNA-processing factor 19	PRP19_MOUSE	19	0.12
Q99KQ4	Nicotinamide phosphoribosyltransferase	NAMPT_MOUSE	29	0.12
Q99LF4	tRNA-splicing ligase RtcB homolog	RTCB_MOUSE	29	0.12
Q9CPY7	Cytosol aminopeptidase	AMPL_MOUSE	32	0.12
Q9CZD3	Glycine--tRNA ligase	SYG_MOUSE	50	0.12
Q9D0K2	Succinyl-CoA:3-ketoacid coenzyme A transferase 1, mitochondrial	SCOT1_MOUSE	25	0.12
Q9D6J6	NADH dehydrogenase [ubiquinone] flavoprotein 2, mitochondrial	NDUV2_MOUSE	16	0.12
Q9D701	Uroplakin-3b-like protein	UPK3L_MOUSE	10	0.12
Q9DBJ3	Brain-specific angiogenesis inhibitor 1-associated protein 2-like protein 1	BI2L1_MOUSE	38	0.12
Q9DCM0	Persulfide dioxygenase ETHE1, mitochondrial	ETHE1_MOUSE	17	0.12
Q9WUM3	Coronin-1B	COR1B_MOUSE	22	0.12
G3X9C2	F-box only protein 50	FBX50_MOUSE	18	0.11
O09117	Synaptophysin-like protein 1	SYPL1_MOUSE	10	0.11
O35658	Complement component 1 Q subcomponent-binding protein, mitochondrial	C1QBP_MOUSE	14	0.11
P17918	Proliferating cell nuclear antigen	PCNA_MOUSE	18	0.11
P32020	Non-specific lipid-transfer protein	NLTP_MOUSE	30	0.11
P40237	CD82 antigen	CD82_MOUSE	11	0.11
P97822	Acidic leucine-rich nuclear phosphoprotein 32 family	AN32E_MOUSE	10	0.11

	member E			
Q04736	Tyrosine-protein kinase Yes	YES_MOUSE	28	0.11
Q0P557	Mitochondria-eating protein	MIEAP_MOUSE	29	0.11
Q3TEA8	Heterochromatin protein 1-binding protein 3	HP1B3_MOUSE	33	0.11
Q3U1J4	DNA damage-binding protein 1	DDB1_MOUSE	53	0.11
Q60864	Stress-induced-phosphoprotein 1	STIP1_MOUSE	41	0.11
Q61792	LIM and SH3 domain protein 1	LASP1_MOUSE	16	0.11
Q8BFR4	N-acetylglucosamine-6-sulfatase	GNS_MOUSE	28	0.11
Q8BL97	Serine/arginine-rich splicing factor 7	SRSF7_MOUSE	17	0.11
Q8JZQ9	Eukaryotic translation initiation factor 3 subunit B	EIF3B_MOUSE	39	0.11
Q8K2I3	Dimethylaniline monooxygenase [N-oxide-forming] 2	FMO2_MOUSE	30	0.11
Q9CR68	Cytochrome b-c1 complex subunit Rieske, mitochondrial	UCRI_MOUSE	16	0.11
Q9D0F9	Phosphoglucomutase-1	PGM1_MOUSE	37	0.11
Q9DBF1	Alpha-aminoadipic semialdehyde dehydrogenase	AL7A1_MOUSE	24	0.11
Q9QZ06	Toll-interacting protein	TOLIP_MOUSE	14	0.11
Q9QZF2	Glypican-1	GPC1_MOUSE	33	0.11
Q9WVK4	EH domain-containing protein 1	EHD1_MOUSE	33	0.11
Q9Z2C6	Uroplakin-1b	UPK1B_MOUSE	12	0.11
O35295	Transcriptional activator protein Pur-beta	PURB_MOUSE	16	0.1
O55029	Coatomer subunit beta~	COPB2_MOUSE	49	0.1
Q11011	Puromycin-sensitive aminopeptidase	PSA_MOUSE	53	0.1
Q61490	CD166 antigen	CD166_MOUSE	29	0.1
Q61699	Heat shock protein 105 kDa	HS105_MOUSE	54	0.1
Q64704	Syntaxin-3	STX3_MOUSE	14	0.1
Q7TSV4	Phosphoglucomutase-2	PGM2_MOUSE	36	0.1
Q8BJZ3	Protein lifeguard 3	LFG3_MOUSE	6	0.1
Q8CI51	PDZ and LIM domain protein 5	PDLI5_MOUSE	33	0.1
Q922Q4	Pyrroline-5-carboxylate reductase 2	P5CR2_MOUSE	17	0.1
Q99MN1	Lysine--tRNA ligase	SYK_MOUSE	30	0.1
Q9CQA3	Succinate dehydrogenase [ubiquinone] iron-sulfur subunit, mitochondrial	SDHB_MOUSE	24	0.1
Q9CR62	Mitochondrial 2-oxoglutarate/malate carrier protein	M2OM_MOUSE	21	0.1

Q9CY50	Translocon-associated protein subunit alpha	SSRA_MOUSE	10	0.1
Q9D0L7	Armadillo repeat-containing protein 10	ARM10_MOUSE	13	0.1
Q9D710	Thioredoxin-related transmembrane protein 2	TMX2_MOUSE	18	0.1
Q9D711	Pirin	PIR_MOUSE	19	0.1
Q9D819	Inorganic pyrophosphatase	IPYR_MOUSE	20	0.1
Q9EP69	Phosphatidylinositide phosphatase SAC1	SAC1_MOUSE	35	0.1
Q9EQ06	Estradiol 17-beta-dehydrogenase 11	DHB11_MOUSE	17	0.1
A2ASQ1	Agrin	AGRIN_MOUSE	89	0.09
O08677	Kininogen-1	KNG1_MOUSE	30	0.09
O35887	Calumenin	CALU_MOUSE	17	0.09
O70133	ATP-dependent RNA helicase A	DHX9_MOUSE	75	0.09
O70400	PDZ and LIM domain protein 1	PDLI1_MOUSE	19	0.09
P10518	Delta-aminolevulinic acid dehydratase	HEM2_MOUSE	15	0.09
P26516	26S proteasome non-ATPase regulatory subunit 7	PSMD7_MOUSE	15	0.09
P45377	Aldose reductase-related protein 2	ALD2_MOUSE	20	0.09
Q61768	Kinesin-1 heavy chain	KINH_MOUSE	64	0.09
Q64191	N(4)-(beta-N-acetylglucosaminyl)-L-asparaginase	ASPG_MOUSE	17	0.09
Q6ZWX6	Eukaryotic translation initiation factor 2 subunit 1	IF2A_MOUSE	22	0.09
Q8BH59	Calcium-binding mitochondrial carrier protein Aralar1	CMC1_MOUSE	38	0.09
Q8BK64	Activator of 90 kDa heat shock protein ATPase homolog 1	AHSA1_MOUSE	24	0.09
Q8CCH2	NHL repeat-containing protein 3	NHLC3_MOUSE	20	0.09
Q8K297	Procollagen galactosyltransferase 1	GT251_MOUSE	40	0.09
Q8VCT3	Aminopeptidase B	AMPB_MOUSE	33	0.09
Q91V61	Sideroflexin-3	SFXN3_MOUSE	20	0.09
Q922P8	Transmembrane protein 132A	T132A_MOUSE	44	0.09
Q922Q8	Leucine-rich repeat-containing protein 59	LRC59_MOUSE	18	0.09
Q99JB2	Stomatin-like protein 2, mitochondrial	STML2_MOUSE	20	0.09
Q99KP3	Lambda-crystallin homolog	CRYL1_MOUSE	20	0.09
Q99L45	Eukaryotic translation initiation factor 2 subunit 2	IF2B_MOUSE	22	0.09
Q9CQ62	2,4-dienoyl-CoA reductase, mitochondrial	DECR_MOUSE	23	0.09
Q9CS42	Ribose-phosphate	PRPS2_MOUSE	19	0.09

	pyrophosphokinase 2			
Q9D0I9	Arginine--tRNA ligase, cytoplasmic	SYRC_MOUSE	42	0.09
Q9D0M3	Cytochrome c1, heme protein, mitochondrial	CY1_MOUSE	16	0.09
Q9D136	2-oxoglutarate and iron-dependent oxygenase domain-containing protein 3	OGFD3_MOUSE	17	0.09
Q9D1P4	Cysteine and histidine-rich domain-containing protein 1	CHRD1_MOUSE	23	0.09
A1A547	Peptidoglycan recognition protein 3	PGRP3_MOUSE	19	0.08
O08529	Calpain-2 catalytic subunit	CAN2_MOUSE	38	0.08
O08911	Mitogen-activated protein kinase 12	MK12_MOUSE	23	0.08
O54984	ATPase Asna1	ASNA_MOUSE	15	0.08
P01901	H-2 class I histocompatibility antigen, K-B alpha chain	HA1B_MOUSE	19	0.08
P30677	Guanine nucleotide-binding protein subunit alpha-14	GNA14_MOUSE	24	0.08
P31938	Dual specificity mitogen-activated protein kinase kinase 1	MP2K1_MOUSE	18	0.08
P51863	V-type proton ATPase subunit d 1	VA0D1_MOUSE	17	0.08
Q00PI9	Heterogeneous nuclear ribonucleoprotein U-like protein 2	HNRL2_MOUSE	41	0.08
Q04447	Creatine kinase B-type	KCRB_MOUSE	21	0.08
Q3UMR5	Calcium uniporter protein, mitochondrial	MCU_MOUSE	17	0.08
Q62087	Serum paraoxonase/lactonase 3	PON3_MOUSE	17	0.08
Q8BYM7	Radial spoke head protein 4 homolog A	RSH4A_MOUSE	27	0.08
Q8K0C9	GDP-mannose 4,6 dehydratase	GMDS_MOUSE	30	0.08
Q8R1F1	Niban-like protein 1	NIBL1_MOUSE	44	0.08
Q8R5C5	Beta-centractin	ACTY_MOUSE	23	0.08
Q91VM5	RNA binding motif protein, X-linked-like-1	RMXL1_MOUSE	33	0.08
Q99KV1	DnaJ homolog subfamily B member 11	DJB11_MOUSE	21	0.08
Q99LC3	NADH dehydrogenase [ubiquinone] 1 alpha subcomplex subunit 10, mitochondrial	NDUAA_MOUSE	23	0.08
Q9CXY6	Interleukin enhancer-binding factor 2	ILF2_MOUSE	21	0.08
Q9D662	Protein transport protein Sec23B	SC23B_MOUSE	39	0.08
Q9D8V0	Minor histocompatibility antigen H13	HM13_MOUSE	15	0.08
Q9DC69	NADH dehydrogenase	NDUA9_MOUSE	27	0.08

	[ubiquinone] 1 alpha subcomplex subunit 9, mitochondrial			
Q9ERH8	Solute carrier family 28 member 3	S28A3_MOUSE	28	0.08
Q9JK81	UPF0160 protein MYG1, mitochondrial	MYG1_MOUSE	27	0.08
Q9WVJ2	26S proteasome non-ATPase regulatory subunit 13	PSD13_MOUSE	26	0.08
O08917	Flotillin-1	FLOT1_MOUSE	31	0.07
O88632	Semaphorin-3F	SEM3F_MOUSE	51	0.07
O88968	Transcobalamin-2	TCO2_MOUSE	23	0.07
P06909	Complement factor H	CFAH_MOUSE	69	0.07
P09055	Integrin beta-1	ITB1_MOUSE	39	0.07
P12367	cAMP-dependent protein kinase type II-alpha regulatory subunit	KAP2_MOUSE	21	0.07
P19324	Serpin H1	SERPH_MOUSE	25	0.07
P37889	Fibulin-2	FBLN2_MOUSE	50	0.07
P46664	Adenylosuccinate synthetase isozyme 2	PURA2_MOUSE	27	0.07
P48722	Heat shock 70 kDa protein 4L	HS74L_MOUSE	60	0.07
P63005	Platelet-activating factor acetylhydrolase IB subunit alpha	LIS1_MOUSE	27	0.07
P63037	DnaJ homolog subfamily A member 1	DNJA1_MOUSE	22	0.07
P70168	Importin subunit beta-1	IMB1_MOUSE	38	0.07
P81117	Nucleobindin-2	NUCB2_MOUSE	24	0.07
P84091	AP-2 complex subunit mu	AP2M1_MOUSE	29	0.07
Q04998	Inhibin beta A chain	INHBA_MOUSE	30	0.07
Q08509	Epidermal growth factor receptor kinase substrate 8	EPS8_MOUSE	45	0.07
Q3THS6	S-adenosylmethionine synthase isoform type-2	METK2_MOUSE	21	0.07
Q60737	Casein kinase II subunit alpha	CSK21_MOUSE	21	0.07
Q60749	KH domain-containing, RNA-binding, signal transduction-associated protein 1	KHDR1_MOUSE	22	0.07
Q60972	Histone-binding protein RBBP4	RBBP4_MOUSE	15	0.07
Q61092	Laminin subunit gamma-2	LAMC2_MOUSE	69	0.07
Q6ZQ38	Cullin-associated NEDD8-dissociated protein 1	CAND1_MOUSE	66	0.07
Q80YQ8	Protein RMD5 homolog A	RMD5A_MOUSE	26	0.07
Q8BGX1	PC-esterase domain-containing protein 1B	PED1B_MOUSE	22	0.07
Q8BWN8	Acyl-coenzyme A thioesterase 4	ACOT4_MOUSE	21	0.07
Q8QZT1	Acetyl-CoA acetyltransferase,	THIL_MOUSE	23	0.07

	mitochondrial			
Q8VE37	Regulator of chromosome condensation	RCC1_MOUSE	18	0.07
Q9CY58	Plasminogen activator inhibitor 1 RNA-binding protein	PAIRB_MOUSE	23	0.07
Q9ER72	Cysteine--tRNA ligase, cytoplasmic	SYCC_MOUSE	51	0.07
Q9WVP1	AP-1 complex subunit mu-2	AP1M2_MOUSE	28	0.07
Q9Z2W1	Serine/threonine-protein kinase 25	STK25_MOUSE	23	0.07
O08528	Hexokinase-2	HXK2_MOUSE	55	0.06
O08810	116 kDa U5 small nuclear ribonucleoprotein component	U5S1_MOUSE	56	0.06
O35114	Lysosome membrane protein 2	SCRB2_MOUSE	24	0.06
P26369	Splicing factor U2AF 65 kDa subunit	U2AF2_MOUSE	19	0.06
P26638	Serine--tRNA ligase, cytoplasmic	SYSC_MOUSE	29	0.06
P30999	Catenin delta-1	CTND1_MOUSE	55	0.06
P50431	Serine hydroxymethyltransferase, cytosolic	GLYC_MOUSE	28	0.06
P97855	Ras GTPase-activating protein-binding protein 1	G3BP1_MOUSE	25	0.06
P98063	Bone morphogenetic protein 1	BMP1_MOUSE	58	0.06
Q0MW30	E3 ubiquitin-protein ligase NEURL1B	NEU1B_MOUSE	23	0.06
Q0VBK2	Keratin, type II cytoskeletal 80	K2C80_MOUSE	33	0.06
Q32NZ6	Transmembrane channel-like protein 5	TMC5_MOUSE	42	0.06
Q3TJD7	PDZ and LIM domain protein 7	PDLI7_MOUSE	28	0.06
Q5XJY5	Coatomer subunit delta	COPD_MOUSE	29	0.06
Q61235	Beta-2-syntrophin	SNTB2_MOUSE	30	0.06
Q61655	ATP-dependent RNA helicase DDX19A	DD19A_MOUSE	34	0.06
Q68FL6	Methionine--tRNA ligase, cytoplasmic	SYMC_MOUSE	49	0.06
Q6P9R2	Serine/threonine-protein kinase OSR1	OXSR1_MOUSE	27	0.06
Q7TT45	Ras-related GTP-binding protein D	RRAGD_MOUSE	23	0.06
Q8BG22	Calcium-activated chloride channel regulator 2	CLCA2_MOUSE	45	0.06
Q8BGH2	Sorting and assembly machinery component 50 homolog	SAM50_MOUSE	29	0.06
Q8BGQ7	Alanine--tRNA ligase, cytoplasmic	SYAC_MOUSE	56	0.06
Q8BVE3	V-type proton ATPase subunit H	VATH_MOUSE	27	0.06
Q8BXZ1	Protein disulfide-isomerase	TMX3_MOUSE	25	0.06

	TMX3			
Q8C522	Endonuclease domain-containing 1 protein	ENDD1_MOUSE	23	0.06
Q8CGC7	Bifunctional glutamate/proline--tRNA ligase	SYEP_MOUSE	94	0.06
Q8CGK3	Lon protease homolog, mitochondrial	LONM_MOUSE	52	0.06
Q8K0E7	Serine incorporator 2	SERC2_MOUSE	12	0.06
Q91YT0	NADH dehydrogenase [ubiquinone] flavoprotein 1, mitochondrial	NDUV1_MOUSE	27	0.06
Q99LD4	COP9 signalosome complex subunit 1	CSN1_MOUSE	26	0.06
Q9CWK8	Sorting nexin-2	SNX2_MOUSE	30	0.06
Q9D1A2	Cytosolic non-specific dipeptidase	CNDP2_MOUSE	26	0.06
Q9DBE0	Cysteine sulfinic acid decarboxylase	CSAD_MOUSE	31	0.06
Q9DBG3	AP-2 complex subunit beta	AP2B1_MOUSE	47	0.06
Q9DBX6	Cytochrome P450 2S1	CP2S1_MOUSE	28	0.06
Q9ES97	Reticulon-3	RTN3_MOUSE	45	0.06
Q9JHU4	Cytoplasmic dynein 1 heavy chain 1	DYHC1_MOUSE	283	0.06
Q9JIF7	Coatomer subunit beta	COPB_MOUSE	56	0.06
Q9JIX9	Fas-activated serine/threonine kinase	FASTK_MOUSE	30	0.06
Q9JLJ2	4-trimethylaminobutyraldehyde dehydrogenase	AL9A1_MOUSE	27	0.06
Q9JLR1	Protein transport protein Sec61 subunit alpha isoform 2	S61A2_MOUSE	17	0.06
Q9WUM4	Coronin-1C	COR1C_MOUSE	24	0.06
O08914	Fatty-acid amide hydrolase 1	FAAH1_MOUSE	26	0.05
O70194	Eukaryotic translation initiation factor 3 subunit D	EIF3D_MOUSE	27	0.05
O89023	Tripeptidyl-peptidase 1	TPP1_MOUSE	22	0.05
P29416	Beta-hexosaminidase subunit alpha	HEXA_MOUSE	25	0.05
P48453	Serine/threonine-protein phosphatase 2B catalytic subunit beta isoform	PP2BB_MOUSE	27	0.05
P50544	Very long-chain specific acyl-CoA dehydrogenase, mitochondrial	ACADV_MOUSE	43	0.05
P51655	Glypican-4	GPC4_MOUSE	29	0.05
P97427	Dihydropyrimidinase-related protein 1	DPYL1_MOUSE	33	0.05
Q3U9G9	Lamin-B receptor	LBR_MOUSE	29	0.05
Q60598	Src substrate cortactin	SRC8_MOUSE	28	0.05
Q60715	Prolyl 4-hydroxylase subunit alpha-1	P4HA1_MOUSE	29	0.05
Q61545	RNA-binding protein EWS	EWS_MOUSE	23	0.05

Q64133	Amine oxidase [flavin-containing] A	AOFA_MOUSE	30	0.05
Q64455	Receptor-type tyrosine-protein phosphatase eta	PTPRJ_MOUSE	54	0.05
Q6DFW4	Nucleolar protein 58	NOP58_MOUSE	27	0.05
Q6PDK8	E3 ubiquitin-protein ligase DTX4	DTX4_MOUSE	32	0.05
Q80UG5	Septin-9	SEPT9_MOUSE	40	0.05
Q8BH04	Phosphoenolpyruvate carboxykinase [GTP], mitochondrial	PCKGM_MOUSE	35	0.05
Q8BU30	Isoleucine--tRNA ligase, cytoplasmic	SYIC_MOUSE	67	0.05
Q8CHT0	Delta-1-pyrroline-5-carboxylate dehydrogenase, mitochondrial	AL4A1_MOUSE	32	0.05
Q8CIE6	Coatomer subunit alpha	COPA_MOUSE	76	0.05
Q8R0X7	Sphingosine-1-phosphate lyase 1	SGPL1_MOUSE	30	0.05
Q8VCM8	Nicalin	NCLN_MOUSE	22	0.05
Q91V92	ATP-citrate synthase	ACLY_MOUSE	61	0.05
Q91WG0	Acylcarnitine hydrolase	EST2C_MOUSE	17	0.05
Q99KG5	Lipolysis-stimulated lipoprotein receptor	LSR_MOUSE	26	0.05
Q9D6Z1	Nucleolar protein 56	NOP56_MOUSE	36	0.05
Q9DBG7	Signal recognition particle receptor subunit alpha	SRPR_MOUSE	41	0.05
Q9ET30	Transmembrane 9 superfamily member 3	TM9S3_MOUSE	21	0.05
Q9R069	Basal cell adhesion molecule	BCAM_MOUSE	35	0.05
E9Q557	Desmoplakin	DESP_MOUSE	207	0.04
O35350	Calpain-1 catalytic subunit	CAN1_MOUSE	45	0.04
P19096	Fatty acid synthase	FAS_MOUSE	131	0.04
P23116	Eukaryotic translation initiation factor 3 subunit A	EIF3A_MOUSE	90	0.04
P23780	Beta-galactosidase	BGAL_MOUSE	28	0.04
P41216	Long-chain-fatty-acid--CoA ligase 1	ACSL1_MOUSE	39	0.04
P70670	Nascent polypeptide-associated complex subunit alpha, muscle-specific form	NACAM_MOUSE	102	0.04
P82198	Transforming growth factor-beta-induced protein ig-h3	BGH3_MOUSE	42	0.04
Q3UPP8	Centrosomal protein of 63 kDa	CEP63_MOUSE	40	0.04
Q3UQ44	Ras GTPase-activating-like protein IQGAP2	IQGA2_MOUSE	96	0.04
Q62318	Transcription intermediary factor 1-beta	TIF1B_MOUSE	33	0.04
Q80VA0	N-acetylgalactosaminyltransferase 7	GALT7_MOUSE	45	0.04
Q8C1A5	Thimet oligopeptidase	THOP1_MOUSE	45	0.04

Q8CG14	Complement C1s-A subcomponent	CS1A_MOUSE	28	0.04
Q8JZQ2	AFG3-like protein 2	AFG32_MOUSE	53	0.04
Q8JZR0	Long-chain-fatty-acid--CoA ligase 5	ACSL5_MOUSE	37	0.04
Q8K0D5	Elongation factor G, mitochondrial	EFGM_MOUSE	45	0.04
Q8R146	Acylamino-acid-releasing enzyme	APEH_MOUSE	36	0.04
Q91VA1	Choline transporter-like protein 4	CTL4_MOUSE	27	0.04
Q91VD9	NADH-ubiquinone oxidoreductase 75 kDa subunit, mitochondrial	NDUS1_MOUSE	42	0.04
Q91W50	Cold shock domain-containing protein E1	CSDE1_MOUSE	55	0.04
Q99MD9	Nuclear autoantigenic sperm protein	NASP_MOUSE	43	0.04
Q9D0R2	Threonine--tRNA ligase, cytoplasmic	SYTC_MOUSE	47	0.04
Q9D2R0	Acetoacetyl-CoA synthetase	AACS_MOUSE	38	0.04
Q9ES07	Solute carrier family 15 member 2	S15A2_MOUSE	29	0.04
Q9JHE3	Neutral ceramidase	ASAH2_MOUSE	25	0.04
Q9QXX4	Calcium-binding mitochondrial carrier protein Aralar2	CMC2_MOUSE	37	0.04
Q9QYB5	Gamma-adducin	ADDG_MOUSE	31	0.04
Q9R0E2	Procollagen-lysine,2-oxoglutarate 5-dioxygenase 1	PLOD1_MOUSE	43	0.04
Q9WTR5	Cadherin-13	CAD13_MOUSE	33	0.04
Q9Z110	Delta-1-pyrroline-5-carboxylate synthase	P5CS_MOUSE	48	0.04
Q9Z185	Protein-arginine deiminase type-1	PADI1_MOUSE	36	0.04
Q9Z2I0	LETM1 and EF-hand domain-containing protein 1, mitochondrial	LETM1_MOUSE	45	0.04
B0V2N1	Receptor-type tyrosine-protein phosphatase S	PTPRS_MOUSE	96	0.03
E9Q5G3	Kinesin-like protein KIF23	KIF23_MOUSE	53	0.03
P17426	AP-2 complex subunit alpha-1	AP2A1_MOUSE	60	0.03
P39054	Dynamin-2	DYN2_MOUSE	56	0.03
P43406	Integrin alpha-V	ITAV_MOUSE	61	0.03
P56399	Ubiquitin carboxyl-terminal hydrolase 5	UBP5_MOUSE	43	0.03
P56677	Suppressor of tumorigenicity 14 protein homolog	ST14_MOUSE	36	0.03
Q07139	Protein ECT2	ECT2_MOUSE	53	0.03
Q3TDQ1	Dolichyl-diphosphooligosaccharide--protein glycosyltransferase subunit STT3B	STT3B_MOUSE	35	0.03

Q60997	Deleted in malignant brain tumors 1 protein	DMBT1_MOUSE	55	0.03
Q61739	Integrin alpha-6	ITA6_MOUSE	62	0.03
Q6P5F9	Exportin-1	XPO1_MOUSE	58	0.03
Q78PY7	Staphylococcal nuclease domain-containing protein 1	SND1_MOUSE	58	0.03
Q8BFY9	Transportin-1	TNPO1_MOUSE	38	0.03
Q8BIJ6	Isoleucine--tRNA ligase, mitochondrial	SYIM_MOUSE	49	0.03
Q8CDG1	Piwi-like protein 2	PIWL2_MOUSE	66	0.03
Q8CFI0	E3 ubiquitin-protein ligase NEDD4-like	NED4L_MOUSE	54	0.03
Q8K310	Matrin-3	MATR3_MOUSE	46	0.03
Q8VDM6	Heterogeneous nuclear ribonucleoprotein U-like protein 1	HNRL1_MOUSE	45	0.03
Q99MR6	Serrate RNA effector molecule homolog	SRRT_MOUSE	49	0.03
Q99P72	Reticulon-4	RTN4_MOUSE	45	0.03
Q9EPL2	Calsyntenin-1	CSTN1_MOUSE	41	0.03
Q9EQH2	Endoplasmic reticulum aminopeptidase 1	ERAP1_MOUSE	52	0.03
Q9JIK5	Nucleolar RNA helicase 2	DDX21_MOUSE	52	0.03
Q9Z1T1	AP-3 complex subunit beta-1	AP3B1_MOUSE	64	0.03
A2A8L5	Receptor-type tyrosine-protein phosphatase F	PTPRF_MOUSE	105	0.02
B2RXS4	Plexin-B2	PLXB2_MOUSE	97	0.02
G5E829	Plasma membrane calcium-transporting ATPase 1	AT2B1_MOUSE	65	0.02
P02468	Laminin subunit gamma-1	LAMC1_MOUSE	83	0.02
P11087	Collagen alpha-1(I) chain	CO1A1_MOUSE	82	0.02
P59509	A disintegrin and metalloproteinase with thrombospondin motifs 19	ATS19_MOUSE	63	0.02
Q05793	Basement membrane-specific heparan sulfate proteoglycan core protein	PGBM_MOUSE	151	0.02
Q3UPL0	Protein transport protein Sec31A	SC31A_MOUSE	53	0.02
Q3UTJ2	Sorbin and SH3 domain-containing protein 2	SRBS2_MOUSE	70	0.02
Q5ND34	WD repeat-containing protein 81	WDR81_MOUSE	91	0.02
Q61001	Laminin subunit alpha-5	LAMA5_MOUSE	158	0.02
Q61595	Kinectin	KTN1_MOUSE	90	0.02
Q62315	Protein Jumonji	JARD2_MOUSE	68	0.02
Q64511	DNA topoisomerase 2-beta	TOP2B_MOUSE	100	0.02
Q68FD7	Folliculin-interacting protein 1	FNIP1_MOUSE	68	0.02
Q6F3F9	G-protein coupled receptor 126	GP126_MOUSE	45	0.02

Q6P5E4	UDP-glucose:glycoprotein glucosyltransferase 1	UGGG1_MOUSE	84	0.02
Q6VH22	Intraflagellar transport protein 172 homolog	IF172_MOUSE	116	0.02
Q7TPV4	Myb-binding protein 1A	MBB1A_MOUSE	78	0.02
Q80XI3	Eukaryotic translation initiation factor 4 gamma 3	IF4G3_MOUSE	97	0.02
Q8BMJ2	Leucine--tRNA ligase, cytoplasmic	SYLC_MOUSE	61	0.02
Q921M3	Splicing factor 3B subunit 3	SF3B3_MOUSE	60	0.02
Q9QXS1	Plectin	PLEC_MOUSE	342	0.02
Q07113	Cation-independent mannose-6-phosphate receptor	MPRI_MOUSE	124	0.01
Q61789	Laminin subunit alpha-3	LAMA3_MOUSE	181	0.01
Q6P4T2	U5 small nuclear ribonucleoprotein 200 kDa helicase	U520_MOUSE	122	0.01
Q8C6K9	Collagen alpha-6(VI) chain	CO6A6_MOUSE	127	0.01
Q8R0W0	Epiplakin	EPIPL_MOUSE	388	0.01
Q99PV0	Pre-mRNA-processing-splicing factor 8	PRP8_MOUSE	145	0.01
Q9D952	Envoplakin	EVPL_MOUSE	126	0.01
Q9QZZ4	Unconventional myosin-XV	MYO15_MOUSE	188	0.01
A2AAJ9	Obscurin	OBSCN_MOUSE	495	0

Table S2: Antibodies used for immuno-detection studies

Primary Antibody	Type	Manufacturer
Anti- Bpifa1	Rabbit polyclonal	Prepared in lab (Musa et al 2012)
Anti- FoxJ1	Mouse monoclonal	Affymetrix eBioscience (2A5 Cat no 14-9965)
Anti- Muc5B	Rabbit polyclonal	Santa Cruz Biotechnology (H-300, Sc-20119)
Anti- P63	Mouse monoclonal	Santa Cruz Biotechnology (4A4, Cat no Sc-8431)
Anti- Lactotransferrin	Rabbit antisera	Milipore (Cat no 07- 685)
Anti- Reg3γ	Rabbit polyclonal	Kindly provided by Professor Lora Hooper (Cash et al 2006)
Anti- Zo1	Rabbit polyclonal	Life Technologies (Cat no 40-2200)

Table S3: Primer sequences and amplicon sizes for end point reverse transcription PCR

Assay	Primer type	Sequence (5'-3')	Product size (bp)
Bpifa1	Forward Reverse	ACAGAGGAGCCGACGTCTAA CCAAGAAAGCTGAAGGTTC	127
Tekt1	Forward Reverse	CAGTGCGAAGTGGTAGACG TTCACCTGGATTTCCTCCTG	373
Muc5B	Forward Reverse	ATGGTGACCAAGAGCCAAAA CAGGACTGTTCACCCAGGTT	178
Muc5AC	Forward Reverse	GCACCAAAGACAGCAGATCA CTGAGAGGTTTGCAGCTCCT	167
Lactotransferrin	Forward Reverse	TCTGTCCCTGTGTATTGGT GTTTCCGGGTGTCATCAAGG	237
SP-D	Forward Reverse	AAGCAGGGGAACATAGGACC GCCTTTTGCCCCTGTAGATC	109
Bpifb1	Forward Reverse	CCCTGACCAAGATCCTTGAA GAGGCTGGAGTGAGCTTGAG	148
Keratin 5	Forward Reverse	ACCTTCGAAACACCAAGCAC TGACTGGTCCAACTCCTTCC	337
Vimentin	Forward Reverse	CAAGCAGGAGTCAAACGAG CCTGTAGGTGGCGATCTCAA	273
Reg3$^{\gamma}$	Forward Reverse	CCTGTCCTCCATGATCAAAGC GCAGACATAGGGTAACTCTAAGT	250
Oaz1	Forward Reverse	ACAGAGGAGCCGACGTCTAA CCAAGAAAGCTGAAGGTTC	274

Movie S1

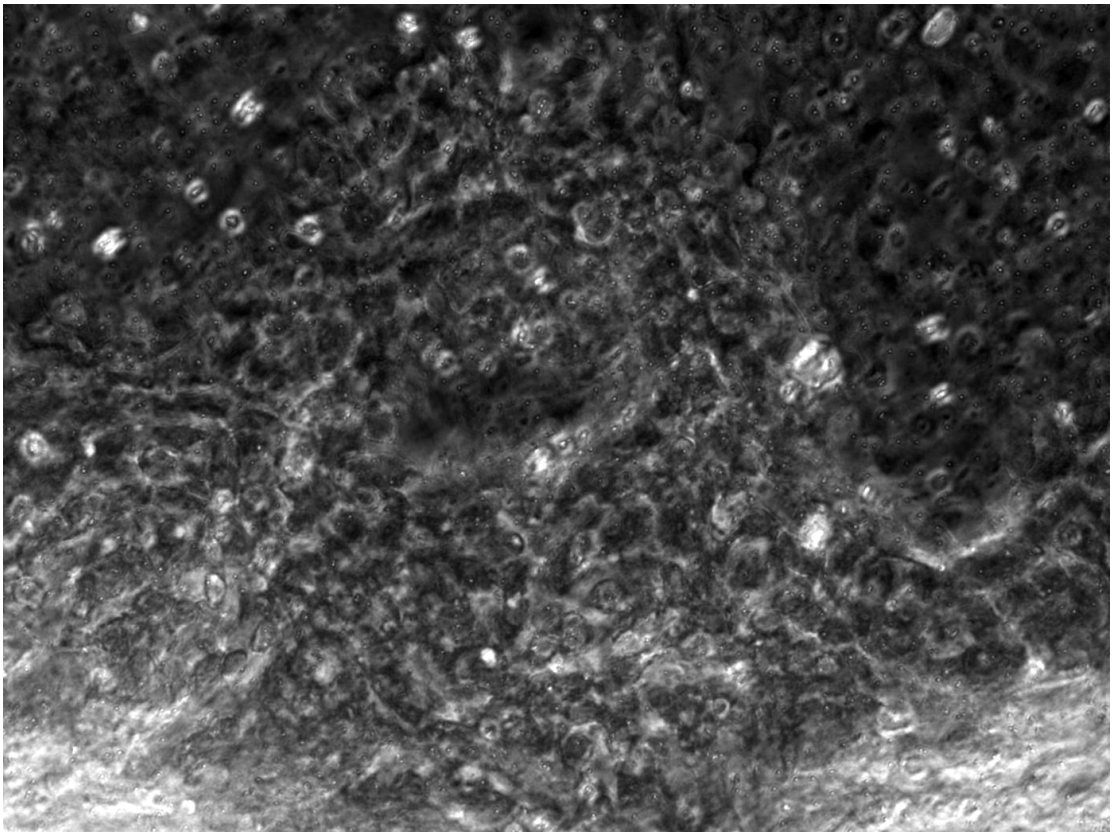

Movie S1: Time lapse images showing ciliary beating in live ALI Day 14 mMEC cells